CALSPAN-UB

RESEARCH CENTER

TECHNICAL REPORT

CALSPAN UB RESEARCH CENTER

CALSPAN-UB RESEARCH CENTER P.O. BOX 400 BUFFALO, NEW YORK 14225

CALSPAN UB RESEARCH CENTER

Development of BEM for Ceramic Composites

Fourth Annual Status Report
January 1991 - December 1991

Grant No. NAG3-888

Prepared by:

D.P. Henry
P.K. Banerjee
G.F. Dargush

Department of Civil Engineering
State University of New York at Buffalo

Prepared for:

National Aeronautics and Space Administration
Lewis Research Center
21000 Brookpark Road
Cleveland, Ohio 44135

Development of BEM for Ceramic Composites

TABLE OF CONTENTS

1. INTRODUCTION

Although from a historical point of view, composite materials have found practical use for centuries, during the past two decades there has been a tremendous increase in the use of composite materials in engineering applications, particularly in aerospace engineering. The main attraction of these materials is the ability to design and manufacture such materials to sustain a specific type of loading in the most efficient manner. If properly produced, composites can often achieve a combination of properties that are far superior to the properties of the individual constituents acting independently.

It is well known that gas turbine engine structures, particularly those components directly in the hot gas flow path, are subjected to extremely severe thermal and mechanical loading that can often lead to creep enhanced distortion, cracking and low cycle fatigue. As the demand for more efficient propulsion systems rise so does the thermal and mechanical loading. It is unlikely that the current generations of metal alloys would be suitable candidates for structural components in the future generations of efficient propulsion systems. Ceramic components are often thought to be ideal as far as their thermal durability is concerned. Unfortunately, ceramics do not have adequate tensile strength to sustain a high level of mechanical loading. In recent years there has been significant effort in the attempt to incorporate fibrous inclusions within a ceramic matrix to develop a class of new materials, known as ceramic composites, for advanced engineering application.

The mechanical behavior of ceramic composites under nonlinear, thermal, and dynamic loading is extremely complex and can only be understood if the observed behavior is interpreted in terms of micromechanical analyses. Such analyses must take care of the complex interaction of the individual fibers or bundles of fibers embedded in the three-dimensional ceramic matrix and must allow for increasing levels of sophistication in terms of the idealization of the fibers as well as the ceramic matrix. In addition complex interface behavior and controlled failure of the fiber must be considered.

It is evident that for proper micromechanical analysis of ceramic composites one needs to use a numerical method that is capable of idealizing the individual fibers or individual bundles of fibers embedded within a three-dimensional ceramic matrix. The analysis must be able to take account of high stress or temperature gradients from diffusion of stress or temperature from the fiber to the ceramic matrix and allow for the interaction between the fibers through the ceramic matrix. The analysis must be sophisticated enough to deal with failure of fibers described by a series of increasingly sophisticated constitutive models. Finally, the analysis must deal with micromechanical modeling of the composite under nonlinear thermal and dynamic loading.

The boundary element method is uniquely suited for the task. BEM has proven its ability to accurately determine stress near a stress concentration. All functional quantities in a BEM system are on the boundary and interface surfaces, therefore, allowing nonlinear interaction on the interface between the matrix and the fiber to be readily described by failure models. Furthermore, recent development has shown the generality and versatility of boundary element method in analyzing large two- and three-dimensional models subjected to static, dynamic, and thermal loads involving materials with nonlinear behavior.

This report details progress made during the first four years towards the development of a boundary element code designed for the micromechanical studies of advanced ceramic composite. Additional effort has been made in generalizing the implementation to allow the program to be applicable to real problems in the aerospace industry.

The ceramic composite formulations developed for this work have been implemented in the three-dimensional boundary element computer code 'BEST3D' which was developed for NASA by Pratt and Whitney and the State University of New York at Buffalo under contract NAS3-23697. BEST3D was adopted as the base for the ceramic composite program, so that many of the enhanced features of this general purpose boundary element code could be utilized. Some of these facilities include sophisticated numerical integration, the capability of local definition of boundary conditions, and the use of quadratic shape

functions for modeling geometry and field variables on the boundary. The multi-region implementation permits a body to be modeled in substructural parts; thus dramatically reducing the cost of the analysis. Furthermore, it allows a body consisting of regions of different ceramic matrices and inserts to be studied.

In the next chapter the elastostatic and steady-state heat conduction boundary element formulation for ceramic composites is developed. The method for the semi-analytic integration of the kernel functions about the fiber is presented and the numerical implementation of the formulation is discussed. This is followed by the development of the uncoupled thermoelastic BEM formulation in Chapter 3. Up to this point, only fibers assumed to be perfectly bonded to the composite matrix were considered. In Chapter 4, the previous formulations are rederived in a form suitable for more general fiber to matrix interface connections. A spring and a nonlinear, coulomb friction constitutive models are developed for use as interface relations, and nonlinear solution algorithm is presented. Chapter 5 contains the transient heat conduction and transient uncoupled thermoelastic BEM formulations. In Chapter 6, nonlinear material behavior in the composite matrix is studied. Chapter 7 outlines the development of the general computer program implementation. In Chapter 8, a number of numerical examples are presented to demonstrate the power of the present implementations. This report is then concluded with a summary and plan for future developments.

2. Steady-State Heat Conduction and Elastostatic BEM Formulation

2.1 Introduction

The conventional boundary integral equations for elastostatic and steady-state heat conduction analyses are used in deriving a boundary element formulation for the analysis of ceramic composite structures. The boundary integral equation written for a point ξ in the interior of the composite matrix is modified by adding the boundary integral equations of each fiber written at the same point ξ to this equation. This eventually eliminates the displacement (or temperature) variables on the fiber-matrix interface from the system, and therefore, reduces the total number of equations required for a solution of the system (see Figure 2-1).

The BEM formulation for the steady-state heat conduction analysis of ceramic composites is identical to the elastostatic formulation, and therefore, the two formulations will be derived as one.

2.2 Boundary Integral Equation Formulations

The direct boundary integral equation for the displacement (or temperature) at a point ξ inside an elastic composite matrix is

$$C_{ij}(\xi)u_i(\xi) = \int_S \left[G_{ij}^M(x,\xi)t_i^O(x) - F_{ij}^M(x,\xi)u_i^O(x)\right]dS(x) + \sum_{n=1}^{N}\int_{S^n}\left[G_{ij}^M(x,\xi)t_i^H(x) - F_{ij}^M(x,\xi)u_i^H(x)\right]dS^n(x) \qquad (2.1)$$

$i,j = 1,2,3$ for elastostatics
$i,j = 1$ for heat conduction

where

G_{ij}^M, F_{ij}^M are the fundamental solutions of the governing differential equations of the ceramic matrix of infinite extent

C_{ij} are constants determined by the geometry at ξ

u_i, t_i are displacements and tractions (or temperature and flux)

S, S^n are the surfaces of the outer boundary of the matrix and the n^{th} hole (left for fiber), respectively

N is the number of individual fibers

Superscripts O and H identify the quantities on the outer surface of the matrix and the quantities on the surface of the hole, respectively.

The conventional boundary integral equation for displacement (or temperature) can also be written for each of the N fibers. For the displacement (or temperature) at a point ξ inside the n^{th} fiber we can write

$$C_{ij}^F(\xi)u_i(\xi) = \int_{S^n} \left[G_{ij}^F(x,\xi)t_i^F(x) - F_{ij}^F(x,\xi)u_i^F(x) \right] dS^n(x) \tag{2.2}$$

$i,j = 1,2,3$ for elastostatics
$i,j = 1$ for heat conduction

G_{ij}^F, F_{ij}^F are the fundamental solutions of the n^{th} fiber

C_{ij}^F are constants determined by the geometry at ξ in fiber n

u_i^F, t_i^F are displacement and tractions (or temperature and flux) associated with the n^{th} fiber

S^n the surface of the n^{th} fiber

Note, each fiber may have different material properties.

We next examine the interface conditions between the composite matrix and the fiber. For a perfect bond the displacement (or temperature) of the matrix and the displacement (or temperature) of the fibers are equal and the tractions (or fluxes) along the interface are equal and opposite.

$$u_i^H(x) = u_i^F(x) \tag{2.3a}$$

$$t_i^H(x) = -t_i^F(x) \tag{2.3b}$$

In elastostatics, when the elastic modulus of the fiber is much greater than the modulus of the composite matrix, the Poisson ratio of the fiber can be assumed equal to that of the

matrix with little error (no approximation is required for the heat conduction analysis). Therefore, upon consideration of the surface normals at the interface and examination of the F_{ij} kernels, we can write the following relation for the n^{th} fiber

$$F_{ij}^{F}(x,\xi) = -F_{ij}^{H}(x,\xi) \tag{2.3c}$$

Substitution of equations (2.3) into equation (2.2) yields the following modified boundary integral equation for fiber n.

$$C_{ij}^{F}(\xi)u_i(\xi) = \int_{S^n} \Big[-G_{ij}^{F}(x,\xi)t_I^{H}(x) + F_{ij}^{M}(x,\xi)u_i^{H}(x) \Big] dS^n(x) \tag{2.4}$$

Finally adding the N fiber equations (2.4) to equation (2.1) and cancelling terms, yields the modified boundary integral equation for the composite matrix

$$\begin{aligned} \bar{C}_{ij}(\xi)u_i(\xi) = &\int_S \Big[G_{ij}^{M}(x,\xi)t_i^{O}(x) - F_{ij}^{M}(x,\xi)u_i^{O}(x) \Big] dS(x) \\ &+ \sum_{n=1}^{N} \int_{S^n} \bar{G}_{ij}(x,\xi)t_i^{H}(x) dS^n(x) \end{aligned} \tag{2.5}$$

where

$$\bar{G}_{ij}(x,\xi) = G_{ij}^{H}(x,\xi) - G_{ij}^{F}(x,\xi)$$

$\bar{C}_{ij}(\xi)$ are constants dependent on the geometry for a point ξ on the outer boundary and $\bar{C}_{ij}(\xi) = \delta_{ij}$ for a point ξ in the interior of the body.

2.3 Analytic Integration Around a Fiber

The boundary element discretization of equations (2.4) and (2.5) in the conventional manner [Banerjee and Butterfield (1981)] requires a very fine discretization about the fiber/hole. Alternatively, a new formulation is introduced in this report for the efficient modeling and analysis of fibers/holes using what the authors refer to as 'Fiber Elements'. The fibers are defined with Fiber Elements by describing the centerline of the (curvilinear, tubular) fiber with nodal points; defining the connectivity of the nodal points; and specifying the radius of the fiber at each of these nodal points (Figure 2.2). Internally

the program generates the surface of the fiber and the hole in which the resulting displacements (or temperatures) and tractions (or fluxes) are described using a trigonometric circular shape function in the circumferential direction and a curvilinear shape function of any order in the longitudinal direction (the present work employs both linear and quadratic shape functions for this purpose). A long hole (which is allowed to vary in diameter) can be described by a number of the fiber elements connected end to end, and any fiber element not connected to another is assumed, by the program, to be closed at the end by a circular disc.

Using the concept of the fiber element, the essential part of the formulation is the conversion of the two-dimensional surface integration of the fiber (and of the hole) to a one-dimensional integration. By performing a semi-analytical integration on the surface of the hole (or fiber) the numerical integration is significantly reduced. In equation (2.5) the integral under the summation is the integral which is to be modified. To facilitate an analytic integration in the circumferential direction, the three-dimensional kernel functions are first expressed in local coordinates with the center of the coordinate system coinciding with the center of the fiber/hole and the z axis aligned with the centerline of the fiber. The relative translation ξ_i' is added to the field coordinate ξ_i and the rotation is applied using the appropriate vector transformation.

$$\xi_i = a_{ij}\bar{\xi}_j + \xi_i'$$

where a_{ij} are the direction cosines between the axis of the local and global coordinate systems and the bar indicates a local variable.

The integration point x_i for a ring can now be expressed in cylindrical coordinates relative to the center of the fiber/hole as

$$x_1 = R\cos\theta$$

$$x_2 = R\sin\theta$$

$$x_3 = 0$$

where R represents the radius of the fiber, i.e., $R = (x_1^2 + x_2^2)^{1/2}$.

The normal vectors are transformed by

$$n_1 = n_r cos\theta$$

$$n_2 = n_r sin\theta$$

$$n_3 = n_z$$

where n_r and n_z represents the normals of the side of the hole in local coordinates and are dependent on the change in the radius of the fiber/hole. On the side of a straight hole $n_r = 1$ and $n_z = 0$, and on the flat surface closing the end of the hole/fiber $n_r = 0$ and $n_z = 1$.

Next a circular shape function is employed to approximate the variation in the traction (or flux) about the circumference of the fiber/hole. The circular shape function is multiplied and integrated with the three-dimensional $\bar{G}_{ij}$ kernel, allowing the nodal values of traction (or flux) to be brought outside the integral. The shape function is expressed as

$$t_i = M^\gamma t_i^\gamma \quad \text{(summation over } \gamma \text{ is implied, } \gamma = 1,2,3)$$

where

$$M^1(\theta) = \frac{1}{3} + \frac{2}{3}cos\theta$$

$$M^2(\theta) = \frac{1}{3} + \frac{\sqrt{3}}{3}sin\theta - \frac{1}{3}cos\theta$$

$$M^3(\theta) = \frac{1}{3} - \frac{\sqrt{3}}{3}sin\theta - \frac{1}{3}cos\theta$$

and t_i^γ is the nodal traction (or flux). See Figure 2.3.

A modified circular shape function is used in the integration over the end of the hole to insure continuity of traction at the center of the end surface. The modified shape function is expressed as:

$$\bar{M}^\gamma = aM^\gamma + b/3 \qquad \gamma = 1,2,3$$

$$a = r/R \qquad\qquad b = (R-r)/R$$

where

R is the radius of the hole at the end,

r is the location of the integration (Gauss) point as it sweeps from $r = 0$ to $r = R$, and

M^γ is the circular shape function defined above.

The traction must also be transformed between the local and the global systems by

$$t_i = a_{ik}\bar{t}_k$$

or

$$\bar{t}_j = a_{mj}t_m$$

Since flux is a scalar quantity, no transformation is necessary in the heat conduction analysis.

The last term in equation (2.5) can now be analytically integrated in the circumferential direction. For the m^{th} hole the two integrals involved can be expressed as

$$\begin{aligned}\int_{S^m} \bar{G}_{ij}(x,\xi)t_i^H(x)ds^m(x) &= \int_{C^m} a_{jk}\int_0^{2\pi} \bar{G}_{\ell k}^{\text{local}}(R,\theta,z,\bar{\xi})M^\gamma R d\theta a_{i\ell}t_i^\gamma dC^m \\ &= \int_{C^m} \bar{G}_{ij}^\gamma(R,z,\bar{\xi})t_i^\gamma dC^m(z)\end{aligned}$$

where the indicated integration over C^m is now a one-dimensional curvilinear integration along the hole and $\bar{G}_{ij}^\gamma$ represent the analytically integrated fiber/hole kernels. Note, since the transformation vector a_{ik} is the independent of angle θ, it may be taken outside the $d\theta$ integration. Similar analytic integration is also performed in equation (2.4).

The final kernel functions of the fiber/hole obtained from the analytical integration are very lengthy and therefore are not presented in this report. They contain functions of elliptical integrals which in general are expressed numerically by common series approximations. For a range of input values (coordinate locations), several higher order elliptical integral functions were found to produce incorrect numerical results. To overcome this problem, several new series were derived using a best fit polynomial approximation (as a function of the modulus of elliptic integrals) using values of the integrals calculated by a very accurate numerical integration in the circumferential direction.

The derivation of the fiber/hole kernels corresponding to the strain equation are accomplished from the displacement equation (2.5) by differentiation and application of the strain-displacement equations. The stress equation is then found using Hooke's Law. Due to the complexity of the resulting fiber/hole kernels, the authors perform the required differentiation before the analytic circumferential integration.

Finally we note, a fiber which has curvature along its length will differ in surface area about the circumference on the curved portion of the fiber. This is neglected in the formulation since the analytical integration is performed on an axisymmetric ring in which the surface area is constant about the circumference. This error, however, is small and disappears completely on a straight tubular fiber which is most commonly encountered. We should also mention that the fibers should not intersect the outer surface of the body or intersect other fibers. This minor restriction can be ignored if results at these locations are not of interest. As long as the fibers do not coincide with nodal points of other elements the errors will be localized and will not affect the overall boundary element solution.

2.4 Numerical Implementation

The integral representations of Section 2.2 are extremely accurate statements of the ceramic composite problem, however, approximations such as finite discretization and numerical integration are necessary in order to obtain a solution to non-trivial problems. The goal of the numerical implementation of the present formulation is to obtain the most accurate and efficient implementation possible.

2.4.1 Discretization

After the analytical integration in the circumferential direction is complete, a fiber in a three-dimensional solid can be modeled as a two-dimensional curvilinear line element with a prescribed radius at each longitudinal node. In the present work, linear and quadratic shape functions are utilized in modeling the geometry and field variables along the fiber element as well as the boundary elements on the outer surface of the 3-D body. In the

discretized form the displacement boundary integral equation for an elastic body containing fibers (equation (2.4)) can be expressed for a single fiber as

$$C_{ij}^{F}(\xi)u_i(\xi) = -\sum_{p=1}^{P}\left[\int_{C^p} G_{ij}^{F\gamma}(x,\xi)N^{\alpha}(\eta)dC^p\right]t_i^{\alpha\gamma} + \sum_{p=1}^{P}\left[\int_{C^p} F_{ij}^{F\gamma}(x,\xi)N^{\alpha}(\eta)dC^p\right]u_i^{\alpha\gamma} \tag{2.6}$$

where

P is the number of fiber elements, and

$N^{\alpha}(\eta)$ represents a shape function over the curvilinear fiber element. Summation over α is implied.

$t_i^{\alpha\gamma}$ and $u_i^{\alpha\gamma}$ are nodal values of traction (or flux) and displacement (or temperature) on the surface of the hole, respectively.

In a similar manner, equation (2.5) can be discretized using one- and two-dimensional shape functions in the following manner.

$$\bar{C}_{ij}(\xi)u_i(\xi) = \sum_{q=1}^{Q}\left[\int_{S^q} G_{ij}^{M}(x,\xi)L^{\beta}(\eta_1,\eta_2)dS^q\right]t_i^{\beta} - \sum_{q=1}^{Q}\left[\int_{S^q} F_{ij}^{M}(x,\xi)L^{\beta}(\eta_1,\eta_2)dS^q\right]u_i^{\beta} + \sum_{p=1}^{P}\left[\int_{C^p} \bar{G}_{ij}^{\gamma}(x,\xi)N^{\alpha}(\eta)dC^p\right]t_i^{\alpha\gamma} \tag{2.7}$$

where

Q is the number of boundary elements on the outer surface of the composite matrix in the region, and

$L^{\beta}(\eta_1,\eta_2)$ represents a two-dimensional shape function. Summation over β is implied.

It is important to note that the displacement and traction (or temperature and flux) on a fiber/hole varies in the longitudinal as well as the circumferential direction, i.e., for displacement (or temperature).

$$u_j = M^{\gamma}N^{\alpha}u_j^{\alpha\gamma}$$

The circular shape function M^{γ} has been analytically integrated into the kernel functions of equations (2.6) and (2.7). The ends of the fibers are assumed to be a flat surface and a one-dimensional numerical integration is carried out in the radial direction. The coefficients obtained from the integration over the end are lumped with their respective coefficients from the integration of the side of the fiber.

Equations for stress, strain, or flux at points in the interior of a body can be discretized and integrated in a similar manner.

2.4.2 Numerical Integration

The complexity of the integral in the discretized equation necessitates the use of numerical integration for their evaluation. The steps in the integration process for a given element is outlined below:

1. Using appropriate Jacobian transformations, a curvilinear fiber element or boundary element is mapped on a unit line or on a flat unit cell, respectively.

2. Depending on the proximity between the field point (ξ) and the element under consideration, there may be element subdivision and additional mapping for improved accuracy.

3. Gaussian quadrature formulas are employed for the evaluation of the discretized integral over each element (or sub-element). These formulas approximate the integral as a sum of weighted function values at designated points. The error in the approximation is dependent on the order of the (Gauss) points employed in the formula. To minimize error while at the same time maintaining computational efficiency, optimization schemes are used to choose the best number of points for a particular field point and element (Watson, 1979).

4. When the field point coincides with a node of the element being integrated, the integration becomes singular. In this case, the value of the coefficients of the F_{ij} kernel corresponding to the singular node cannot be calculated accurately by numerical inte-

gration. Instead, after the integration of all elements is complete, this value is determined so as to satisfy a rigid body displacement of the body (Banerjee and Butterfield, 1981).

2.4.3 Assembly of Equations

After the derivation of the modified boundary integral equations and the analytical circumferential integration of the kernel functions, the next critical step in the formulation is the assembly of the fibers in the system equations. Here, efficiency is of utmost importance. The approach to writing an efficient algorithm is to keep the number of system equations to a minimum by eliminating all unnecessary unknowns from the system. The strategy is to retain in the system only traction variables on the fiber-matrix interface. This is in contrast to a general multi-region problem where both displacement and tractions are retained on an interface. The elimination of the displacement on the interface is achieved through a backsubstitution of the fiber equations in the system equations which are made up exclusively from equations written for the composite matrix (on the outer surface and on the surface of the holes). The procedure is described below.

Equation (2.7) is used to generate a system of equations for nodes on the outer surface of the composite matrix and for nodes on the surface of the holes containing the fibers. Written in matrix form we have

$$\text{On the Matrix Outer Surface:} \qquad \mathbf{G^M t^O - F^M u^O + \bar{G} t^H = 0} \tag{2.8a}$$

$$\text{On the Matrix Hole Surface:} \qquad \mathbf{G^M t^O - F^M u^O + \bar{G} t^H = I u^H} \tag{2.8b}$$

where

$\mathbf{t^O}$ and $\mathbf{u^O}$ are traction and displacement (or flux and temperature) vectors on the outer surface of the composite matrix

$\mathbf{t^H}$ and $\mathbf{u^H}$ are traction and displacement (or flux and temperature) vectors on the hole

$\mathbf{I}$ is the identity matrix

$\mathbf{G^M}$ and $\mathbf{F^M}$ matrices contain coefficients from the integration over the outer boundary.

$\bar{\mathbf{G}}$ matrix contains coefficients integrated about the fiber/hole

Our goal is to eliminate $\mathbf{u^H}$ from the system. To this end, equation (2.6) is written for every node on a fiber, collocating slightly outside the boundary of the fiber [at a distance of (1.25)*(fiber radius)] where $C^F_{ij}(\xi) = 0$.

$$\mathbf{F^{F2}u^F = G^{F2}t^F}$$

Superscript **F2** identifies the equations written at points located slightly outside the boundary of the fibers.

Noting $\mathbf{u^H = u^F}$ and $\mathbf{t^H = -t^F}$ we have

$$\mathbf{F^{F2}u^H = -G^{F2}t^H} \tag{2.9}$$

Post multiplying equation (2.8b) by the $\mathbf{F^{F2}}$ matrix in equation (2.9) yields

$$\mathbf{F^{F2}G^Mt^O - F^{F2}F^Mu^O + F^{F2}\bar{G}t^H = F^{F2}u^H} \tag{2.10}$$

Equation(2.9) can now be set equal to equation (2.10) and the final form of the system is derived.

$$\text{On Outer Surface:} \qquad \mathbf{G^Mt^O - F^Mu^O + \bar{G}t^H = 0}$$

$$\text{On Hole:} \qquad \mathbf{F^{F2}G^Mt^O - F^{F2}F^Mu^O + (F^{F2}\bar{G} + G^{F2})t^H = 0} \tag{2.11}$$

At every point on the outer surface, either the traction or the displacement (or the temperature or the flux) is specified and on the surface of the hole only the tractions (or fluxes) are retained. Therefore, the number of equations in the system are equal to the final number of unknowns, and hence, the system can be solved. Thereafter, equation (2.8b) is used to determine the displacement on the fiber-matrix interface.

It should be noted that since the displacement (or temperature) about a particular hole is present only in the fiber equation corresponding to that hole, backsubstitution can

be performed one fiber at a time in a more efficient manner than backsubstitution of all fibers at once. Further, nowhere in the assembly process is a matrix inversion necessary. This efficient assembly process was made possible due to the unique formulation of the modified boundary integral equations developed earlier in this chapter.

When the composite matrix is divided into a multi-region model, the above fiber assembly is performed for each region independently. Thereafter, equilibrium and compatibility conditions are invoked at common interfaces of the substructured matrix composite. After collecting together the known and unknown boundary quantities, the final system can be expressed as

$$\mathbf{A}^b\mathbf{x} = \mathbf{B}^b\mathbf{y} \tag{2.12}$$

where

- $\mathbf{x}$ is the vector of unknown variables at outer boundary unknown tractions (or fluxes) along the fiber-matrix interface
- $\mathbf{y}$ is the vector of known variables on the outer boundary of the composite matrix, and
- $\mathbf{A}^b, \mathbf{B}^b$ are the coefficient matrices

Standard numerical procedures are used to solve the unknowns in equation (2.12). Details are described in the computer development section (Chapter 6).

Once the unknowns are determined, the resulting displacements (or temperatures) on the fiber-matrix interfaces can be found using equation(2.8b) rendering a complete boundary solution for both the fibers and composite matrix.

2.5 Interior Quantities

Once all of the displacements and tractions (or temperature and fluxes) are known on the matrix outer surface and on the fiber-matrix interface, interior quantities of displacement, stress and strain (or temperature and flux) can be determined at any point in the composite matrix or fiber. For displacement (or temperature), either the conventional

boundary displacement (or temperature) integral equation (2.1) or (2.2) can be employed or alternatively the modified equations (2.3) or (2.5) can be used.

Equations for strains can be derived from the forementioned displacement equations and the strain-displacement relations. Thereafter, equations for stress are obtained by substituting the resulting strain equations into Hooke's law.

The resulting equations, however, are not only invalid on the surface, but also difficult to evaluate numerically at points close to it. For points on the surface, the stresses can be calculated by constructing a local Cartesian coordinate system with the axes 1 and 2 directed along the tangential directions and the axis 3 in the direction of the outward normal. The stresses $\bar{\sigma}_{ij}$ referred to these local axes (indicated by overbars) are then given by:

$$
\begin{aligned}
\bar{\sigma}_{11} &= \frac{\nu}{1-\nu}\bar{t}_3 + \frac{E\nu}{1-\nu^2}\left(\bar{\varepsilon}_{11}+\bar{\varepsilon}_{22}\right) + \frac{E}{1+\nu}\bar{\varepsilon}_{11} \\
\bar{\sigma}_{12} &= \bar{\sigma}_{21} = \frac{E}{2(1+\nu)}\bar{\varepsilon}_{12} \\
\bar{\sigma}_{22} &= \frac{\nu}{1-\nu}\bar{t}_3 + \frac{E\nu}{1-\nu^2}\left(\bar{\varepsilon}_{11}+\bar{\varepsilon}_{22}\right) + \frac{E}{1+\nu}\bar{\varepsilon}_{22} \\
\bar{\sigma}_{33} &= \bar{t}_3 \\
\bar{\sigma}_{32} &= \bar{\sigma}_{23} = \bar{t}_2 \\
\bar{\sigma}_{31} &= \bar{\sigma}_{13} = \bar{t}_1
\end{aligned}
\tag{2.13}
$$

where E is the Young's modulus, $\bar{\varepsilon}_{ij}$ defines the components of the strains in the local axes system and $\bar{t}_i$ are the traction on the boundary. This method of evaluating the stresses on the surface was originally devised by (Rizzo and Shippy, 1968).

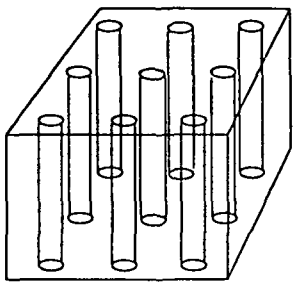

$$C_{ij}(\xi)u_i(\xi) = \int_S \left[G_{ij}^M(x,\xi)t_i^O(x) - F_{ij}^M(x,\xi)u_i^O(x)\right]dS(x) + \sum_{n=1}^{N}\int_{S^n}\left[G_{ij}^M(x,\xi)t_i^H(x) - F_{ij}^M(x,\xi)u_i^H(x)\right]dS^n(x)$$

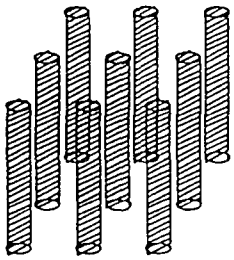

$$C_{ij}^F(\xi)u_i(\xi) = \int_{S^n}\left[G_{ij}^F(x,\xi)t_i^F(x) - F_{ij}^F(x,\xi)u_i^F(x)\right]dS^n(x)$$

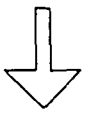

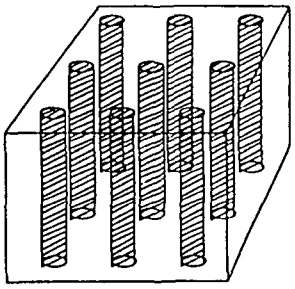

$$\bar{C}_{ij}(\xi)u_i(\xi) = \int_S \left[G_{ij}^M(x,\xi)t_i^O(x) - F_{ij}^M(x,\xi)u_i^O(x)\right]dS(x) + \sum_{n=1}^{N}\int_{S^n}\bar{G}_{ij}(x,\xi)t_i^H(x)dS^n(x)$$

where

$$\bar{G}_{ij}(x,\xi) = G_{ij}^H(x,\xi) - G_{ij}^F(x,\xi)$$

$i,j = 1,2,3$ for elastostatics
$i,j = 1$ for heat conduction

Fig. 2.1 Boundary Integral Equation Formulation for Fiber Composite Materials

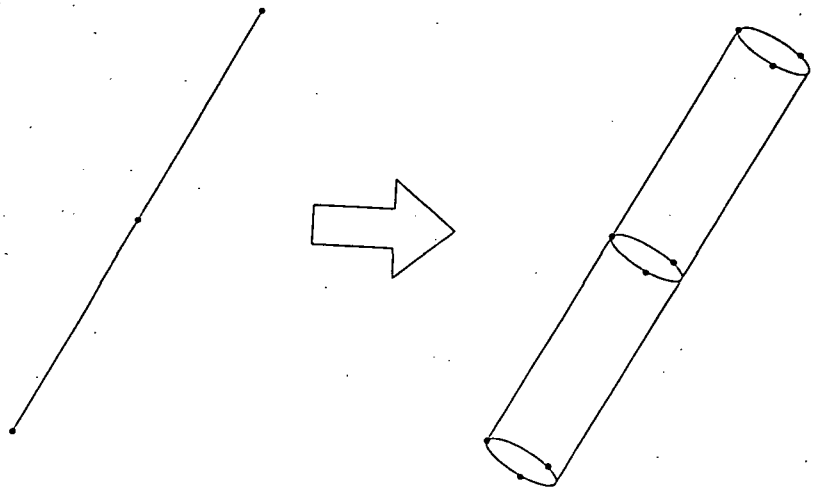

Fig. 2.2 The User Defines the Centerline of the Fiber and the Radius. The Surface of the Fiber (and the Surface of the Hole Containing the Fiber) is Automatically Generated by the Program

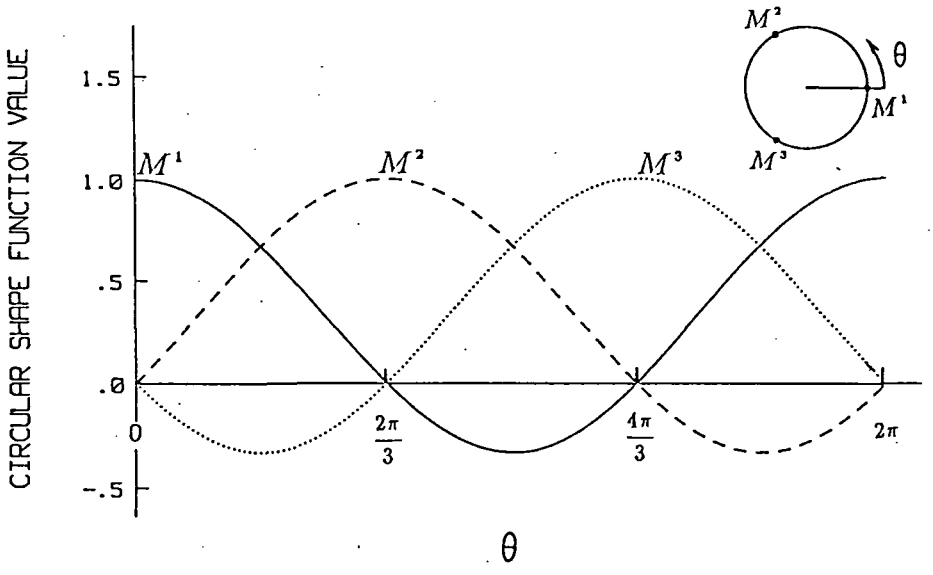

Fig. 2.3 Value of the 3-Nodal Circular Shape Function about the Fiber/Hole

3. Steady-State Uncoupled Thermoelastic BEM Formulation

3.1 Introduction

The boundary element formulation for the steady-state uncoupled thermoelastic analysis of perfectly bonded ceramic composite structures is similar to the elastostatic/heat conduction BEM formulation of Chapter 2. The primary difference is the inclusion of one-way coupling terms which, for the present formulation, requires the solution of the heat conduction equation prior to solving the thermoelastic equation set. This, however, is favorable since solving two uncoupled subsystems independently is more efficient than solving the system as a whole.

3.2. Boundary Integral Equation Formulation

Once again, the conventional boundary integral equation is the starting point for the uncoupled thermoelastic ceramic formulation. The displacement/temperature for a point ξ inside the elastic composite matrix is

$$C_{ij}(\xi)u_i(\xi) = \int_S \left[G_{ij}^M(x,\xi)t_i^O(x) - F_{ij}^M(x,\xi)u_i^O(x)\right]dS(x) + \sum_{n=1}^{N}\int_{S^n}\left[G_{ij}^M(x,\xi)t_i^H(x) - F_{ij}^M(x,\xi)u_i^H(x)\right]dS^n(x) \qquad (3.1)$$

$$i,j = 1,2,3,4$$

where

G_{ij}^M, F_{ij}^M are the uncoupled thermoelastic fundamental solutions of the governing differential equations of the ceramic matrix of infinite extent [Dargush, 1987]

C_{ij} are constants determined by the geometry at ξ

u_i, t_i are displacements and tractions for $i = 1,2,3$, and temperatures and fluxes for $i = 4$

S, S^n are surfaces of the outer boundary of the matrix and the n^{th} hold (left for fiber), respectively

N is the number of individual fibers

Superscripts O and H identify the quantities on the outer surface of the matrix and the quantities on the surface of the hole, respectively.

The conventional boundary integral equation for displacement/temperature can also be written for each of the N fibers. For the displacement/temperature at a point ξ inside the n^{th} fiber we can write

$$C_{ij}^F(\xi)u_i(\xi) = \int_{S^n} \left[G_{ij}^F(x,\xi)t_i^F(x) - F_{ij}^F(x,\xi)u_i^F(x) \right] dS^n(x) \tag{3.2}$$

$$i,j = 1,2,3,4$$

G_{ij}^F, F_{ij}^F are the fundamental solutions of the n^{th} fiber

C_{ij}^F are constants determined by the geometry at ξ in fiber n

u_i^F, t_i^F are displacement and tractions ($i = 1,2,3$) and temperature and fluxes ($i = 4$) associated with the n^{th} fiber

S^n the surface of the n^{th} fiber

Note, each fiber may have different material properties.

We next examine the interface conditions between the composite matrix and the fiber. For a perfect bond the displacement/temperature of the matrix and the displacement/temperature of the fibers along the interface are equal and the tractions/fluxes are equal and opposite.

$$u_i^H(x) = u_i^F(x) \tag{3.3a}$$

$$t_i^H(x) = -t_i^F(x) \tag{3.3b}$$

Substitution of equations (3.3) into equation (3.2) yields the following modified boundary integral equation for fiber n.

$$C_{ij}^F(\xi)u_i(\xi) = \int_{S^n} \left[-G_{ij}^F(x,\xi)t_I^H(x) + F_{ij}^M(x,\xi)u_i^H(x) \right] dS^n(x) \tag{3.4}$$

Finally adding N fiber equations (3.4) to equation (3.1) and canceling terms, yields the modified boundary integral equation for the composite matrix

$$\bar{C}_{ij}(\xi)u_i(\xi) = \int_S \left[G_{ij}^M(x,\xi)t_i^O(x) - F_{ij}^M(x,\xi)u_i^O(x) \right] dS(x)$$

$$+\sum_{n=1}^{N}\int_{S^n}\left[\bar{G}_{ij}(x,\xi)t_i^H(x)-\bar{F}_{ij}(x,\xi)u_i^H(x)\right]dS^n(x) \tag{3.5}$$

where

$$\bar{G}_{ij}(x,\xi)=G_{ij}^H(x,\xi)-G_{ij}^F(x,\xi) \tag{3.6}$$

$$\bar{F}_{ij}(x,\xi)=F_{ij}^H(x,\xi)+F_{ij}^F(x,\xi) \tag{3.7}$$

$\bar{C}_{ij}(\xi)$ are constants dependent on the geometry for a point ξ on the outer boundary and $\bar{C}_{ij}(\xi)=\delta_{ij}$ for a point in the interior of the body.

3.3 Assembly of Equations

The approach to writing an efficient algorithm is to keep the number of system equations to a minimum by eliminating all unnecessary unknowns from the system. Once again the strategy used is to retain in the system only traction/flux variables on the fiber-matrix interface. This is in contrast to a general multi-region problem where both displacement/temperatures, and tractions/fluxes are retained on an interface. The elimination of the displacement/temperatures on the interface is achieved through a backsubstitution of the fiber equations into the system equations which are made up exclusively from equations written for the composite matrix (on the outer surface and on the surface of the holes). The procedure is described below.

Equations (3.4) and (3.5) can be discretized and integrated as described in chapter 2. The thermoelastic and heat conduction equations are integrated simultaneously. Therefore, using equation (3.4) a system of equations can be generated for the nodal points on the discretized composite matrix model. The equations for the nodes on the outer boundary of the matrix and for the nodes on the hole surface can be written separately in matrix notation as:

On the Matrix Outer Surface: $$\mathbf{G^M t^O - F^M u^O + \bar{G} t^H - \bar{F} u^H = 0} \tag{3.8a}$$

On the Matrix Hole Surface: $$\mathbf{G^M t^O - F^M u^O + \bar{G} t^H - \bar{F} u^H = I u^H} \tag{3.8b}$$

$\mathbf{t^O}$ and $\mathbf{u^O}$ are traction/flux and displacement/temperature vectors on the outer surface of the composite matrix

$\mathbf{t^H}$ and $\mathbf{u^H}$ are traction/flux and displacement/temperature vectors on the hole

$\mathbf{I}$ is the identity matrix

$\mathbf{G^M}$ and $\mathbf{F^M}$ matrices contain coefficients from the integration over the outer boundary.

$\bar{\mathbf{G}}$ and $\bar{\mathbf{F}}$ matrices contain coefficients integrated about the fiber/hole

Our goal is to eliminate $\mathbf{u^H}$ from the system. To this end, equation (3.4) is written for every node on a fiber, collocating slightly outside the boundary of the fiber [at a distance of (1.25)* (radius of fiber)] where $C^F_{ij}(\xi) = 0$.

$$\mathbf{G^{F2}t^F - F^{F2}u^F = 0}$$

Superscript **F2** identifies the equations written at points located slightly outside the boundary of the fibers.

Noting $\mathbf{u^H = u^F}$, and $\mathbf{t^H = -t^F}$ we have

$$\mathbf{F^{F2}u^H = -G^{F2}t^H} \tag{3.9}$$

Post multiplying equation (3.8b) by the $\mathbf{F^{F2}}$ matrix in equation (3.9) yields

$$\mathbf{F^{F2}G^Mt^O - F^{F2}F^Mu^O + F^{F2}\bar{G}t^H - F^{F2}\bar{F}u^H = F^{F2}u^H} \tag{3.10}$$

Equation (3.9) can now be set equal to equation (3.10) and the final form of the system is derived.

$$\text{On Outer Surface:} \qquad \mathbf{G^Mt^O - F^Mu^O + \bar{G}t^H - \bar{F}u^H = O} \tag{3.11a}$$

$$\text{On Hole:} \qquad \mathbf{F^{F2}G^Mt^O - F^{F2}F^Mu^O + (F^{F2}\bar{G} + G^{F2})t^H - F^{F2}\bar{F}u^H = O} \tag{3.11b}$$

Matrix $\bar{\mathbf{F}}$ of equation (3.11) are coefficients derived from the integration of the $\bar{F}_{ij}$ kernel defined in equation (3.7) as

$$\bar{F}_{ij} = F^H_{ij} + F^F_{ij}$$

In the elastostatic/heat conduction formulation of Chapter 2 this kernel is zero according to equation (2.3c). This allowed the displacement/temperature vector $\mathbf{u^H}$ to be removed from the formulation leaving an equal number of unknowns and equations for which a solution can be obtained. In the present formulation, if we once again assume the Poisson ratio of the fiber to be the same as the composite matrix, all but three of the sixteen components in the $\bar{F}_{ij}$ kernel vanish. F_{41}, F_{42}, and F_{43} are non-zero when the coefficient of thermal expansion of the fiber is not the same as the matrix. Examining the $\bar{F}_{ij}$ kernel more closely the following simplification is possible.

$$\bar{F}_{ij}(u,\xi)u_i^H(x) = \frac{\alpha^M - \alpha^F}{\alpha^M} \begin{bmatrix} 0 & 0 & 0 & F_{41}^M \\ 0 & 0 & 0 & F_{42}^M \\ 0 & 0 & 0 & F_{43}^M \\ 0 & 0 & 0 & 0 \end{bmatrix} \begin{Bmatrix} u_1^H \\ u_2^H \\ u_3^H \\ u_4^H \end{Bmatrix} \tag{3.12}$$

where

u_1^H, u_2^H, u_3^H are the displacement components of the hole

u_4^H are the temperature component of the hole

$F_{41}^M, F_{42}^M, F_{43}^M$ are components of the F_{ij}^M kernel on the hole surface of the matrix, and

α^F, α^M are the coefficients of thermal expansion of the fiber and the matrix, respectively.

From the above equation it is clear the displacement about the fiber/hole once again vanishes from the formulation, however, the temperature θ^H ($\theta^H = u_4^H$) is present as a coupling term, in the displacement equations (components 1,2 and 3 of the kernel) and vanishes in the temperature equation (component 4). Equation (3.11) may therefore be uncoupled and written as follows.

Heat conduction system

$$\text{Outer Surface: } \mathbf{G^M t^o - F^M u^o + \bar{G} t^H = 0} \tag{3.13a}$$

$$\text{Hole Surface: } \mathbf{F^{F2} G^M t^o - F^{F2} F^M u^o + (F^{F2} \bar{G} + G^{F2}) t^H = 0} \tag{3.13b}$$

Thermal elastic system

$$\text{Outer Surface: } \mathbf{G^M t^o - F^M u^o + \bar{G} t^H = \bar{B} \theta^H} \tag{3.13c}$$

$$\text{Hole Surface: } \mathbf{F^{F2} G^M t^o - F^{F2} F^M u^o + (F^{F2} \bar{G} + G^{F2}) t^H = \bar{B}^2 \theta^H} \tag{3.13d}$$

where

$$\bar{\mathbf{B}}\theta^{\mathbf{H}} = \bar{\mathbf{F}}\mathbf{u}^{\mathbf{H}}$$

and

$$\bar{\mathbf{B}}^{\mathbf{2}}\theta^{\mathbf{H}} = \mathbf{F}^{\mathbf{F2}}\bar{\mathbf{F}}\mathbf{u}^{\mathbf{H}} \tag{3.14b}$$

In the heat conduction system the number of unknowns is equal to the number of equations. The heat conduction system can be solved and the nodal temperatures on the hole determined using an uncoupled form of equation (3.8b). With the nodal temperatures on the hole known, the number of unknowns in the thermoelastic equation system is reduced to exactly the number of equations, and therefore, this system can be solved. With the use of equation (3.8b) all remaining nodal boundary variables can be determined on the fiber-matrix interface rendering a complete solution to the boundary value problem. Displacement, temperature, traction, flux, stress, or strain measures can now be determined at any point on the boundary or in the interior of the body as described in chapter 2.

4. Nonlinear Interface Connections Between the Fiber and the Matrix

4.1 Introduction

In order to accurately analyze a ceramic composite structure the interaction between the fiber and the composite matrix must be properly modeled. Interface phenomena such as perfect bonding, progressive debonding (with gap openings), frictional slipping, and plastic behavior along the fiber-matrix interface must be included. The failure mode of an interface is dependent on the state of stress at the interface. Therefore, the general mode of failure will be nonlinear and irreversible rendering a path dependent, quasistatic analysis.

In this chapter the steady-state uncoupled thermoelastic boundary element formulations of chapter 3 is rederived in a form suitable for the inclusion of nonlinear interface connections. In addition to the perfectly bonded interface, two new types of interface connections are presented in a general form so as to be interchangeable upon input by the user. Finally the assembly of the numerically integrated BEM equations is presented and an incremental algorithm for their solution is described. The elastostatic and steady-state heat conduction formulations are obtained from the uncoupled thermoelastic formulation.

4.2. Boundary Integral Equation Formulation

The conventional boundary integral equation for displacement/temperature is the starting point for the steady-state uncoupled thermoelastic ceramic formulation with nonlinear fiber-matrix interface connections. The displacement/temperature for a point ξ inside the elastic composite matrix is

$$C_{ij}(\xi)u_i(\xi) = \int_S \left[G_{ij}^M(x,\xi)t_i^O(x) - F_{ij}^M(x,\xi)u_i^O(x)\right]dS(x) + \sum_{n=1}^{N}\int_{S^n}\left[G_{ij}^M(x,\xi)t_i^H(x) - F_{ij}^M(x,\xi)u_i^H(x)\right]dS^n(x) \qquad (4.1)$$

$$i,j = 1,2,3,4$$

where

G_{ij}^M, F_{ij}^M are the fundamental solutions of the governing differential equations of the ceramic matrix of infinite extent [Dargush, 1987]

C_{ij} are constants determined by the geometry at ξ

u_i, t_i are displacements and tractions

S, S^n are the surfaces of the outer boundary of the matrix and the n^{th} hole (left for fiber), respectively

N is the number of individual fibers

Superscripts O and H identify the quantities on the outer surface of the matrix and the quantities on the surface of the hole, respectively.

The conventional boundary integral equation for displacement can also be written for each of the N fibers. For the displacement/temperature at a point ξ inside the n^{th} fiber we can write

$$C_{ij}^F(\xi)u_i(\xi) = \int_{S^n} \left[G_{ij}^F(x,\xi)t_i^F(x) - F_{ij}^F(x,\xi)u_i^F(x) \right] dS^n(x) \tag{4.2}$$

$$i,j = 1,2,3,4$$

G_{ij}^F, F_{ij}^F are the fundamental solutions based on material properties of the n^{th} fiber

C_{ij}^F are constants determined by the geometry at ξ in fiber n

u_i^F, t_i^F are displacement and tractions associated with the n^{th} fiber

S^n the surface of the n^{th} fiber

Note, each fiber may have different material properties.

We next examine the interface conditions between the composite matrix and the fiber. The difference between the displacement/temperature of the fiber and the displacement/ temperature of the fiber is defined by a variable d_i. The traction/flux on the hole is equal and opposite to the traction/flux on the fiber. Therefore

$$u_i^H(x) = u_i^F(x) + d_i(x) \tag{4.3a}$$

$$t_i^H(x) = -t_i^F(x) \tag{4.3b}$$

Substitution of equations (4.3b) into equation (4.2) yields the following modified boundary integral equation for fiber n.

$$C_{ij}^F(\xi)u_i(\xi) = \int_{S^n} \Big[- G_{ij}^F(x,\xi)t_i^H(\xi) - F_{ij}^F(x,\xi)u_i^F(x) \Big] dS^n(x) \tag{4.4}$$

Finally adding N fiber equations (4.4) to equation (4.1) and invoking equation (4.3a), yields the modified boundary integral equation for the composite matrix

$$\begin{aligned} C_{ij}(\xi)u_i(\xi) + \sum_{n=1}^{N} \left(C_{ij}^F(\xi)\right)^n u_i(\xi) = & \int_S \Big[G_{ij}^M(x,\xi)t_i^O(x) - F_{ij}^M(x,\xi)u_i^O(x) \Big] dS(x) \\ & + \sum_{n=1}^{N} \int_{S^n} \Big[\bar{G}_{ij}(x,\xi)t_i^H(x) - F_{ij}^M(x,\xi)d_i(x) - \bar{F}_{ij}(x,\xi)u_i^F(x) \Big] dS^n(x) \end{aligned} \tag{4.5}$$

where

$$\bar{G}_{ij}(x,\xi) = G_{ij}^M(x,\xi) - G_{ij}^F(x,\xi)$$

$$\bar{F}_{ij}(x,\xi) = F_{ij}^M(x,\xi) + F_{ij}^F(x,\xi)$$

For a point in the interior of the matrix

$$C_{ij}(\xi) = \delta_{ij} \quad \text{and} \quad \left(C_{ij}^F(\xi)\right)^n = 0 \quad \text{for all } n \tag{4.6a}$$

For a point in the interior of the k^{th} fiber

$$C_{ij}(\xi) = 0 \quad \text{and} \quad \left(C_{ij}^F(\xi)\right)^n = \begin{cases} 0 & \text{for} \quad n \neq k \\ \delta_{ij} & \text{for} \quad n = k \end{cases} \tag{4.6b}$$

For a point on the outer boundary of the matrix

$$C_{ij}(\xi) \text{ is dependent on the geometry at } \xi, \text{ and}$$

$$\left(\left(C_{ij}^F(\xi)\right)^n = 0 \qquad \text{for all } n \right. \tag{4.6c}$$

For a point on the k^{th} fiber-matrix

$$C_{ij}(\xi) + \left(\left(C_{ij}^F(\xi)\right)^k = \delta_{ij}$$

$$\left(\left(C_{ij}^F(\xi)\right)^n = 0 \quad \text{for} \quad n \neq k \right. \tag{4.6d}$$

For a point ξ on the k^{th} matrix-fiber interface the left-hand side of equation (4.5) may be rewritten using equation (4.3a) and (4.6d) as

$$C_{ij}(\xi)u_i^H(\xi) + \left(C_{ij}^F(\xi)\right)^k u_i^F(\xi) + \sum_{\substack{n=1 \\ n\neq k}}^{N} \left(C_{ij}^F(\xi)\right)^n u_i(\xi)$$
$$= C_{ij}(\xi)u_i^F(\xi) + C_{ij}(\xi)d_i(\xi) + \left(C_{ij}^F(\xi)\right)^k u_i^F(\xi) = \delta_{ij}u_i^F(\xi) + C_{ij}(\xi)d_i(\xi) \qquad (4.7)$$

4.3 Interface Constitutive Relationships

4.3.1 Introduction

The interface constitutive relationships of ceramic composite materials are, in general, nonlinear. This requires that their BEM solution be found using an incremental (quasistatic) algorithm. Therefore, the linear BEM equations of Section 4.2 are interpreted as incremental relations and the interface constitutive relationships are defined in terms of the incremental displacements/temperatures $\dot{u}_j$ and the incremental tractions/fluxes $\dot{t}_i$ as

$$\dot{t}_i = k_{ij}^{ep}\dot{d}_j \qquad (4.8a)$$

$i, j = 1$ to 3 for elastostatics
$i, j = 1$ for heat conduction
$i, j = 1$ to 4 for uncoupled thermoelasticity

where k_{ij}^{ep} is the nonlinear constitutive matrix dependent on the current state of stress,

$$\dot{d}_j = \dot{u}_j^H - \dot{u}_j^F, \qquad (4.8b)$$

$$\dot{t}_i = t_i^F = -\dot{t}_i^H \qquad (4.8c)$$

The elastostatic constitutive relationships that are derived in this section are expressed using a local coordinate system where the first component corresponds to the direction normal to the interface and the second and third components correspond to arbitrary tangential directions on the fiber-matrix interface. The local constitutive matrix is transformed to the global coordinate system when incorporated in the BEM equations as follows

$$\left(k_{ij}^{ep}\right)^{\text{global}} = a_{\ell i}\left(k_{\ell m}^{ep}\right)^{\text{local}} a_{mj}$$

where a_{mj} is the directional cosine transformation tensor.

4.3.2 Linear Spring Interface Connection

The general form of the linear spring interface connection may be expressed as (k^e_{ij} replaces k^{ep}_{ij})

$$t_i = k^e_{ij} d_j \tag{4.9}$$

In the current elastostatic implementation the special case $k^e_{11} = k_n, k^e_{22} = k^e_{33} = k_t$, and $k^e_{ij} = 0$ for $i \neq j$, is assumed (see Figure 4.1). k_n is the spring constant in the normal direction and k_t is the spring constant in the tangential direction. The general form does not pose any more difficulty in implementation then the special case, but the additional generality is usually not required in practice. The limiting form as $k_n \to \infty$ and $k_t \to \infty$ approaches the case of a perfect bond, and $k_n = k_t = 0$ corresponds to a completely debonded interface. $k_n \to \infty$ and $k_t = 0$ corresponds to a sliding interface with a perfect connection in the normal direction. Results using the present formulation with values $k_n = k_t = (E^{\text{matrix}} + E^{\text{fiber}}) * 10^6$ compared very closely to results obtained for the same problem assuming a perfect bond. Similar comparisons were found to hold true for problems with $k_n = k_t = 0$ verses $E^{\text{fiber}} = 0$ (hole solution).

In the heat conduction implementation $k_{11} = -k$ where k is the thermal conductivity, $k = 0$ does not permit heat flow across the interface which is analogous to an insulated hole and $k \to \infty$ is analogous to a perfect bond between the fiber and the matrix.

The k_{ij} for uncoupled thermoelastic analysis is derived by combining the elastostatic and heat conduction k_{ij} to form a completely uncoupled k_{ij} matrix $k_{11} = k_n, k_{22} = k_{33} = k_t, k_{44} = -k$, and $k_{ij} = 0$ for $i \neq j$.

4.3.3 Spring-Friction Nonlinear Interface (Coulomb Friction)

An interface model shown in Figure (4.2) exhibits a linear spring behavior normal to the interface when the normal tractions are in compression. Linear spring resistance is also observed in the tangential direction when the principal tangential traction is below

the slip limit defined by the coulomb friction criteria. When the slip limit is reached the traction that the interface can sustain in the tangential direction has reached a maximum and any additional tangential traction will result in an irrecoverable shift of the relative displacement between the fiber and the matrix, and a redistribution of stress (and therefore interface tractions) is required to bring the structure back in equilibrium. Furthermore, the model does not support tensile tractions normal to the interface. Instead the tractions at this point are set to zero through the constitutive relation $k_{ij} = 0$ $(i, j = 1 \text{ to } 3)$ and a gap between the fiber and the matrix will form. Once again a redistribution in stress is required to bring the structure back in equilibrium.

The nonlinear interface constitutive relationship for a point on the interface exhibiting the spring-coulomb friction phenomena can be derived in a manner analogous to the incremental theory of plasticity [Selvadurai, 1988]. This requires a description and use of

(1) A flow rule relating the irrecoverable nonlinear part of the displacement difference rate to the traction state at the interface.

(2) A consistency relation requiring the new traction state to lie on the newly formed yield surface (defined by the hardening rule and yield function).

(3) A yield function defining the limits of elastic behavior, and

(4) A hardening rule defining the subsequent yield surfaces.

The variable for the incremental displacement difference across the interface is assumed to be composed of an elastic part $\dot{d}_i^e$ and a plastic part $\dot{d}_i^p$

$$\dot{d}_i = \dot{d}_i^e + \dot{d}_i^p \tag{4.10}$$

where the elastic component is related to the interface traction by the linear constitutive relation defined in Section 4.3.2.

$$\dot{t}_i = k_{ij}^e \dot{d}_j^e$$

or

$$\dot{t}_i = k^e_{ij}(\dot{d}_j - \dot{d}^p_j) \tag{4.11}$$

Next a flow rule is defined as

$$\dot{d}^p_j = \dot{\lambda}\frac{\partial Q}{\partial t_j}$$

where $\dot{\lambda}$ is an unknown flow factor dependent on the current state of traction and Q is a nonlinear potential. Substituting the flow rule into equation (4.11) yields

$$\dot{t}_i = k^e_{ij}\dot{d}_j - k^e_{ij}\dot{\lambda}\frac{\partial Q}{\partial t_j} \tag{4.12}$$

The consistency relation is defined as

$$\frac{\partial F}{\partial t_i}\dot{t}_i = 0 \tag{4.13}$$

Substitution of equation (4.12) into the consistency relationship and rearranging yields a relationship for $\dot{\lambda}$.

$$\dot{\lambda} = \frac{1}{G}\frac{\partial F}{\partial t_i}k^e_{ij}\dot{d}_j \tag{4.14}$$

where $G = \frac{\partial F}{\partial t_m}k^e_{mn}\frac{\partial Q}{\partial t_n}$

Finally substitution of equation (4.14) into equation (4.12) yields

$$\dot{t}_i = k^{ep}_{ij}\dot{d}_j \tag{4.15}$$

where

$$k^{ep}_{ij} = k^e_{ij} - k^p_{ij} \tag{4.16}$$

and

$$k^p_{ij} = \frac{1}{G}k^e_{iq}k^e_{pj}\frac{\partial F}{\partial t_p}\frac{\partial Q}{\partial t_q} \tag{4.17}$$

The nonlinear interface constitutive relationship is complete once F and Q are defined.

Assuming the coulomb friction criteria, the yield function F is given by

$$F = (t_2^2 + t_3^2)^{1/2} + \mu t_n = 0 \tag{4.18}$$

where t_n is the total traction normal to the interface, t_2 and t_3 are the total tangential tractions and μ is the coefficient of friction between the fiber and the matrix.

This relation holds only for $t_n < 0$. If $F < 0$, the interface is assumed elastic and a spring connection is used. If $F = 0$ the nonlinear interface relation (4.15) is used. $F < 0$ is meaningless in theory, however, since in practice we assume a finite size load step the function may become slightly positive in which case it is treated as $F = 0$. When $t_n \geq 0$, $k_{ij} = 0$ $(i, j = 1 \text{ to } 3)$ is assumed.

This relationship is assumed constant for the entire analysis and therefore to complete the analogy with classical plasticity, we can say we have zero hardening. The nonlinear potential Q is assumed to be the magnitude of the principal tangential traction.

$$Q = (t_2^2 + t_3^2)^{1/2} \tag{4.19}$$

If we assume the special elastostatic case described in Section 4.3.2 for k_{ij}^e where $k_{11} = k_n, k_{22} = k_{33} = k_t$, and $k_{ij}^e = 0$ for $i \neq j$ we can write for k_{ij}^p

$$k_{ij}^p = \begin{bmatrix} 0 & 0 & 0 \\ \mu k_n \hat{t}_2 & k_t \hat{t}_2 \hat{t}_2 & k_t \hat{t}_2 \hat{t}_3 \\ \mu k_n \hat{t}_3 & k_t \hat{t}_2 \hat{t}_3 & k_t \hat{t}_3 \hat{t}_3 \end{bmatrix} \tag{4.20}$$

where $\hat{t}_2$ and $\hat{t}_3$ are the normalized components of total tangential tractions, i.e.

$$\hat{t}_2 = \frac{t_2}{(t_2^2 + t_3^2)^{1/2}} \qquad \text{and} \qquad \hat{t}_3 = \frac{t_3}{(t_2^2 + t_3^2)^{1/2}}$$

In the present heat conduction and uncoupled thermoelastic implementation, only a linear (uncoupled) relation is allowed between the increment of flux and the temperature difference rate variable across the interface. This of course will be updated in the newly proposed work.

4.4 Assembly of Equations for General Fiber-Matrix Interface Connections

In the assembly of the perfectly bonded fibers the number of equations in the final system was reduced by eliminating all unnecessary unknowns from the problem. In the previous case all unknown displacement/temperature nodal variables on the fiber-matrix

interface were eliminated leaving only the unknown tractions/fluxes. In the present case the tractions/fluxes will be eliminated retaining only the fiber-matrix displacement difference variables along the interface.

The steady-state uncoupled thermoelastic equations (4.4) and (4.5) can be discretized and integrated as described in Chapter 2. Therefore, using equations (4.4), (4.6c), and (4.7) a system of equations can be generated for the nodes on the discretized model of the composite matrix. The equations for the nodes on the outer boundary of the matrix and for the nodes on the hole surface can be written separately in matrix notation as:

$$\text{On the Matrix Outer Surface:} \qquad \mathbf{G^M t^O - F^M u^O + \bar{G} t^H - F^H d - \bar{F} u^F = 0} \tag{4.21a}$$

$$\text{On the Matrix Hole Surface:} \qquad \mathbf{G^M t^O - F^M u^O + \bar{G} t^H - F^H d - \bar{F} u^F = I u^F} \tag{4.21b}$$

where

$\mathbf{t^o}$ and $\mathbf{u^o}$ are traction/flux and displacement/temperature vectors on the outer surface of the composite matrix

$\mathbf{t^H}$ is the traction/flux vector on the hole

$\mathbf{u^F}$ is the displacement/temperature vector on the fiber

$\mathbf{d}$ vector of displacement/temperature difference between the hole and fiber

$\mathbf{I}$ is the identity matrix

$\mathbf{G^M}$ and $\mathbf{F^M}$ matrices contain coefficients from the integration over the outer boundary

$\bar{\mathbf{G}}, \bar{\mathbf{F}}$ and $\mathbf{F^H}$ matrices contain coefficients from the integration over the fiber/hole

Vectors $\mathbf{u^O}$ and $\mathbf{d}$ are arranged in the same order as the equations are written so as to produce a strong main diagonal in matrices $\mathbf{F^M}$ and $\mathbf{F^H}$.

Equation (4.6c) is used in writing equation (4.21a). The $C_{ij}(\xi)u_i(\xi)$ term is lumped with its respective (diagonal block) coefficient in matrix $\mathbf{F^M}$. The sum of these two terms are accurately calculated indirectly using the rigid body technique [Banerjee and Butterfield,

1981]. Equation (4.7) is used in writing equation (4.21b). The $C_{ij}(\xi)d_i(\xi)$ term is lumped with its respective (diagonal block) coefficient in matrix $\mathbf{F^H}$ (also calculated by the rigid body technique). Similarly, the term $\delta_{ij}u_i^F(\xi)$ could be lumped with matrix $\bar{\mathbf{F}}$, but instead it is put on the right-hand side (forming an identity matrix $\mathbf{I}$ for use in subsequent matrix algebraic operations. Next, equation (4.5) is written for every shape function node on a fiber, collocating slightly outside the boundary of the fiber [at a distance of (1.25)*(radius of fiber)] where $C_{ij}^F(\xi) = 0$.

$$\mathbf{G^{F2}t^F - F^{F2}u^F = 0} \tag{4.22}$$

Superscript **F2** identifies the equations written at points located slightly outside the boundary of the fibers. Equation (4.22) can be rewritten as

$$\mathbf{F^{F2}u^F = -G^{F2}t^H} \tag{4.23}$$

Post multiplying equation (4.21b) by matrix $\mathbf{F^{F2}}$ of equation (4.23) yields

$$\mathbf{F^{F2}G^Mt^O - F^{F2}F^Mu^O + F^{F2}\bar{G}t^H - F^{F2}F^Hd - F^{F2}\bar{F}u^F = F^{F2}u^F} \tag{4.24}$$

For efficiency, this operation can be carried out one fiber at a time. Equation (4.23) can now be set equal to equation (4.10). This yields,

$$\mathbf{F^{F2}G^Mt^O - F^{F2}F^Mu^O + G^3t^H - F^3d - F^{F2}\bar{F}u^F = 0} \tag{4.25}$$

where

$$\mathbf{G^3 = F^{F2}\bar{G} + G^{F2}} \quad \text{, and}$$

$$\mathbf{F^3 = F^{F2}F^H}$$

The nonlinear interface relation $\mathbf{t^H = -K^{ep}d}$ is substituted in equation (4.21a) and (4.25) and noting equations (3.12) and (3.14) the final form of the system can be written as

On Outer Surface: $$\mathbf{G^Mt^O - F^Mu^O - (\bar{G}K^{ep} + F^H)d = \bar{B}\theta^F} \tag{4.26a}$$

On Hole Surface: $$\mathbf{F^{F2}G^Mt^O - F^{F2}F^Mu^O - (G^3K^{ep} + F^3)d = \bar{B}^2\theta^F} \tag{4.26b}$$

For each degree of freedom on every node on the outer surface, either the displacement/temperature or traction/flux is specified and on the fiber/matrix interface the displacement/temperature difference variable and the fiber temperature variable are present. Therefore the number of unknowns in the system is greater than the number of equations by exactly the number of nodes on the interface (exceeded due to the fiber temperature variables). However, as was the case in uncoupled thermoelasticity with a perfectly bonded fiber-matrix interface, the $\bar{\mathbf{B}}$ and $\bar{\mathbf{B}}^2$ matrices influence only the thermoelastic solution, i.e., the coefficients corresponding to the heat conduction equations are zero. Therefore, in the heat conduction equations these terms do not appear. The heat conduction equation can be uncoupled from the system in a manner similar to equation (3.13) rendering an equal number of heat conduction equations and unknowns. The heat conduction system is solved and the fiber nodal temperatures are determined using equation (4.21b). With the fiber nodal temperatures known, the number of unknown in the thermoelastic equation system is reduced to exactly the number of equations, and therefore the system can be solved. With the use of equations (4.8) and (4.21b) all remaining nodal boundary variables can be determined on the fiber-matrix interface rendering a complete solution to the boundary value problem. Displacement, temperature, traction, flux, stress, or strain measures can now be determined at any point on the boundary or in the interior of the body as described in Chapter 2.

The elastostatic and steady-state heat conduction formulations are derived from equation (4.26). Noting the $\bar{F}_{ij}$ kernel vanishes in elastostatic and heat conduction analysis, equation (4.21) is used setting matrix $\bar{\mathbf{F}} = \mathbf{0}$. The final system is similar to equation (4.26) with $\bar{\mathbf{B}} = \bar{\mathbf{B}}^2 = \mathbf{0}$. The number of unknowns are equal to the number of equations in a well posed problem and the system can be solved in one step.

4.5 Numerical Algorithm for Nonlinear Interface Connections

The nonlinear constitutive relationships are incorporated in the linear BEM equations and solved using the incremental (quasistatic) algorithm described below.

Nonlinear Solution Algorithm

(a) The boundary (and body force loading if present) is divided into a number of small sub-increments. Ten sub-increments have been found to be sufficient.

Initial Load Step (Iterative Start-up Loop):

(b) Assemble the BEM system equation (4.26) as described in Section 4.4 using the interface relations calculated in step (d). In the initial assembly step, linear spring connections (Section 4.3.2) are assumed at each interface node.

(c) Apply the sub-increment of load to the system equations (4.26).

(d) Determine the traction state at each interface node and derive the appropriate interface constitutive relation for that node.

- If the normal traction a the interface is positive, assume a gap opening with zero traction, i.e., $k_{ij}^{ep} = 0$
- If $F < 0$ assume a spring connection (Section 4.3.2)
- If $F \leq 0$ assume a nonlinear connection (Section 4.3.3) and evaluate the constitutive relationship using the current traction state (from current loading).

(e) Changing the interface connections from a linear spring to nonlinear relationship in the first sub-load step may cause a major redistribution in the tractions on the interface. Therefore, the constitutive relations calculated in step (c) will change. Repeat step (b), (c) and (d) until a coverage solution is achieved for the first load step.

Subsequent Load Steps:

(f) Steps (b), (c), and (d) are repeated once for each additional load step. In general, iteration within a subsequent sub-load step is not required since the constitutive relationships at interface nodes change in a gradual manner once the start-up loop is complete. The solution of any sub-increment is the accumulation of all previous sub-load steps. It is this current solution that is used in step (d) to evaluate the current interface constitutive relationships used in the next sub-incremental load step (step (c)).

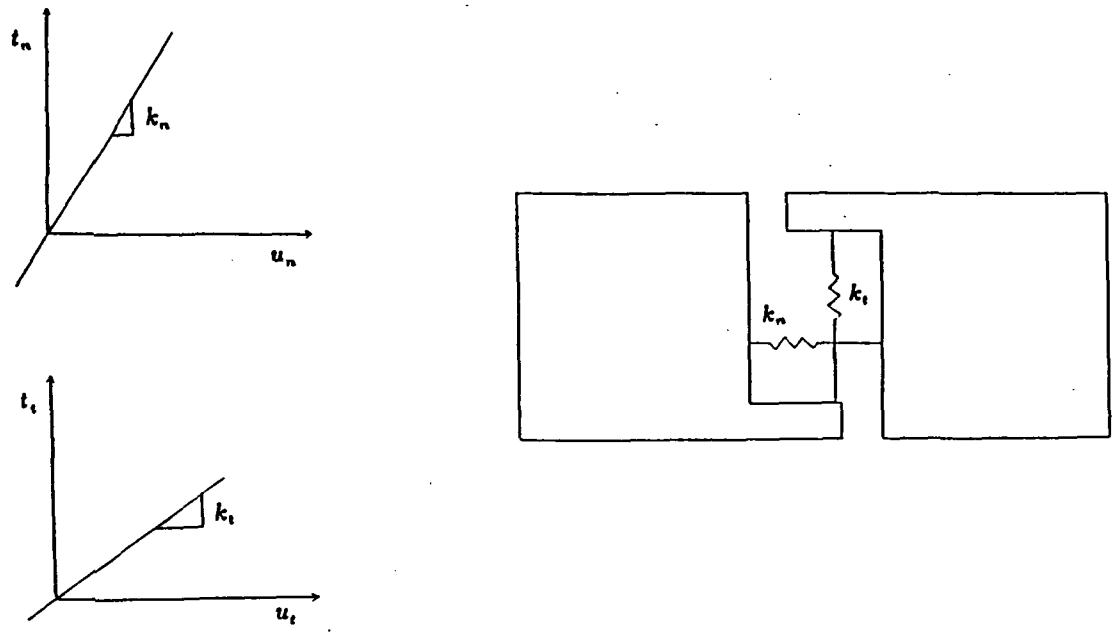

Fig. 4.1. Spring Interface Connection

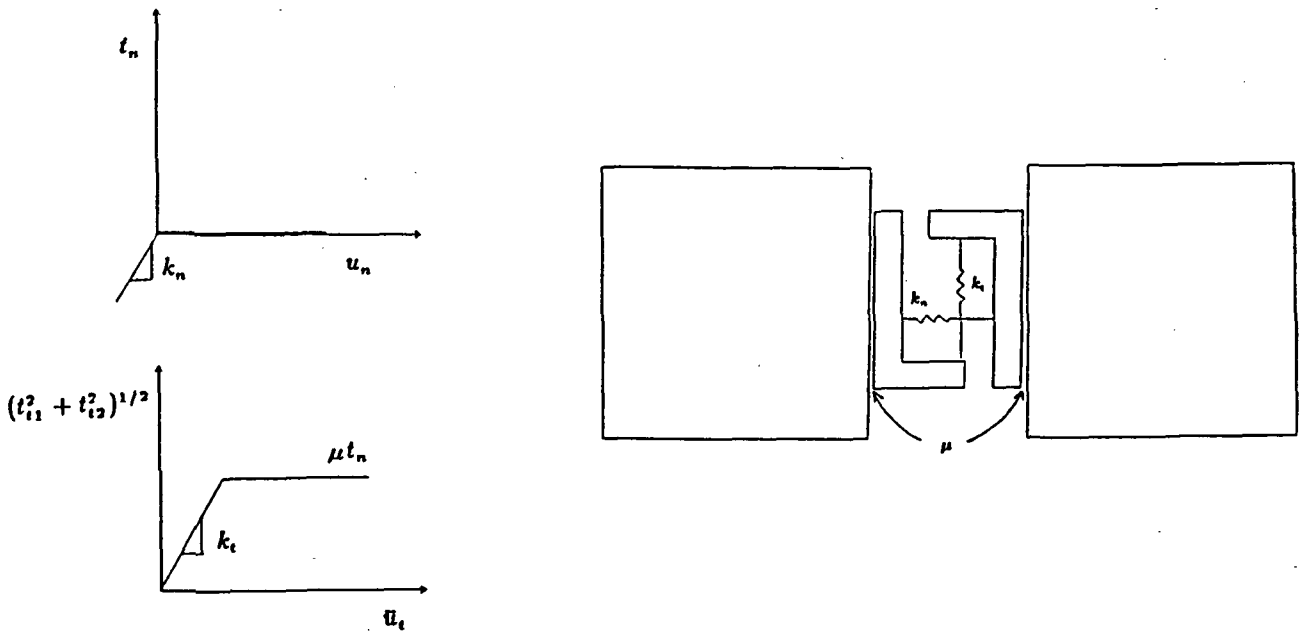

Fig. 4.2. Nonlinear Spring/Coulomb-frictional Interface Connection

5. TRANSIENT HEAT CONDUCTION AND TRANSIENT UNCOUPLED THERMOELASTIC BEM FORMULATIONS

5.1 Introduction

The analysis of a body in a transient state is inherently more complicated than a steady-state analysis. The boundary element formulation for transient analysis contains convoluted integrals which must be integrated in time as well as in space. Therefore, a transient BEM analysis is expected to be more complicated and more expensive than its steady-state counterpart. To compound these difficulties, the cost saving techniques developed for the steady-state ceramic composite analyses cannot be employed for the transient case. First, the efficient modified boundary integral formulations and the resultant assembly schemes of Chapters 2-4 do not lend themselves to transient fiber formulations for composites with general material properties. Secondly, due to the complexity of the transient kernel functions, the integration about the circumference of the fiber must now be carried out using numerical integration, thus adding to the cost of the analysis.

Nevertheless, an efficient numerical integration scheme as well as an efficient assembly algorithm have been derived for the transient heat conduction and thermoelastic BEM analyses. In the assembly algorithm the equations of the fibers are backsubstituted into the equation system of the composite matrix, hence, reducing the size of the overall system. This is carried out prior to decomposition at a point when the equations for each fiber can be handled individually in the most efficient manner. This assembly, as well as the decomposition, is required only for the initial time step. Later time steps require only a new calculation of the system's right-hand side.

5.2 Transient Boundary Integral Equation Formulation

The transient, uncoupled thermoelastic boundary integral equation (Dargush and Banerjee, 1991) for the displacement (and temperature) at a point ξ in a composite matrix is

$$C_{\beta\alpha}(\xi)u_\beta(\xi,t) = \int_S [g^M_{\beta\alpha} * t^O_\beta(X,t) - f^M_{\beta\alpha} * u^O_\beta(X,t)]\, dS(X)$$
$$+ \sum_{m=1}^{M} \int_{S^m} [g^M_{\beta\alpha} * t^H_\beta(X,t) - f^M_{\beta\alpha} * u^H_\beta(X,t)]\, dS^m(X) \qquad (5.1)$$

where

α, β indices varying from 1 to 4 for uncoupled thermoelasticity and equaled to 4 for heat conduction

$C_{\beta\alpha}$ constants determined by the geometry at ξ

u_β, t_β generalized displacement and traction

$u_\beta = [u_1,\ u_2,\ u_3,\ \theta]^T$

$t_\beta = [t_1,\ t_2,\ t_3,\ q]^T$

θ, q temperature, heat flux

$g^M_{\alpha\beta}, f^M_{\alpha\beta}$ generalized displacement and traction kernels

S, S^m are the surfaces of the outer boundary of the matrix and the mth hole (left for fiber)

M is the number of individual fibers

and, for example

$$g^M_{\beta\alpha} * t_\beta = \int_0^t g^M_{\beta\alpha}(X,t;\xi,\tau) t_\beta(X,\tau) d\tau$$

denotes a Riemann convolution integral.

Superscripts O and H are used to highlight the quantities associated with the outer surface of the matrix and the quantities associated with the surface of the hole, respectively.

The boundary integral equation for mth fiber can be written as

$$C_{\beta\alpha}(\xi)u_\beta(\xi) = \int_{S^m} [g^F_{\beta\alpha} * t^F_\beta(X,t) - f^F_{\beta\alpha} * u^F_\beta(X,t)]\, dS^m(X) \qquad (5.2)$$

where

$g^F_{\beta\alpha}, f^F_{\beta\alpha}$ are the fundamental solutions for a body with material properties corresponding to the mth fiber.

$C_{\beta\alpha}$ are constants determined by the geometry at ξ in fiber m

u^F_β, t^F_β are the generalized displacement and tractions associated with the mth fiber

S^m the surface of the mth fiber

In principle, at each instant of time progressing from time zero, these equations can be written at every point on the respective boundary. The collection of the resulting equations could then be solved simultaneously, producing exact values for all the unknown boundary quantities. In reality, of course, discretization is needed to limit this process to a finite number of equations and unknowns. Techniques useful for the discretization of (5.1) and (5.2) are the subject of the following section.

5.3 Numerical Implementation

The boundary integral equations (5.1) and (5.2) developed in the last section, are exact statements. No approximations have been introduced other than those used to formulate the boundary value problem. However, in order to apply (5.1) and (5.2) for the solution of practical engineering problems, approximations are required in both time and space. In this section, an overview of a general-purpose, state-of-the-art numerical implementation is presented for transient analysis.

5.3.1 Temporal Discretization

Consider, first, the time integrals represented in (5.1) and (5.2) as convolutions. Clearly, without any loss of precision, the time interval from zero to t can be divided into N equal increments of duration at Δt.

By assuming that the primary field variables, t_β and u_β, are constant within each Δt time increment, these quantities can be brought outside of the time integral. That is,

$$g_{\beta\alpha} * t_\beta(X,t) = \sum_{n=1}^{N} t^n_\beta(X) \int_{(n-1)\Delta t}^{n\Delta t} g_{\beta\alpha}(X-\xi, t-\tau)d\tau \qquad (5.3a)$$

$$f_{\beta\alpha} * u_\beta(X,t) = \sum_{n=1}^{N} u^n_\beta(X) \int_{(n-1)\Delta t}^{n\Delta t} f_{\beta\alpha}(X-\xi, t-\tau)d\tau \qquad (5.3b)$$

where the superscript on the generalized tractions and displacements represents the time increment number. Notice, also, that within an increment, these primary field variables are now only functions of position. Since the integrands remaining in (5.3) are known in explicit form from the fundamental solutions, the required temporal integration can be performed analytically, and written as

$$G_{\beta\alpha}^{N+1-n}(X-\xi) = \int_{(n-1)\Delta t}^{n\Delta t} g_{\beta\alpha}(X-\xi, t-\tau)d\tau \tag{5.4a}$$

$$F_{\beta\alpha}^{N+1-n}(X-\xi) = \int_{(n-1)\Delta t}^{n\Delta t} f_{\beta\alpha}(X-\xi, t-\tau)d\tau. \tag{5.4b}$$

These kernel functions, $G_{\beta\alpha}^{n}(X-\xi)$ and $F_{\beta\alpha}^{n}(X-\xi)$, are detailed in Appendix B. Combining (5.3) and (5.4) with (5.1) and (5.2) produces

$$\begin{aligned} C_{\beta\alpha}(\xi)u_{\beta}^{N}(\xi) = \sum_{n=1}^{N}\Bigg\{ &\int_{S}\left[G_{\beta\alpha}^{N+1-n}(X-\xi)t_{\beta}^{n}(X) - F_{\beta\alpha}^{N+1-n}(X-\xi)u_{\beta}^{n}(X)\right]dS(X) \\ &+ \sum_{m=1}^{M}\int_{S^m}\left[G_{\beta\alpha}^{N+1-n}(X-\xi)t_{\beta}^{n}(X) - F_{\beta\alpha}^{N+1-n}(X-\xi)u_{\beta}^{n}(X)\right]dS^m(X)\Bigg\} \end{aligned} \tag{5.5a}$$

and for the mth fiber

$$C_{\beta\alpha}(\xi)u_{\beta}^{N}(\xi) = \sum_{n=1}^{N}\left\{\int_{S^m}\left[G_{\beta\alpha}^{N+1-n}(X-\xi)t_{\beta}^{n}(X) - F_{\beta\alpha}^{N+1-n}(X-\xi)u_{\beta}^{n}(X)\right]dS^m(X)\right\} \tag{5.5b}$$

which are the boundary integral statements after the application of the temporal discretization.

5.3.2 Spatial Discretization

With the use of generalized primary variables and the incorporation of a piecewise constant time stepping algorithm, the boundary integral equation (5.5) begins to show a strong resemblance to the equations of the steady-state analyses, particularly for the initial time step (i.e., $N = 1$). In this subsection, those similarities will be exploited to develop the spatial discretization for the uncoupled quasistatic problem. This approximate spatial

representation will, subsequently, permit numerical evaluation of the surface integrals appearing in (5.5). The techniques described here, actually, originated in the finite element literature, but were later applied to boundary elements by Lachat and Watson (1976).

The process begins by subdividing the entire surface of the body (including the fibers) into individual elements of relatively simple shapes. The geometry of each element is, then, completely defined by the coordinates of the nodal points and associated interpolation functions, as described in Chapter 2.

In the present work, the geometry is exclusively defined by quadratic shape functions. On the other hand, the variation of the primary quantities can be described, within an element, by either quadratic or linear shape functions. (The introduction of linear variations proves computationally advantageous in some instances.)

Once this spatial discretization has been accomplished and the body has been subdivided into Q boundary elements and P fiber elements, the boundary integral equation can be rewritten for the matrix as

$$\begin{aligned} C_{\beta\alpha}(\xi)u^N_\beta(\xi) = \sum_{n=1}^{N}\Bigg\{ & \sum_{q=1}^{Q}\left[\int_{S^q} G^{N+1-n}_{\beta\alpha}(X(\zeta)-\xi)L_\omega(\zeta)dS^q(X(\zeta))\right] t^n_{\beta\omega} \\ & - \sum_{q=1}^{Q}\left[\int_{S^q} F^{N+1-n}_{\beta\alpha}(X(\zeta)-\xi)L_\omega(\zeta)dS^q(X(\zeta))\right] u^n_{\beta\omega} \\ & + \sum_{p=1}^{P}\left[\int_{S^p} G^{N+1-n}_{\beta\alpha}(X(\zeta)-\xi)N_\omega(\zeta)M_\gamma(\theta)dS^p(X(\zeta),\theta)\right] t^n_{\beta\omega\gamma} \\ & - \sum_{p=1}^{P}\left[\int_{S^p} F^{N+1-n}_{\beta\alpha}(X(\zeta)-\xi)N_\omega(\zeta)M_\gamma(\theta)dS^p(X(\zeta),\theta)\right] u^n_{\beta\omega\gamma}\Bigg\} \end{aligned} \tag{5.6a}$$

and

$$\begin{aligned} C_{\beta\alpha}(\xi)u^N_\beta(\xi) = \sum_{n=1}^{N}\Bigg\{ & \sum_{p=1}^{P}\left[\int_{S^p} G^{N+1-n}_{\beta\alpha}(X(\zeta)-\xi)N_\omega(\zeta)M_\gamma(\theta)dS^p(X(\zeta),\theta)\right] t^n_{\beta\omega\gamma} \\ & - \sum_{p=1}^{P}\left[\int_{S^p} F^{N+1-n}_{\beta\alpha}(X,(\zeta)-\xi)N_\omega(\zeta)M_\gamma(\theta)dS^p(X(\zeta),\theta)\right] u^n_{\beta\omega\gamma}\Bigg\} \end{aligned} \tag{5.6b}$$

where

Q is the number of boundary elements on the outer surface of the composite matrix in the region,

P is the number of fiber elements in the region,

L_ω represents a two-dimensional shape function,

N_γ represents a one-dimensional shape function,

M_γ is the circular shape function defined in Chapter 2,

t, u are nodal values of generalized traction and displacement, respectively.

In the above equation, the nodal quantities $t^n_{\beta\omega}$ and $u^n_{\beta\omega}$ were brought outside the surface integrals. This positioning of the nodal primary variables outside the integrals is, of course, a key step since now the integrands contain only known functions. However, before discussing the techniques used to numerically evaluate these integrals, a brief discussion of the singularities present in the kernels $G^n_{\beta\alpha}$ and $F^n_{\beta\alpha}$ is in order.

The fundamental solutions to the uncoupled quasistatic problem contain singularities when the load point and field point coincide, that is, is when $r = 0$. The same is true of $G^n_{\beta\alpha}$ and $F^n_{\beta\alpha}$, since these kernels are derived directly from the fundamental solutions. Series expansions of terms present in the evolution functions can be used to deduce the level of singularities existing in the kernels.

A number of observations concerning the results of these expansions should be mentioned. First, as would be expected $F^1_{\alpha\beta}$ has a stronger level of singularity than does the corresponding $G^1_{\alpha\beta}$, since an additional derivative is involved in obtaining $F^1_{\alpha\beta}$ from $G^1_{\alpha\beta}$. Second, the coupling terms do not have as high degree of singularity as do the corresponding non-coupling terms. Third, all of the kernel functions for the first time step could actually be rewritten as a sum of steady-state and transient components. That is,

$$G^1_{\alpha\beta} = {}^{ss}G_{\alpha\beta} + {}^{tr}G^1_{\alpha\beta}$$

$$F^1_{\alpha\beta} = {}^{ss}F_{\alpha\beta} + {}^{tr}F^1_{\alpha\beta}$$

Then, the singularity is completely contained in the steady-state portion. Furthermore, the singularity in G^1_{ij} and F^1_{ij} is precisely equal to that for elastostatics, while $G^1_{\theta\theta}$ and $F^1_{\theta\theta}$

singularities are identical to those for potential flow. This observation is critical in the numerical integration of the $F_{\alpha\beta}$ kernel to be discussed in the next subsection. However, from a physical standpoint, this means that, at any time t, the closer one moves toward the load point, the closer the quasistatic response field corresponds with a steady-state field. Eventually, when the sampling and load points coincide, the quasistatic and steady-state responses are indistinguishable. As a final item, after careful examination of Appendix B, it is evident that the steady-state components in the kernels $G^n_{\alpha\beta}$ and $F^n_{\alpha\beta}$, with $n > 1$, vanish. In that case, all that remains is a transient portion that contains no singularities. Thus, all singularities reside in the ${}^{ss}G_{\alpha\beta}$ and ${}^{ss}F_{\alpha\beta}$ components of $G^1_{\alpha\beta}$ and $F^1_{\alpha\beta}$, respectively.

5.3.3 Numerical Integration

Having clarified the potential singularities present in the coupled kernels, it is now possible to consider the evaluation of the integrals in equation (5.6).

To assist in this endeavor, the following three distinct categories can be identified.

(1) The point ξ does not lie on the element m.

(2) The point ξ lies on the element m, but only non-singular or weakly singular integrals are involved.

(3) The point lies on the element m, and the integral is strongly singular.

In practical problems involving many elements, it is evident that most of the integration occurring in equation (5.6) will be of the category (1) variety. In this case, the integrand is always non-singular, and standard Gaussian quadrature formulas can be employed. Sophisticated error control routines are needed, however, to minimize the computational effort for a certain level of accuracy. This non-singular integration is the most expensive part of a boundary element analysis, and, consequently, must be optimized to achieve an efficient solution. In the present implementation, error estimates, based upon the work of Stroud and Secrest (1966), are employed to automatically select the proper order of the quadrature rule. Additionally, to improve accuracy in a cost-effective manner, a graded subdivision of the element is incorporated, especially when ξ is nearby.

The integration over the surface of the hole and fiber elements must be carried out using numerical integration. The complexity of the transient kernel function prohibits an analytic integration about the circumference of the fiber in a manner similar to the steady-state case. Therefore, numerical integration must be performed in both the longitudinal and the circumferential directions. An efficient integration scheme is adopted in which one-dimensional Gaussian integration formulas are applied independently in the two directions. This allows the subsegmentation and mapping, as well as the order of the Gaussian formulas to vary independently in the two directions so that the accuracy and the cost of the integration can be optimized.

Turning next to category (2), one finds that again Gaussian quadrature is applicable, however, a somewhat modified scheme must be utilized to evaluate the weakly singular integrals. This is accomplished through element subsegmentation about the singular point so that the product of shape function, Jacobian and kernel remains well behaved.

Unfortunately, the remaining strongly singular integrals of category (3) exist only in the Cauchy principal value sense and cannot, in general, be evaluated numerically, with sufficient precision. It should be noted that this apparent stumbling block is limited to the strongly singular portions, ${}^{ss}F_{ij}$ and ${}^{ss}F_{\theta\theta}$, of the $F^1_{\alpha\beta}$ kernel. The remainder of $F^1_{\alpha\beta}$, including ${}^{tr}F^1_{ij}$ and ${}^{tr}F^1_{\theta\theta}$, can be computed using the procedures outlined for category (2). However, as will be discussed in the next subsection, even category (3) ${}^{ss}F_{ij}$ and ${}^{ss}F_{\theta\theta}$ kernels can be accurately determined by employing an indirect 'rigid body' method originally developed by Cruse (1974).

5.3.4 Assembly of Equations

The complete discretization of the boundary integral equation, in both time and space, has been described, along with the techniques required for numerical integration of the kernels. Now, a system of algebraic equations can be developed to permit the approximate solution of the original quasistatic problem. This is accomplished by systematically writing (5.6) at each node on the outer surface, on the surface of the hole, and on the surface of

the fiber. The ensuing nodal collocation process, then produces a global set of equations given here in matrix form, for time N.

For the nodes on matrix:

$$[G_M^1]\{t_O^N\} - [F_M^1]\{u_O^N\} + [G_M^1]\{t_H^N\} - [F_M^1]\{u_H^n\} = \{D^N\} \tag{5.7a}$$

For the nodes on the fibers:

$$[G_F^1]\{t_F^N\} - [F_F^1]\{u_F^N\} = \{D_F^N\} \tag{5.7b}$$

where $\{D^N\}$ and $\{D_F^N\}$ are the values of the convolution from the previous $N-1$ time steps defined as

$$-\{D^N\} = \sum_{n-1}^{N-1} \{[G_M^{N+1-n}]\{t_O^n\} - [F_M^{N+1-n}]\{u_O^n\} + [G_M^{N+1-n}]\{t_H^n\} - [F_M^{N+1-n}]\{u_H^n\}\} \tag{5.8a}$$

and

$$-\{D_F^N\} = \sum_{n=1}^{N-1} \{[G_F^{N+1-n}]\{t_F^n\} - [F_F^{N+1-n}]\{u_F^n\}\} \tag{5.8b}$$

In these equations, subscripts O, H and F are used to denote the quantities associated with the outer surface of the matrix, the surface of the hole containing the fiber, and surface of the fiber, respectively. Furthermore, the $C_{\alpha\beta}(\xi)$ term of each equation is lumped with the respective coefficient in the F^1 matrix.

To calculate the coefficients of the singular points by the 'rigid body' technique, consider now, the first step. Thus, for $N = 1$, equation(5.7) becomes

$$[G_M^1]\{t_O^1\} - [F_M^1]\{u_O^1\} + [G_M^1]\{t_H^1\} - [F_M^1]\{u_H^1\} = \{0\} \tag{5.9a}$$

$$[G_F^1]\{t_F^1\} - [F_F^1]\{u_F^1\} = \{0\}. \tag{5.9b}$$

At this point, the coefficients of the F matrices corresponding to the singular node of the equations has not been completely determined due to the strongly singular nature of the kernel function. To determine the values of these coefficients, we first decompose the F_{ij} kernel into transient and steady-state parts. Following Cruse (1974) and, later Banerjee

et al (1986) in elastodynamics, the steady-state part of the coefficients can be calculated indirectly by imposing a uniform 'rigid body' generalized displacement field on the same body under steady-state conditions. The steady-state part of the singular coefficients are simply the summation of the non-singular, steady-state coefficients. The remaining transient portion of the coefficients are non-singular, and hence can be evaluated to any desired precision.

For a fiber that is perfectly bonded to the matrix, the displacement of the surface on the hole containing the fiber is equal to the displacement of the surface of the fiber, and the surface tractions are equal in magnitude but opposite in direction.

$$\{u_H^n\} = \{u_F^n\} \tag{5.10a}$$

$$\{t_H^n\} = -\{t_F^n\} \tag{5.10b}$$

Substitution of equation (5.10) into equations (5.7b) and (5.8b) and rearranging yields

$$\{t_H^N\} = -[H][F_F^1]\{u_H^N\} - [H]\{D_F^N\} \tag{5.11a}$$

$$\{D_F^N\} = \sum_{n=1}^{N-1} \{[G_F^{N+1-n}]\{t_H^n\} + [F_F^{N+1-n}]\{u_H^n\}\} \tag{5.11b}$$

where

$$[H] = [G_F^1]^{-1}$$

Note, since the boundary integral equation for each fiber is independent of the equations for the other fibers, the inversion of $[G_F^1]$ can be reduced to a number of smaller inversions, one corresponding to each fiber.

Equation (5.11a) can now be back substituted in equation (5.7a) to yield

$$[G_M^1]\{t_O^N\} - [F_M^1]\{u_O^N\} - [F^X]\{u_H^N\} = \{D^N\} + [G_H^1][H]\{D_F^N\} \tag{5.12}$$

where

$$[F^X] = [G_H^1][H][F_F^1] + [F_H^1]$$

In a well-posed problem, at time Δt, the set of global generalized nodal displacements and tractions will contain exactly $(4 \times P)$ unknown components (and P unknowns for heat conduction analysis).

Then, as the final stage in the assembly process, equation (5.12) can be arranged to form

$$[A^1]\{x^N\} = [B^1]\{y^N\} + \{D^N\} + [G_H^1][H]\{D_F^N\} \tag{5.13}$$

in which

$\{x^N\}$ unknown components of $\{u^N\}$ and $\{t^N\}$

$\{y^N\}$ known components of $\{u^N\}$ and $\{t^N\}$

$[A^1,][B^1]$ associated matrices

Note, the entire matrix $[F^X]$ becomes part of $[A^1]$ since all the (generalized) displacements on the interface are unknown quantities.

5.3.5 Solution

A solution of equation (5.13) may be achieved for any time using a time marching algorithm. For the initial time $N = 1$, $\{D^1\} = \{D_F^1\} = \{0\}$ and equation (5.13) can be rewritten as

$$[A^1]\{x^1\} = [B^1]\{y^1\} \tag{5.14}$$

To obtain a solution for the unknown nodal quantities of this equation, a decomposition of matrix $[A^1]$ is required. In general, $[A^1]$ is a densely populated, unsymmetric matrix. The out-of-core solver, utilized here, was developed originally for elastostatics from the LINPACK software package (Dongarra et al, 1979) and operates on a submatrix level. Within each submatrix, Gaussian elimination with single pivoting reduces the block to upper triangular form. The final decomposed form of $[A^1]$ is stored in a direct-access file for reuse in subsequent time steps. Backsubstitution then completes the determination of $\{x^1\}$. Additional information on this solver is available in Banerjee et al (1985).

After returning from the solver routines, the entire nodal response vectors, $\{u^1\}$ and

$\{t^1\}$, at time Δt are known. For solutions at later times, a simple marching algorithm is employed. Assuming that the same set of nodal components are unknown as in (5.14) for the first time step, equation (5.13) is reformulated as

$$[A^1]\{x^2\} = [B^1]\{y^2\} + \{D^2\} + [G_H^1][H]\{D_F^2\} \tag{5.15}$$

Since the right-hand side contains only known quantities, (5.15) can be solved for $\{x^2\}$. However, the decomposed form of $[A^1]$ already exists on a direct-access file, so only the relatively inexpensive backsubstitution phase is required for the solution.

The generalization of (5.15) to any time step N is simply equation (5.13)

$$[A^1]\{x^N\} = [B^1]\{y^N\} + \{D^N\} + [G_H^1][H]\{D_F^N\} \tag{5.16}$$

in which the vectors $\{D^N\}$ and $\{D_F^N\}$ contain summations which represent the effect of past events. By systematically storing all of the matrices and nodal response vectors computed during the marching process, surprisingly little computing time is required at each new time step. In fact, for any time step beyond the first, the only major computational task is the integration needed for form $[G^N]$ and $[F^N]$. Even this process is somewhat simplified, since now the kernels are non-singular. Also, as time marches on, the effect of events that occurred during the first time step diminishes. Consequently, the terms containing $[G^N]$ and $[F^N]$ will eventually become insignificant compared to those associated with recent events. Once that point is reached, further integration is unnecessary, and a significant reduction in the computing effort per time step can be achieved.

It should be emphasized that the entire boundary element method developed, in this section, has involved surface quantities exclusively. A complete solution to the well-posed linear uncoupled quasistatic problem with composite fibers can be obtained in terms of the nodal response vectors, without the need for any volume discretization. In many practical situations, however, additional information, such as, the temperature at interior locations or the stress at points on the boundary, is required. The next section discusses the calculations of these quantities.

5.4 Interior Quantities

Once equation (5.16) is solved, at any time step, the complete set of nodal displacements and tractions are known. Subsequently, the response at points within the body can be calculated in a straightforward manner. For any point ξ in the interior, the generalized displacement can be determined from (5.6a) or (5.6b) with $C_{\beta\alpha} = \delta_{\beta\alpha}$. Now, all the nodal variables on the right-hand side are known, and, as long as ξ is not on the boundary nor on the interface between the fiber and the matrix. The kernel functions in (5.6) remain non-singular. However, when ξ is on the boundary or on the interface, the strong singularity in ${}^{ss}F_{\beta\alpha}$ prohibits accurate evaluation of the generalized displacement via (5.6), and an alternate approach is required. The apparent dilemma is easily resolved by recalling that the variation of surface quantities is completely defined by the elemental shape functions. Thus, for points on the outer boundary of the matrix, the desired relationship is simply

$$u_\alpha^N(\xi) = L_\omega(\zeta) u_{\alpha\omega}^N \tag{5.17a}$$

Where L_ω are the shape functions for the appropriate element and ζ are the intrinsic coordinates corresponding to ξ within that element. Obviously, from (5.17), neither integration nor the explicit contribution of past events are needed to evaluate generalized boundary displacements.

In many problems, additional quantities, such as heat flux and stress, are also important. The boundary integral equation for heat flux, can be written

$$\begin{aligned} q_i^N(\xi) = \sum_{n=1}^{N} \Bigg\{ & \sum_{q=1}^{Q} \left[\int_{S^q} E_{\beta\theta i}^{N+1-n}(X(\zeta) - \xi) L_\omega(\zeta) dS^q(X(\zeta)) \right] t_{\beta\omega}^n \\ & - \sum_{q=1}^{Q} \left[\int_{S^q} D_{\beta\theta i}^{N+1-n}(X(\zeta) - \xi) L_\omega(\zeta) dS^q(X(\zeta)) \right] u_{\beta\omega}^n \\ & + \sum_{p=1}^{P} \left[\int_{S^p} E_{\beta\theta i}^{N+1-n}(X(\zeta) - \xi) N_\omega(\zeta) M_\gamma(\theta) dS^p(X(\zeta)) \right] t_{\beta\omega\gamma}^n \\ & - \sum_{p=1}^{P} \left[\int_{S^p} D_{\beta\theta i}^{N+1-n}(X(\zeta) - \xi) N_\omega(\zeta) M_\gamma(\theta) dS^p(X(\zeta)) \right] u_{\beta\omega\gamma}^n \Bigg\}. \end{aligned} \tag{5.18}$$

where

$$E^n_{\beta\theta i}(X(\zeta)-\xi) = -k\frac{\partial G^n_{\beta\theta}(X(\zeta)-\xi)}{\partial \xi_i} \tag{5.19a}$$

$$D^n_{\beta\theta i}(X(\zeta)-\xi) = -k\frac{\partial F^n_{\beta\theta}(X(\zeta)-\xi)}{\partial \xi_i} \tag{5.19b}$$

A similar equation can be written for the heat flux inside a fiber. This is valid for interior points, whereas, when ξ is on the boundary, the shape functions can again be used. In this latter case,

$$L_\omega(\zeta) q^N_\omega = n_i(\xi) q^N_i(\xi) \tag{5.20a}$$

$$\frac{\partial L_\omega(\zeta)}{\partial \zeta}\theta^N_\omega = -\frac{1}{k}\frac{\partial x_i}{\partial \zeta} q^N_i(\xi) \tag{5.20b}$$

which can be solved for boundary flux. Meanwhile, interior stresses can be evaluated from

$$\begin{aligned}
\sigma^N_{ij}(\xi) = \sum_{n=1}^{N}\Bigg\{ & \sum_{q=1}^{Q}\left[\int_{S^q} E^{N+1-n}(X(\zeta)-\xi)L_\omega(\zeta)dS^q(X(\zeta))\right] t^n_{\beta\omega} \\
& - \sum_{q=1}^{Q}\left[\int_{S^q} D^{N+1-n}_{\beta ij}(x(\zeta)-\xi)L_\omega(\zeta)dS^q(X(\zeta))\right] u^n_{\beta\omega} \\
& + \sum_{p=1}^{P}\left[\int_{S^p} E^{N+1-n}_{\beta ij}(x(\zeta)-\xi)N_\omega(\zeta)M_\gamma(\theta)dS^p(x(\zeta))\right] t^n_{\beta\omega\gamma} \\
& - \sum_{p=1}^{P}\left[\int_{S^p} D^{N+1-n}_{\beta ij}(x(\zeta)-\xi)N_\omega(\zeta)M_\gamma(\theta)dS^p(x(\zeta))\right] u^n_{\beta\omega\gamma}\Bigg\}
\end{aligned} \tag{5.21}$$

in which

$$E^n_{\beta ij}(X(\zeta)-\xi) = \frac{2\mu\nu}{1-2\nu}\delta_{ij}\frac{\partial G^n_{\beta\ell}}{\partial \xi_\ell} + \mu\left(\frac{\partial G^N_{\beta i}}{\partial \xi_j} + \frac{\partial G^n_{\beta j}}{\partial \xi_i}\right) - \beta\delta_{ij}G^n_{\beta\theta} \tag{5.22a}$$

$$D^n_{\beta ij}(X(\zeta)-\xi) = \frac{2\mu\nu}{1-2\nu}\delta_{ij}\frac{\partial F^n_{\beta\ell}}{\partial \xi_\ell} + \mu\left(\frac{\partial F^N_{\beta i}}{\partial \xi_j} + \frac{\partial F^n_{\beta j}}{\partial \xi_i}\right) - \beta\delta_{ij}F^n_{\beta\theta}. \tag{5.22b}$$

A similar equation could be derived if stress measurements are required inside a fiber. Equation (5.22) is, of course, developed from (5.6). Since strong kernel singularities appear when (5.22) is written for outer boundary points, an alternate procedure is needed to determine surface stress. This alternate scheme exploits the interrelationships between generalized displacement, traction, and stress and is the straightforward extension of the

technique typically used in elastostatic implementation (Dargush and Banerjee, 1990). Specifically, the following can be obtained

$$n_j(\xi)\sigma_{ij}^N = L_\omega(\zeta)t_{i\omega}^N \tag{5.23a}$$

$$\sigma_{ij}^N(\xi) - \frac{D_{ijkl}^e}{2}\left(u_{k,l}^N(\xi) + u_{l,k}^N(\xi)\right) = -\beta\delta_{ij}L_\omega(\zeta)u_{\theta\omega}^N \tag{5.23b}$$

$$\frac{\partial x_j}{\partial\zeta}u_{i,j}^N(\xi) = \frac{\partial L_\omega(\zeta)}{\partial\zeta}u_{i\omega}^N \tag{5.23c}$$

in which $u_{\theta\omega}^N$ is obviously the nodal temperatures, and,

$$D_{ijkl}^e = \lambda\delta_{ij}\delta_{kl} + 2\mu\delta_{ik}\delta_{jl}.$$

Equations (5.23) form an independent set that can be resolved numerically for $\sigma_{ij}^N(\xi)$ and $u_{i,j}^N(\xi)$ completely in terms of known nodal quantities $u_{\alpha\omega}^N$ and $t_{\alpha\omega}^N$, without the need for kernel integration nor convolution. Notice, however, that shape function derivatives appear in (5.23c), thus constraining the representation of stress on the surface element to something less than full quadratic variation. The interior stress kernel functions, defined by (5.22) are also detailed in Appendix B.

6. NONLINEAR MATERIAL FORMULATION

6.1 Introduction

Due to the material discontinuity in a composite structure, large localized stress gradients develop on the fiber-matrix interface when a specimen is loaded. These large stress gradients induce plastic yielding in a composite about the fibers. It is therefore, important to include these material nonlinearities in an analysis of a composite structure loaded beyond its elastic limit. As a first step in this analysis, a formulation to account for the plastic yielding of the composite matrix is developed. The nonlinear effects are included in the boundary element formulation through a volume integral.

In this chapter, new methods are developed for the efficient evaluation of the volume integrals which appear in the integral formulations. An elastoplastic-fracture constitutive law is used to model the nonlinear behavior of ceramic composite material, and an iterative control algorithm is implemented for the solution of the nonlinear system.

6.2 Integral Equation Formulation for Elastoplasticity

The governing equation of plasticity can be written in the following form [Banerjee and Butterfield, 1981]:

$$(\lambda + \mu)\dot{u}_{j,ij} + \mu\dot{u}_{i,jj} = \dot{\sigma}^c_{ij,j} \tag{6.1}$$

$$i, j = 1, 2, 3$$

where λ and μ are Lamé constants, $\dot{u}_i$ is displacement rate and $\dot{\sigma}^c_{ii}$ is an initial stress rate (or a corrective stress rate) resulting from the nonlinearities present in the plastic domain. For the purpose of the plasticity algorithm the initial stress rate is defined as

$$\dot{\sigma}^c_{ij} = D^e_{ijkl}\dot{\epsilon}_{kl} - D^{ep}_{ijkl}\dot{\epsilon}_{kl}$$

where D^e_{ijkl} and D^{ep}_{ijkl} is the elastic and elastoplastic constitutive tensors, respectively, and $\dot{\epsilon}_{kl}$ is the strain rate.

The boundary integral equation for the displacement at a point ξ in the matrix can be expressed as

$$C_{ij}(\xi)\dot{u}_i(\xi) = \int_S [G^M_{ij}(x,\xi)\dot{t}^O_i(x) - F^M_{ij}(x,\xi)\dot{u}^O_i(x)]dS(x) + \int_V B^M_{ikj}(z,\xi)\dot{\sigma}^C_{ik}(z)dV(z)$$
$$+ \sum_{n=1}^{N} \int_{S^n} [G^M_{ij}(x,\xi)\dot{t}^H_i(x) - F^M_{ij}(x,\xi)\dot{u}^H_i(x)]dS^n(x) \tag{6.2}$$

where

G^M_{ij}, F^M_{ij}, and B^M_{ijk} are the fundamental solutions of a ceramic matrix of infinite extent,

C_{ij} are constants determined by the geometry at ξ,

$\dot{u}_i, \dot{t}_i$ are the displacement and traction rates,

S, S^n are the surfaces of the outer boundary and the nth hole (encompassing the fiber), respectively and

N is the number of individual fibers.

Superscript O and H identify the quantities of the outer surface of the matrix and the quantities on the surface of the hole, respectively.

A similar equation can be written for the displacement rate of a point ξ in the nth fiber as

$$C^F_{ij}\dot{u}_i(\xi) = \int_{S^n} [G^F_{ij}(x,\xi)\dot{t}^F_i(x) - F^F_{ij}(x,\xi)\dot{u}^F_i(x)]dS^n(x) \tag{6.3}$$

where

G^F_{ij}, F^F_{ij} are the fundamental solutions of the nth fiber,

C^F_{ij} are constants determined by the geometry at ξ,

$\dot{u}^F_i, \dot{t}^F_i$ are displacement and traction rates associated with the nth fiber

S^n the surface of the nth fiber

Note, each fiber may have different material properties.

For a perfectly bonded fiber-matrix interface the displacement rates of the matrix and the fiber are equal and the traction rates are equal and opposite:

$$\dot{u}^H_i(x) = \dot{u}^F_i(x) \tag{6.4a}$$

$$\dot{t}^H_i(x) = -\dot{t}^F_i(x) \tag{6.4b}$$

As in the derivation of the integral equation for elastostatic fiber composite analysis of Chapter 2, the Poisson's ratio of the fiber and the Poisson's ratio of the matrix is assumed to be equal. This leads to the following relation:

$$F_{ij}^{F}(x,\xi) = -F_{ij}^{H}(x,\xi) \tag{6.5}$$

Finally, using relations (6.4) and (6.5), equation (6.3) can be backsubstituted in equations (6.2) to yield the integral equation for the displacement rate at a point ξ in a fiber composite structure in which material nonlinearities are present in the matrix:

$$\begin{aligned}\bar{C}_{ij}(\xi) = &\int_S [G_{ij}^{M}(x,\xi)\dot{t}_i^{O}(x) - F_{ij}^{M}(x,\xi)\dot{u}_i^{O}(x)]dS(x) + \int_V B_{ikj}^{M}(z,\xi)\dot{\sigma}_{ik}^{C}(z)dV(z) \\ &+ \sum_{n=1}^{N}\int_{S^n} \bar{G}_{ij}(x,\xi)\dot{t}_i^{H}(x)dS^n(x)\end{aligned} \tag{6.6}$$

where

$$\bar{G}_{ij}(x,\xi) = G_{ij}^{H}(x,\xi) - G_{ij}^{F}(x,\xi)$$

$\bar{C}_{ij}(\xi)$ are constants dependent on the geometry for a point ξ on the outer boundary, and

$\bar{C}_{ij}(\xi) = \delta_{ij}$ for a point ξ in the interior of the composite.

6.3 Cylinder Volume Cells

The volume integral in equation (6.6) is evaluated assuming a variation based on a 30 node shape function over a cylindrical volume cell (Figure 6.1). The initial stress rates have a variation through the volume cell which are quadratic in the longitudinal direction, linear in the radial direction, and trigometric in the circumferential direction. The variation in the circumferential direction is based on a 5-noded circular shape function shown in Figure 6.2. It is similar to the 3-noded circular shape function used for the displacement and traction rates on the fiber/hole, however, in addition to the constant, *sine* and *cosine* terms, the 5-noded function contains $\sin 2\theta$ and $\cos 2\theta$ terms. Hence, the shape function can model

initial stress rates which have two peak values in the circumferential direction. In two-dimensional numerical experimentation, this was observed as a minimum requirement for reasonable approximation of the actual initial stress rate variation.

The integration is carried out analytically about the circumference of the volume cell to keep numerical costs down. However, due to the complexity of the resulting integrand, numerical integration was employed in the radial and longitudinal directions.

6.4 Interior Stress Rate Equations

The solution algorithm in a plasticity analysis requires the determination of stress (and strain) rates at nodes of the volume cell. The integral equation for stress (and strain) rates in the composite matrix are derived from the displacement rate integral equations (6.2) through the application of the strain-displacement equation and the nonlinear stress-strain relations, i.e.,

$$\sigma_{ij} = D^e_{ijkl}\epsilon_{kl} - \sigma^C_{ij} \tag{6.7}$$

Nonlinear effects are incorporated in the stress rate integral equation via a volume integral. This volume integral is strongly singular, however, and special considerations must be given to this integral as described in Henry and Banerjee (1987).

The integral equation for stress rates, however, are strongly singular for a point on the fiber-matrix interface. In this instance the stress rates are best determined using a boundary stress calculation similar to equation (2.13). However, in a nonlinear analysis the nonlinear stress-strain rate constitutive relationship involving initial stress rates [Henry, 1987] must be used. The calculation is very efficient because the calculation does not require surface nor volume integration.

6.5 Plasticity-Fracture Constitutive Model for Ceramic Composites

An elastic-plastic strain hardening-fracture model (Chen, 1975) is used to model the inelastic behavior of the ceramic material. The yield function describing the inelastic behavior is bounded by two surfaces: the elastic limit or initial discontinuous surface; and

a failure surface. When the stress level violates the elastic limit, plastic yielding occurs with strain hardening. At this point unloading would behave linear-elastically, however, permanent deformation will have occurred. A new elastic limit surface, uniquely defined by the invariants p and J_2 (described below), corresponds to the highest stress state achieved in prior loading history. Loading can continue until the failure surface is reached. At this time the material will fracture and the stress will be reduced to zero at this point.

An important feature that this model exhibits to accurately represent ceramic material behavior is its ability to sustain stress in compression many times greater than in tension. Further, this phenomenon is magnified during plastic hardening since both the isotropic and kinematic hardening rules are employed. The strain-hardening model is illustrated in Figures 6.3 and 6.4.

The loading function shown in Figure 6.4 has the following form:

in the compression domain:

$$f(\sigma_{ij}) = \frac{J_2 + \frac{1}{3}Ap}{1 - \frac{1}{3}Bp} = \tau^2 \tag{6.8a}$$

in the tension and tension-compression domains:

$$f(\sigma_{ij}) = \frac{J_2 - \frac{1}{6}p^2 + \frac{1}{3}Ap}{1 - \frac{1}{3}Bp} = \tau^2 \tag{6.8b}$$

where

$p = (\sigma_x + \sigma_y + \sigma_z)/3$,

$J_2 = \frac{1}{6}\left[(\sigma_x - \sigma_y)^2 + (\sigma_y - \sigma_z)^2 + (\sigma_z - \sigma_x)^2\right] + \sigma_{xy}^2 + \sigma_{xz}^2 + \sigma_{yz}^2$,

$A = \frac{A_0\tau_u^2 - A_u\tau_a^2}{\tau_u^2 - \tau_0^2}$,

$B = \frac{A_u - A_0}{\tau_u^2 - \tau_0^2}$,

τ is a function of hardening, and

A_0, τ_0, A_u, τ_u are material constants which can be obtained from uniaxial and biaxial tests.

By employing the normality condition the final form of the constitutive equation relating the stress increment to the strain increment can be derived.

$$\dot{\sigma}_{kl} = \left[D^e_{klij} - P D^e_{klmn} \frac{\partial f}{\partial \sigma_{mn}} \frac{\partial f}{\partial \sigma_{qr}} D^e_{qrij} \right] \dot{\epsilon}_{ij} \tag{6.9}$$

where

$\frac{1}{P} = 2\sigma_e H' \left(\frac{\partial f}{\partial \sigma_{pq}} \frac{\partial f}{\partial \sigma_{pq}} \right)^{\frac{1}{2}} + \frac{\partial f}{\partial \sigma_{rs}} D^e_{rsvw} \frac{\partial f}{\partial \sigma_{vw}}$

D^e_{klij} is the elastic constitutive matrix relation

H' is the current slope of the equivalent stress-equivalent plastic strain hardening curve, and

$\sigma_e = \sqrt{f}$ is the definition of equivalent stress

6.6 Assembly of Equations

The discretization and integration of the integral equations for displacement and stress rates follows the procedure outlined in Chapter 2. After the integration of the kernel functions, the next critical step in the formulation is the assembly of the system equations. Here, efficiency is of utmost importance. The approach to writing an efficient algorithm is to keep the number of system equations to a minimum by eliminating all unnecessary unknowns from the system. The strategy is to retain in the system only traction variables on the fiber-matrix interface. This is in contrast to a general multi-region problem where both displacement and tractions are retained on an interface. The elimination of the displacement on the interface is achieved through a backsubstitution of the fiber equations in the system equations which are made up exclusively from equations written for the composite matrix (on the outer surface and on the surface of the holes). The procedure is described below.

Equation (6.6) is used to generate a system of equations for nodes on the outer surface of the composite matrix and for nodes on the surface of the holes containing the fibers. Written in matrix form we have

$$\text{On the Matrix Outer Surface:} \qquad \mathbf{G^M \dot{t}^O - F^M \dot{u}^O + \bar{G} \dot{t}^H + B^M \dot{\sigma}^C = 0} \tag{6.10a}$$

On the Matrix Hole Surface: $\mathbf{G^M \dot{t}^O - F^M \dot{u}^O + \bar{G} \dot{t}^H + B^M \dot{\sigma}^C = I \dot{u}^H}$ (6.10*b*)

where

$\mathbf{t^O}$ and $\mathbf{u^O}$ are traction and displacement rates

$\mathbf{\dot{t}^H}$ and $\mathbf{\dot{u}^H}$ are traction and displacement rates

$\boldsymbol{\sigma^C}$ is the initial stress rate vector

$\mathbf{I}$ is the identity matrix

$\mathbf{G^M}$ and $\mathbf{F^M}$ matrices contain coefficients from the integration over the outer boundary.

$\mathbf{\bar{G}}$ matrix contains coefficients integrated about the fiber/hole

$\mathbf{B^M}$ matrix contains coefficients from the integration over the volume cells

Our goal is to eliminate $\mathbf{\dot{u}^H}$ from the system. To this end, equation (6.3) is written for every node on a fiber, collocating slightly outside the boundary of the fiber [at a distance of (1.25)*(fiber radius)] where $C_{ij}^F(\xi) = 0$.

$$\mathbf{F^{F2} u^F = G^{F2} t^F}$$

Superscript **F2** identifies the equations written at points located slightly outside the boundary of the fibers.

Noting $\mathbf{\dot{u}^H = \dot{u}^F}$ and $\mathbf{\dot{t}^H = -\dot{t}^F}$ we have

$$\mathbf{F^{F2} \dot{u}^H = -G^{F2} \dot{t}^H} \tag{6.11}$$

Post multiplying equation (6.10b) by the $\mathbf{F^{F2}}$ matrix in equation (6.12) yields

$$\mathbf{F^{F2} G^M \dot{t}^O - F^{F2} F^M \dot{u}^O + F^{F2} \bar{G} \dot{t}^H + F^{F2} B^M \dot{\sigma}^C = F^{F2} \dot{u}^H} \tag{6.12}$$

Equation (6.11) can now be set equal to equation (6.12) and the final form of the system is derived.

On Outer Surface: $\mathbf{G^M \dot{t}^O - F^M \dot{u}^O + \bar{G} \dot{t}^H + B^M \dot{\sigma}^C = 0}$

On Hole: $\mathbf{F^{F2} G^M \dot{t}^O - F^{F2} F^M \dot{u}^O + (F^{F2} \bar{G} + G^{F2}) \dot{t}^H + F^{F2} B^M \dot{\sigma}^C = 0}$ (6.13)

At every point on the outer surface, either the traction or the displacement rate is specified and on the surface of the hole only the traction rates are retained. Therefore, the number of displacement rate equations in the system are equal to the final number of boundary unknowns. The initial stress rate vector, however, is unknown and must be determined by a quasistatic, iterative solution algorithm. This requires the use of stress rate equations and a constitutive law. The stress rate equation can be written in matrix form as

$$\dot{\sigma} = \mathbf{G}^{\sigma}\dot{\mathbf{t}}^{\mathbf{O}} - \mathbf{F}^{\sigma}\dot{\mathbf{u}}^{\mathbf{O}} + \mathbf{G}^{\sigma}\dot{\mathbf{t}}^{\mathbf{H}} - \mathbf{F}^{\sigma}\dot{\mathbf{u}}^{\mathbf{H}} + \mathbf{B}^{\sigma}\dot{\sigma}^{\mathbf{C}} \tag{6.14}$$

Note, the displacement rate vector $\mathbf{u}^{\mathbf{H}}$ for the hole is known from equation (6.10b) and could be eliminated from equation (6.14). For numerical efficiency, however, a two step procedure is used in which $\mathbf{u}^{\mathbf{H}}$ is first determined using equation (6.10b) and then substituted in equation (6.14). Nevertheless, for illustration purposes, a backsubstitution of equation (6.10b) into equation (6.14) will be implied. Hence, the displacement rate and stress rate equations (6.13) and (6.14) are assembled by collecting the known and unknown values of traction and displacement rates and their coefficients together. The final system equations can be cast as:

$$\mathbf{A}^{\mathbf{b}}\dot{\mathbf{x}} = \mathbf{B}^{\mathbf{b}}\dot{\mathbf{y}} + \mathbf{C}^{\mathbf{b}}\dot{\sigma}^{\mathbf{C}} \tag{6.15a}$$

$$\dot{\sigma} = \mathbf{A}^{\sigma}\dot{\mathbf{x}} + \mathbf{B}^{\sigma}\dot{\mathbf{y}} + \mathbf{C}^{\sigma}\dot{\sigma}^{\mathbf{C}} \tag{6.15b}$$

where $\dot{\mathbf{x}}$ is the vector of unknown variables at boundary and interface nodes; $\dot{\mathbf{y}}$ is the vector of known variables; $\dot{\sigma}^{\mathbf{c}}$ is the vector of initial stress rates; $\mathbf{A}^{\mathbf{b}}, \mathbf{B}^{\mathbf{b}}, \mathbf{C}^{\mathbf{b}}$ are the coefficient matrices of the boundary (displacement rate) system equations (6.13); and $\mathbf{A}^{\sigma}, \mathbf{B}^{\sigma}, \mathbf{c}^{\sigma}$ are the coefficient matrices of the stress rate equation (6.14). It should be noted that $\mathbf{A}^{\mathbf{b}}$ is a square matrix. Furthermore, in a substructured system the matrices $\mathbf{A}^{\mathbf{b}}$ and $\mathbf{B}^{\mathbf{b}}$ are block banded while matrices $\mathbf{C}^{\mathbf{b}}, \mathbf{A}^{\sigma}, \mathbf{B}^{\sigma}$, and $\mathbf{C}^{\sigma}$ are block diagonal.

6.7 Nonlinear Iterative Solution Algorithm

The algorithm described below provides the solution of the system equations given by (6.15). This requires complete knowledge of the initial stress rate distribution $\dot{\sigma}^{\mathbf{C}}$ within the yielded region that is induced by the imposition of the boundary loading. Unfortunately the nonlinear initial stress rates are not known a priori for a particular load increment and therefore an iterative process must be employed within each loading stage.

An important feature incorporated in the iterative algorithm of the present work is an acceleration scheme based on the initial stress rates generated by the past history. In this procedure, the path followed by the previous load increment is used to extrapolate the initial stress rates at the beginning of the current increment before the start of the iterative operations. This results in substantial reduction in computer time. This procedure is graphically illustrated in Figure 6.5 for a simple tension problem with a variable hardening parameter. The initial loading from point A generates initial stress rates which are distributed during the iterations to arrive at the solution at B. Upon loading from state B the extrapolated path BC is followed. At C the resulting initial stress rates are distributed to reach state D.

The steps of the incremental plasticity algorithm is described below:

1. Obtain the elastic solution $\dot{\mathbf{x}}$ for an arbitrary increment of boundary loading $\dot{\mathbf{y}}$ from

$$\mathbf{A}^{\mathbf{b}}\dot{\mathbf{x}} = \mathbf{B}^{\mathbf{b}}\dot{\mathbf{y}} \tag{6.16a}$$

   and determine the stress rates at the nodes of the volume cells from

$$\dot{\sigma} = \mathbf{A}^{\sigma}\dot{\mathbf{x}} + \mathbf{B}^{\sigma}\dot{\mathbf{y}} \tag{6.16b}$$

2. Scale the elastic solution such that the node with the highest stress rate is at yield. In the case of nonproportional loading, this onset of yielding cannot be reached by scaling. Instead, incremental loads must be applied until yielding is reached.
3. Impose a small load increment $\dot{\mathbf{y}}$, (usually less than 5% of the yield load) plus the estimated value of the initial stress rates accumulated from the previous load step and

evaluate $\dot{\mathbf{x}}$ and $\boldsymbol{\sigma}$ using

$$\mathbf{A}^{\mathbf{b}}\dot{\mathbf{x}} = [\mathbf{B}^{\mathbf{b}}\dot{\mathbf{y}} + \mathbf{C}^{\mathbf{b}}\dot{\sigma}^{\mathbf{C}}] \tag{6.17a}$$

$$\dot{\sigma} = \mathbf{A}^{\sigma}\dot{\mathbf{x}} + \mathbf{B}^{\sigma}\dot{\mathbf{y}} + \mathbf{C}^{\sigma}\dot{\sigma}^{\mathbf{C}} \tag{6.17b}$$

where $\dot{\boldsymbol{\sigma}}^{\mathbf{c}}$ is the estimated initial stress rates. If no prior plastic history exists the value of the estimated initial stress rates are zero.

4. Accumulate all incremental quantities of stress, traction, and displacement rates and use Eq. (6.7) to calculate the strain for this increment.
5. Evaluate the current constitutive matrix using the new stress rate history and calculate the current initial stress rates via

$$\dot{\sigma}_{ij}^{C} = (D_{ijkl}^{e} - D_{ijkl}^{ep})\dot{\epsilon}_{kl} \tag{6.18}$$

Accumulate the initial stress rate history of this load increment for use as the estimated initial stress rate of the next load increment in step 3.

6. If the current increment of initial stress rates computed in Eq. (6.18) is greater than a prescribed tolerance (normally 0.005 times the yield stress) then calculate the incremental quantities ($\dot{\mathbf{x}}$ and $\dot{\sigma}$) due to these rates using

$$\mathbf{A}^{\mathbf{b}}\dot{\mathbf{x}} = \mathbf{C}^{\mathbf{b}}\dot{\sigma}^{\mathbf{c}} \quad \text{and} \quad \dot{\sigma} = \mathbf{A}^{\sigma}\dot{\mathbf{x}} + \mathbf{C}^{\sigma}\dot{\sigma}^{\mathbf{c}}$$

and return to step 4 for the next iteration. If the value is less than the prescribed tolerance, go to step 7. Note the boundary loading is zero for this calculation. If the number of iterations is greater than a specified limit (usually 50) the system is assumed to have reached the state of failure.

7. Return to step 3 and apply the next load increment and the accumulated initial stress rates from this load step. (If the size of the load increment changes the estimated initial stress rates should be scaled proportionally.)

Any residual initial stress at the end of the iteration is carried forward and applied to the system with the next load increment.

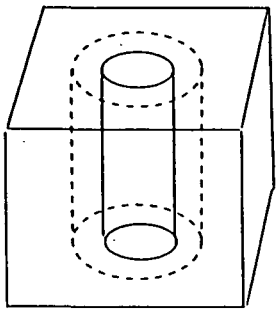

$$C_{ij}(\xi)\dot{u}_i(\xi) = \int_S [G^M_{ij}(x,\xi)\dot{t}^O_i(x) - F^M_{ij}(x,\xi)\dot{u}^O_i(x)]dS(x) + \int_V B^M_{ikj}(z,\xi)\dot{\sigma}^C_{ik}(z)dV(z)$$
$$+ \sum_{n=1}^{N} \int_{S^n} [G^M_{ij}(x,\xi)\dot{t}^H_i(x) - F^M_{ij}(x,\xi)\dot{u}^H_i(x)]dS^n(x)$$

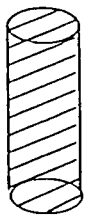

$$C^F_{ij}\dot{u}_i(\xi) = \int_{S^n} [G^F_{ij}(x,\xi)\dot{t}^F_i(x) - F^F_{ij}(x,\xi)\dot{u}^F_i(x)]dS^n(x)$$

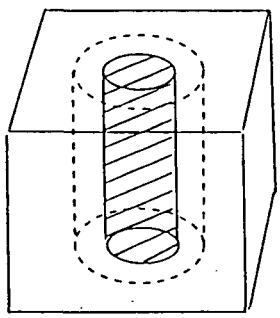

$$\tilde{C}_{ij}(\xi) = \int_S [G^M_{ij}(x,\xi)\dot{t}^O_i(x) - F^M_{ij}(x,\xi)\dot{u}^O_i(x)]dS(x) + \int_V B^M_{ikj}(z,\xi)\dot{\sigma}^C_{ik}(z)dV(z)$$
$$+ \sum_{n=1}^{N} \int_{S^n} \tilde{G}_{ij}(x,\xi)\dot{t}^H_i(x)dS^n(x)$$

where

$$\tilde{G}_{ij}(x,\xi) = G^H_{ij}(x,\xi) - G^F_{ij}(x,\xi)$$

$$i,j = 1,2,3$$

Fig. 6.1 Integral Equation Formulation for the Nonlinear Analysis of Fiber Composite Materials. A 30-Node Cylindrical Volume Cell is Generated Automatically.

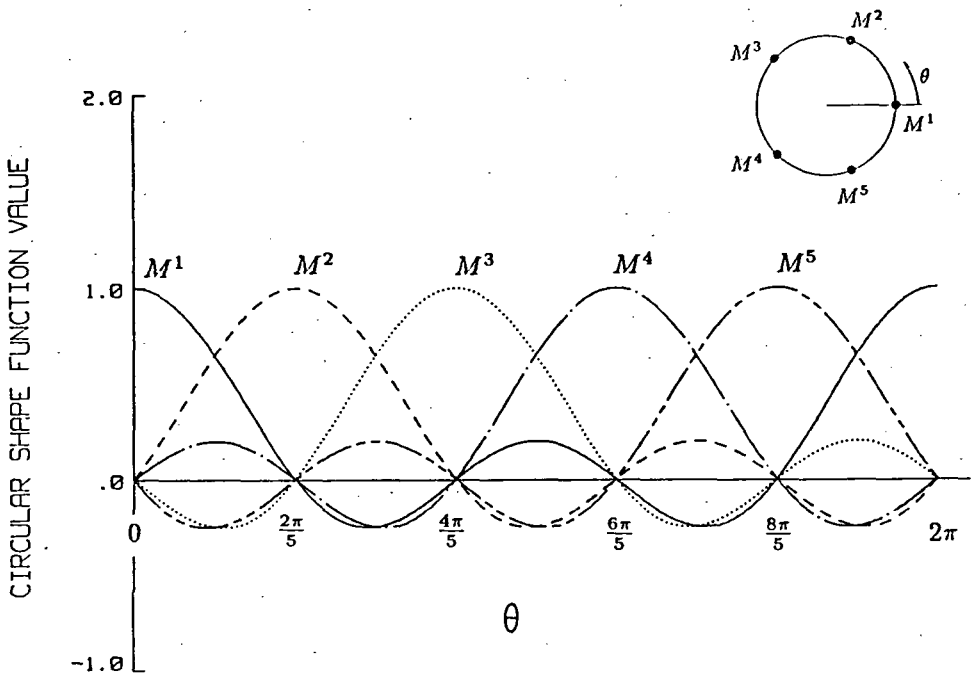

Fig. 6.2 Value of the 5-Noded Circular Shape Function about the Circumference of the Cylindrical Volume Cell

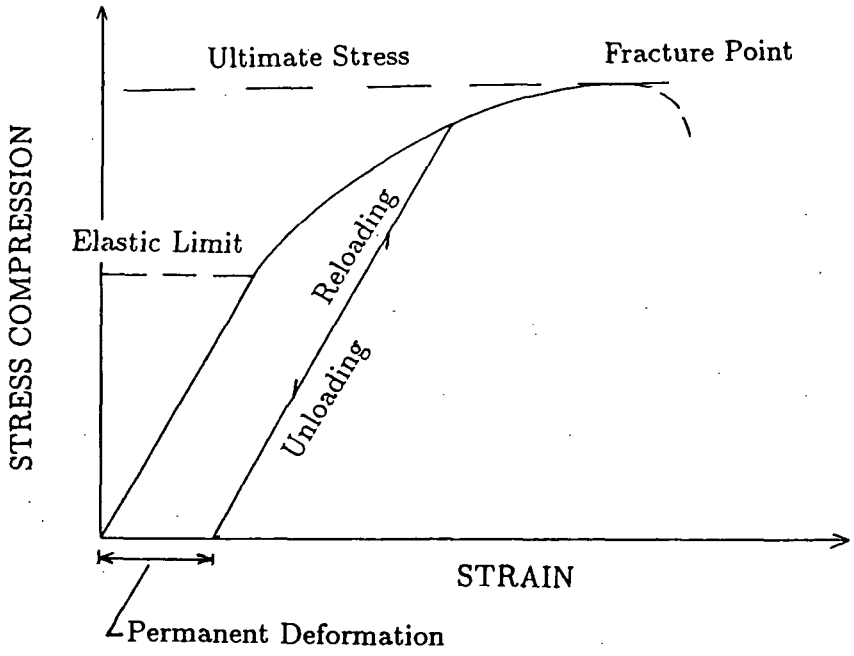

Fig. 6.3 Typical Stress-Strain Curve in Equivalent Stress-Strain Space

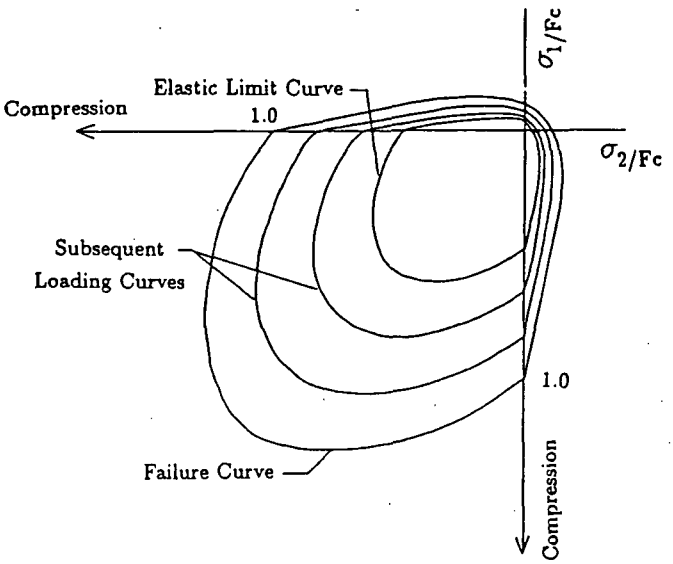

Fig. 6.4 Loading Function in Biaxial Principal Stress Space

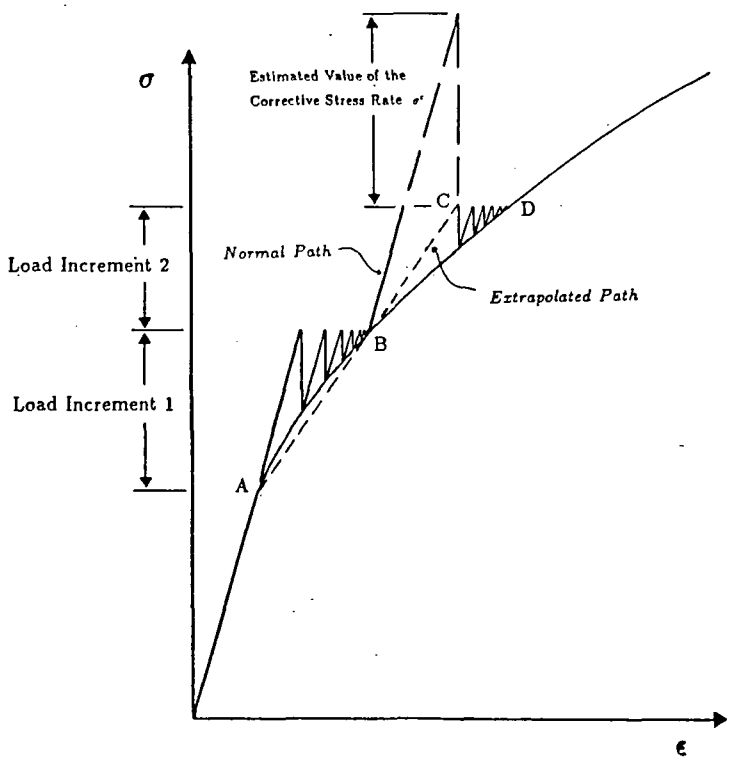

Fig. 6.5 Accelerated Iterative Plasticity Algorithm

7. COMPUTER PROGRAM DEVELOPMENT

7.1 Introduction

The goal of the 'BEST-CMS' computer program developed for ceramic composites is the accurate and efficient implementation of the formulation described in Chapters 2-6. Of equal importance is the degree of generality required in the definition of component geometry, loading and material properties. This is necessary if the program is to be applicable to real problems in the aerospace industry.

For this reason the ceramic composite formulation has been implemented in the three-dimensional boundary element computer code 'BEST3D' (Boundary Element Stress Technology - Three-dimensional) which was developed for NASA by Pratt and Whitney and SUNY/Buffalo under contract NAS 3-23697. Since its development, BEST3D has been proven to be a highly accurate and numerically efficient boundary element program.

The development of the computer program 'BEST-CMS' is discussed in the following sections.

7.2 Program Structure

BEST-CMS is designed to be a fully general ceramic composite analysis system employing the boundary element method. The program is written using standard FORTRAN 77. Development has been carried out at SUNY/Buffalo on an HP 9000 minicomputer, a SUN-4 workstation, and a SUN Sparcstation-1. The nature of the method is such that, for any realistic problem, not all required data can reside simultaneously in core. For this reason extensive use is made of both sequential and direct access scratch files.

The program first executes an input segment. After the input has been processed, the surface integrals are calculated and assembled into the set of system equations using specified boundary conditions, followed by the fiber assembly and the inclusion of the fiber equations in the general system. The system matrix is then decomposed and saved on disk, followed by the calculation of the solution vector. The full displacement and traction

(and/or temperature and flux) solution on each boundary element and fiber element is then reconstructed from the solution vector. In a time dependent problem the process of constructing the load vector for the system equations is repeated at each time step, but the integration, formation and decomposition of the system matrix are done only once. However, in an analysis with nonlinear fiber-matrix interface connections, the assembly and decomposition must be carried out several times.

The current program limits are as follows:

- 20 time points (solutions for different loadings)
- 15 generic modeling regions (GMR)
- 600 elements (300 elements per GMR) including fiber elements
- 100 fiber elements per generic modeling region
- 500 fiber elements per problem
- 2500 modeling nodes
- 1200 source points (600 source points per GMR)

Various aspects of the computer program are discussed below.

7.3 Program Input

The input for BEST-CMS is free field. Meaningful keywords are used to identify data types and to name particular data sets. The input is divided into five types:

1. Case Control Cards

The case control cards define global characteristics of the problem. In addition to the problem title, the times for multiple time steps are defined. The reading or writing of restart data is also defined at this point. **The restart facility allows one to change the arrangements to fibers without recalculating the various coefficients.**

2. Material Property Definition

The material property input allows the definition of material properties for a variety of materials. The Young's modulus can be prescribed in tabular form for a user-defined set of temperatures. Temperature independent values of Poisson's ratio are also defined.

3. Geometry Input

Geometry input is defined one GMR (generic modeling region, or subregion) at a time. To initiate the input, a tag is provided to identify the GMR, a material name and reference temperature are defined to allow initialization of material properties.

The next block of geometry input consists of the Cartesian coordinates of the user input points for the outer surface geometry definition of the composite matrix, together with identifiers (normally positive integers) for these geometric nodes.

Following the definition of an initial set of nodal points, the surface connectivity of the outer surface of the composite matrix is defined through the input of one or more named surfaces. Each surface is made up of a number of elements, with each element defined in terms of several geometric nodes. Three sided elements, defined using six rather than eight geometric nodes, are used for mesh transition purposes. The terms quadrilateral and triangle are normally used to refer to the eight and six noded elements, although the real geometry represented is, in general, a nonplanar surface patch. Nine noded elements are made available by adding a central node to the eight noded elements.

Over each element the variation of displacement and traction (and/or temperature and flux) can be defined using either the linear, quadratic or quartic shape functions. Linear and quadratic elements can share a common side, which is then constrained to have linear displacement and traction (and/or temperature and flux) variation. Quadradic/quartic mixtures assumes a quadratic variation, and linear/quartic mixtures assumes a linear variation.

Finally an option is available to allow quadratic and quartic functional variation to be used in conjunction with linear geometry (4 or 3 nodes). In this case the program generates

the additional nodes automatically at mid-point of the sides. The characteristics of the various element types are summarized below.

Surface Element Type	Geometry Nodes	Displacement/Traction Nodes (and/or Temperature/Flux Nodes)
Linear Quadrilateral	3, 8 or 9	4
Linear Triangle	4, 6 or 7	3
Quadratic Quadrilateral	4, 8 or 9	8 or 9
Quadratic Triangle	3 or 6	6
Quartic Triangle	3, 8 or 9	13 or 15
Quartic Quadrilateral	3 or 6	17 or 25

Following the definition for the composite matrix outer surface, the embedded fibers are then defined. These are defined as curvilinear line elements with a prescribed radius of the cross-section. The fibers are generally straight, however as noted, curved fibers are also allowed. The user first defines the nodal coordinates of the centerline of the fiber. Thereafter, the radius and the fiber connectivity is defined. Linear and quadratic elements are available for both geometry and functional variation, however, quadratic functional variation over linear geometry is not presently available. The various options for the fiber elements are summarized below.

Fiber Element Type	Geometry Nodes	Displacement/Traction Nodes (and/or Temperature/Flux Nodes)
Linear-Linear	2	2
Quadratic-Linear	3	2
Quadratic-Quadratic	3	3

Note only the surface of the fiber needs to be defined, i.e., the hole in the composite matrix which encompasses the fiber does not have to be explicitly defined.

4. Interface Conditions

The interface input describes the connection of surfaces or elements of one region to another and between the matrix and the fibers. Special types of fiber-matrix interface conditions which are available presently include fully-bonded and sliding contact (including coulomb friction) and springs.

5. Boundary Condition Input

The final input section provides for the definition of boundary conditions, as functions of both position and time. Data can be input for an entire surface, or for a subset (elements or nodes) of a surface. Input can be in global coordinates, or can define rollers or pressure (or flux) in the local coordinate system. Input simplifications are available for the frequently occurring cases of boundary data which is constant with respect to space and/or time variation. Each boundary condition set can be defined at a different set of times.

7.4 Surface Integral Calculation

Following the processing of the input data, the surface integrals are evaluated numerically. This is the most time consuming portion of the analyses. In BEST-CMS the results of these integrations are stored as they are calculated, rather than being assembled into the final equation system immediately. Although this is somewhat more costly in terms of storage and CPU (central processing unit) time, it has led to much greater clarity in the writing of BEST-CMS. In addition, it provides much greater flexibility in the implementation of various restart and boundary condition options.

The calculations proceed first by GMR (generic modeling region), then by source point (the equation being constructed) and finally by surface element and fiber element. The results for each source point element pair are written to disk. All of the calculations are carried out and stored in the global (Cartesian) coordinate system.

The integration of the BEM equations is the most complex part of the code. In this process either singular or nonsingular integrals can be encountered. The integrals are singular if the source point for the equations being constructed lies on the element being integrated. Otherwise, the integrals are nonsingular, although numerical evaluation is still difficult if the source point and the element being integrated are close together.

In both the singular and nonsingular cases Gaussian integration is used. The basic technique is developed in Banerjee and Butterfield, 1981. In the nonsingular case an

approximate error estimate for the integral was developed based on the work of Stroud and Secrest (1966). This allows the determination of element subdivisions and orders of Gaussian integration which will retain a consistent level of error throughout the structure. Numerical tests have shown that the use of 3, 4 and 5 point Gauss rules provide the best combination of accuracy and efficiency. In the present code the 4 point rule is used for nonsingular integration, and error is controlled through element subdivision. The origin of the element subdivision is taken to be the closest point to the source point on the element being integrated.

If the source point is very close to the element being integrated, the use of a uniform subdivision of the element can lead to excessive computing time. This frequently happens in the case of aerospace structures, due either to mesh transitions or to the analysis of thin walled structures. In order to improve efficiency, while retaining accuracy, a graded element subdivision was employed. Based on one-dimensional tests, it was found that the subelement divisions could be allowed to grow geometrically away from the origin of the element subdivision. Numerical tests on a complex three-dimensional problem have shown that a mesh expansion factor as high as 4.0 can be employed without significant degradation of accuracy.

In each case of singular integration (source point on the elements being integrated) the element is first divided into subelements. The integration over each subelement is carried out using a Jacobian transformation in mapping. This coordinate transformation produces nonsingular behavior in all except one of the required integrals. Normal Gauss rules can then be employed. The remaining integral (that of the traction kernel F_{ij} times the isoparametric shape function which is 1.0 at the source point) is still singular, and cannot be numerically evaluated with reasonable efficiency and accuracy. Its calculation is carried out indirectly, using the fact that the stresses due to a rigid body translation are zero (Lachat and Watson, 1976). It has been found that subdivision in the circumferential direction of a two-dimensional surface element is required to preserve accuracy in the

singular integration of the outer surface. A maximum included angle of 15 degrees is used. Subdivision in the radial direction has not been required.

The integrals required for calculation of displacement, stress, temperature, and flux at interior points are of the same type as those involved in the generation of the system equations, except that only nonsingular integrals are involved. If the source point involved is located on the surface of the body, then numerical integration is not required. Instead, the required quantities are calculated using the displacements and tractions (or temperature and flux) on the element (or elements) containing the source point, as discussed in Section 2.5.

7.5 System Matrix Assembly

The first step in the assembly process is the reduction of the rectangular matrix of **F** integrals to a square matrix. This matrix is the prototype of the system matrix. The columns of the matrix are transformed or replaced, as required by the boundary conditions, as the assembly process proceeds.

The next step in the process is the incorporation of the fiber equations in the system. As was described in detail for each specific analysis in Chapters 2-6, the fiber assembly consists of a fiber by fiber matrix multiplication and backsubstitution. The backsubstitution minimizes the number of equations required in the system by eliminating some of the unknown quantities on the fibers.

A key problem in the entire process is the proper definition of appropriate coordinate systems, on a nodal basis. This is a problem common in any direct boundary element method which treats structures with nonsmooth surfaces. It arises because the tractions at a point are not uniquely determined unless the normal direction to the surface varies continuously at the point in question.

The original surface integral calculations are all done in global coordinates. If the displacement (or temperature) boundary condition is specified at a given node, in global coordinates, then no new coordinate system definition is required. It is only necessary to

keep track of the subset of elements, containing the given node, on which the fixed displacement (or temperature) is to be reacted. However, if a displacement (or temperature) is specified in a nonglobal direction at a given node, then a new nodal coordinate system must be defined and, potentially, updated as further boundary conditions are processed. The associated nonzero reactions must then be expressed in the new coordinate system.

Following this preparatory work, the final assembly of the system equations is carried out. It is performed in three major steps:

1. Transformation of the columns of the matrices to appropriate local coordinate systems and incorporation of any boundary conditions involving springs.
2. Incorporation of compatibility and equilibrium conditions on interfaces.
3. Application of specified displacements and tractions (and/or temperatures and fluxes).

Two particular features of the equation assembly deserve special comment. First, in multi-GMR problems the system matrix is not full. Rather it can be thought of as consisting of an NxN array of submatrices, each of which is either fully populated or completely zero. Only the nonzero portions of the system equations are preserved during system matrix assembly. In order to improve the numerical conditioning of the system matrix for the solution process, the columns are reordered so that the variables from the two regions, lying on the same interface, are as close together as possible.

Second, rather than simply assembling an explicit load vector at each time point in the solution process, load vector coefficient matrices are assembled and stored. These allow the updating of the load vector at any required time point simply by interpolating the time dependent boundary conditions and performing a matrix multiplication. A Similar process is used in the calculation of interior and boundary stresses.

7.6 System Equation Solution

The solver employed in BEST-CMS operates at the submatrix level, using software from the LINPACK package (Dongarra, 1979) to carry out all operations on submatrices. The system matrix is stored, by submatrices, on a direct access file. The decomposition process is a Gaussian reduction to upper triangular (submatrix) form. The row operations required during the decomposition are stored in the space originally occupied by the lower triangle of the system matrix. Pivoting of rows within diagonal submatrices is permitted.

The calculation of the solution vector is carried out by a separate subroutine, using the decomposed form of the system matrix from the direct access file. The process of repeated solution, required for problems with multi-time steps, is highly efficient.

7.7 Nonlinear Solution Process

The nonlinear solution algorithm starts with an elastic analysis (with linear elastic spring interface or bonded connection between the matrix and the fiber) of the problem for the first loading increment (complete with the specified boundary and body force loading). At the end of the elastic increment the state variables are calculated and the nonlinear constitutive relations are established. The difference between the actual values and the elastic (or previous) values is estimated. A new equation system is assembled with the calculated nonlinear constitutive relations. The process is essentially repeated until the constitutive equations yield values that are negligibly different from the previous step. A new loading increment is taken and the process is repeated for each subsequent increment.

7.8 Output Description

The output from BEST-CMS is relatively straightforward. It consists of ten sections, as follows:

1. Complete echo of the input data set.
2. Summary of case control and material property input.
3. Complete definition for each GMR, including all surface fiber nodes, surface and fiber

elements.

4. Complete summary for each interface and boundary condition set, including the elements and nodes affected.
5. Boundary solution (on an element basis), including displacements and tractions (and/or temperature and fluxes) at each node of each element.
6. The resultant load on each element and on the entire GMR is calculated and printed.
7. Solution for the displacements and tractions (and/or temperatures and fluxes) at the Fiber-Matrix composite interface (on an element basis).
8. Displacement, stress and strain (and/or temperature and fluxes) on a nodal basis, at all surface nodes, for each GMR.
9. Displacements (and/or temperatures) at interior nodes.
10. Stresses at interior nodes.

8. EXAMPLES OF FIBER COMPOSITE ANALYSIS

8.1 Introduction

In this section a number of examples are presented to verify and demonstrate the applications of the ceramic composite formulation of the previous chapters.

In the mesh diagrams of the models containing the fibers, a double line is used to indicate the centerline of the fiber elements. The length of these elements are shown in proper proportion for the three-dimensional views, however, the radii of the fibers are not indicated on these diagrams. The double line is a symbolic representation of the fiber elements and does not in any way indicate the diameter of the fiber. Refer to the example description for the values of the radii.

Throughout this section consistent units are used in the definition of the examples. This means all lengths are defined in the same units and the tractions and the elastic moduli are defined in terms of these lengths as force/length^2. No confusion should arise since the results are reported as non-dimensional quantities.

8.2 Cube with a Single Fiber

The first test of the formulation is on a unit cube with a single fiber of radius 0.1 through the center of the cube. The cube is subjected to tension and shear in the direction parallel and perpendicular to the fiber. The cube has a modulus of 100.0 and a Poisson ratio of 0.3. Consistent units are used for all information described in this problem. A fiber with two different moduli of 1,000 and 10,000 is studied. The Poisson ratio of the fiber is assumed to be the same as that of the cube.

The problem is analyzed by both the present formulation and by a full three-dimensional multi-region BEM approach. As shown in Fig. 8.2.1, the model for the fiber formulation consists of fourteen quadratic boundary elements and the fiber contains three quadratic fiber elements. The two-region, three-dimensional model shown in Fig. 8.2.2 contains twenty quadratic boundary elements in the first region and sixteen in the second. Note

9-noded elements are used in describing the fiber and hole to accurately capture the curvilinear geometry.

In Fig. 8.2.3, the profile of the end displacement of the cube under a uniform normal traction of 100.0 (in parallel with the fiber) is shown. The present formulation is in good agreement with the full three-dimensional results for $Ef/E = 10$. For the case $Ef/E = 100$, the fiber formulation exhibits greater stiffness than the 3-D results. This difference is contributed to the way the load is distributed from the fiber to the composite matrix. In the full 3-D model, the applied traction and the resulting reactions at the fixed end act directly on the end of the fiber. In the composite formulation, the fiber is assumed not to intersect the boundary surface and therefore the fiber is moved back slightly from the end of the cube. The load is therefore transferred through the composite matrix to the end of the fiber and to its sides in a manner that is slightly different from the full 3-D analysis.

In Fig. 8.2.4, the stress distribution through the center of the cube (from A to B as indicated in the figure) is shown. Again the results are very good for $Ef/E = 10$, and deviates slightly from the full 3-D results in the second case.

In Figs. 8.2.5 and 8.2.6, the lateral displacements along the side of the cube are shown for a cube subjected to a shear traction of 100. For the case of applied shear perpendicular to the fiber (Fig. 8.2.5), the results for both the fiber and full 3-D model show good agreement. Once again a slight deviation is observed for $Ef/E = 100$. In the case of the shear traction in the plane of the fiber (Fig. 8.2.6) the fiber has little effect on the displacement (as anticipated) and all results fall in close proximity.

8.3 Lateral Behavior of a Cube with Multiple Fibers

Existing methods of analysis of composite material based on mechanics of materials have been relatively successful in predicting the behavior of composite material for loading in the longitudinal direction. The properties perpendicular to the direction of the fibers are not so readily predictable by present means. The focus of the present example concerns this lateral behavior.

Four cubes (Fig. 8.3.1) with one, two, five and nine fibers are fixed with a roller boundary condition on one side and subjected to a uniform traction, perpendicular to the fibers. The material properties, given in consistent units, are

$$E^{fiber} = 1000 \qquad E^{matrix} = 100$$

$$\nu^{fiber} = 0.3 \qquad \mu^{matrix} = 0.3$$

For the cube with one and two fibers, the boundary mesh consists of two quadratic surface elements on each lateral side and four elements on the top and bottom. For the cubes with five and nine fibers, one additional element was added to the side with the applied traction and to the side with the roller boundary condition. The top and bottom faces contain six elements to match the pattern of the sides. In all cases, each fiber contained three one-dimensional quadratic elements.

The profile for the end displacement of the cube with one fiber and five fibers are shown in Figs. 8.3.2 and 8.3.3. The results are seen to be in good agreement with the two-dimensional results. The 2-D results are approximations since plane stress is assumed. The 3-D solutions for the one fiber are within 2% error of the 2-D solution and within 3% for the case of 5 fibers.

Also shown in Fig. 8.3.4 are the average end displacements for the one, two, five and nine fibers. Results show good agreement with 2-D results. For one, two and five fibers, the solutions are within 2% error of the 2-D results and 6% for the case of nine fibers where the volume ratio of the fibers to the total volume is 28.2%. The result is also displayed in a plot of Effective Modulus vs. fiber Volume Ratio in Fig. 8.3.5. The effective modulus is defined as the average stress/average strain. The three-dimensional results follow closely to the two-dimensional solution.

8.4 Thick Cylinder with Circumferential Fiber Supports

The strength of a cylinder under internal pressure can be increased by adding circumferential fiber supports. In the present example, a three-dimensional, open-end, thick cylinder with four fiber supports is analyzed. The inner and outer radii of the cylinder are 10 and 20 inches respectively, the height is 2 inches, and the radius of the fully-bonded fiber is 0.5 inches. By using roller boundary conditions on the faces of symmetry, only a fifteen degree slice of the thick cylinder needs to be modeled. As shown in Figure 7.4.1, eighteen quadratic boundary elements are used to define the geometry of the model (nine-node boundary elements are used on both the internal and external faces of the cylinder) and three fiber elements are used per fiber. Three analyses are carried out with three different elastic moduli of fibers: 100, 500, and 1000 psi. The elastic modulus of the cylinder is assumed to be 100.0 psi. The Poisson ratio is 0.3 for both the matrix and the fibers. The cylinder is subjected to an internal pressure of 100 psi.

Two analyses are carried out for each fiber type in which the functional variation over the boundary elements of the outer surface assumed a quadratic variation in one case and a quartic variation in another. These two analyses are compared with a multi-region, axisymmetric BEM analysis in which quadratic boundary elements are used to model the outer surface, the hole surfaces, and the fiber surfaces (Figure 8.4.2).

The radial displacement along the top face of the cylinder is shown in Figure 8.4.3. Both the quadratic and quartic element approaches are in excellent agreement with the axisymmetric solution in the analysis in which the modulus of elasticity of the fibers and the matrix are the same. The quadratic and quartic element results deviate slightly from the axisymmetric solution for the fiber-matrix modulus ratios of 5 to 1 and 10 to 1. The results of the quartic elements are in better agreement with the axisymmetric results than are the quadratic element results.

In Figure 8.4.4, the circumferential stress is shown for points along the top of the cylinder. The quartic element solution is in excellent agreement for all three fiber-matrix

ratios, while the quadratic element solution increases in error with increasing fiber modulus ratios.

In Figure 8.4.5 the radial stress is shown along the top of the cylinder. Once again the results of the quartic elements are superior to the results of the quadratic elements.

8.5 Cube with Multiple Fibers with Random Orientation

In an attempt to analyze a material with a random fiber structure, cubes with multiple fibers oriented in random directions are studied. The cubes are of unit length and have four boundary elements per side (Fig. 8.5.1a). Randomly oriented fibers of variable length with radii of 0.05 are placed in five cubes in quantities of 5, 10, 15, 20 and 25 (Fig. 8.5.1b-f). Three cases of material properties are considered for each cube. The modulus of the composite matrix is 100 for all cases, however, the modulus of the fibers are 500, 10,000 and 200,000 for the three cases studied. Poisson's ratio is uniformly 0.3 throughout. Roller boundary conditions are employed on three adjacent sides and a uniform normal traction of 100 is applied to a fourth face.

The normal end displacement at the center of the face on the side with the applied traction is plotted against the number of fibers in a cube for the three materials (Fig. 8.5.2). The displacement decreases with increasing number of fibers per cube and increasing Ef/E values as expected.

8.6 A Beam with Fiber Reinforcement in Bending

In the last example, the applicability of the present formulation to the study of the micromechanical behavior of the ceramic composite is apparent. The present formulation, however, is equally applicable to typical problems encountered by civil engineers. Reinforced concrete can now be modeled exactly as a three-dimensional body and studied in detail for the first time. The present example considers a reinforced concrete beam. Here the concrete plays the role of the composite matrix and the reinforcement bars play the role of the fiber fiber. In Fig. 8.6.1, a $4 \times 1 \times 1$ beam with four fibers is modeled using twenty-eight quadratic boundary elements. The effect of the ratio of fiber modulus to

matrix modulus (Ef/E) is studied for a range of values between 1 and 100. The Poisson ratio is 0.3 for both the beam and reinforced rods.

The beam is completely fixed at one end and a downward shear traction of 100 is applied to the other end. The non-dimensional vertical displacement of the end obtained from the present analysis is shown in Fig. 8.6.2 as a function of Ef/E. The non-dimensional displacement is defined as the end displacement of the reinforced beam divided by the displacement of a homogeneous beam under similar boundary conditions.

The end displacement obtained from the mechanics of material solution is also displayed in Fig. 8.6.2 in non-dimensional form. The curvature of the two plots are very similar but differ in magnitude. This difference is contributed to the fact that although the mechanics of material solution accounts for the stiffening due to the fibers, it does not include the effect of interaction between fibers.

8.7 Laminated Fiber Composite

A laminated composite fabricated from a fiber composite material is shown in Fig. 8.7.1. The fiber composite is constructed with a single row of fully-bonded fibers oriented in the same direction. A two-ply laminate is then constructed from the fiber composite with the fibers of the two layers oriented at 90° angles. A boundary element model created for the study of this material is shown in Fig. 8.7.2. A small slice containing two fibers in each layer is used. The model consists of two regions. The outer surface of each region is modeled with sixteen quadratic boundary elements and each fiber contains two quadratic fiber elements. The interface between the two regions is assumed to be a perfect bond, however, the present version of the program also allows for sliding and spring connections.

The composite structure is subjected to bi-axial tension. This is accomplished with normal tractions of 100 applied to two adjacent roller boundary conditions applied to the opposite ends. The elastic modulus of the composite matrix of both regions are assumed to be 100, and the moduli of the fibers very between 100 and 10,000. The Poisson ratio is 0.3 for both the composite matrix and fibers at all times.

Figure 8.7.3 displays the displacement as a function of fiber moduli for a point on the interface at the corner of the plate adjacent to the sides with the applied traction. The material exhibits less displacement as the modulus is increased, as expected.

8.8 Heat Conduction: Cube with Random Fibers

The cube with randomly oriented fibers shown in Fig. 8.5.1 was analyzed for heat conduction analysis. The left end was subjected to a prescribed temperature of 100°F and for the right end a temperature of 0° was specified. All other surfaces were assumed to be insulated. Figure 8.8.1 shows the equivalent thermal conductivity of a cube for different fiber arrangements. In this analysis the ratio of thermal conductivities between the fiber and the matrix was assumed to be 100.

8.9 Thermoelasticity: Effective Coefficient of Thermal Expansion

The addition of fiber fibers in a material alters the thermal expansion of the material. The effective coefficient of thermal expansion of a composite material is dependent on many factors such as: The elastic and thermal properties of the individual constituents; the size, shape, orientation, and number of fibers; and the interface interaction between the fiber and matrix. Some investigators [Hopkins and Chamis, 1985] have formulated equations for the determination of the effective material properties of fiber composite materials, including the coefficient of thermal expansion. These equations are, however, limited to specific types of fiber arrangements and interface connections. For general arrangements, experiments can be carried out for the prediction of effective material properties. Experiments, however, are expensive and time consuming. The finite element method may be employed for this purpose, however, the convergence of the solution may be slow and the solution may be expensive and difficult to achieve. The present uncoupled thermoelastic BEM implementation is an ideal alternative for the prediction of effective material properties for general, tubular fiber composite materials. The analysis is relatively simple and cost efficient.

A boundary element model of a cube with nine fibers is shown in Fig. 8.9.1. The fibers are assumed to be perfectly bonded to the composite matrix. Twenty-four boundary elements are used to model the outer surface of the cube and one fiber element is used to model each of the nine fibers. The cube is subjected to a uniform temperature increase by simply specifying the temperature on one face of the cube and zero flux on the other five sides. The cube is allowed to expand freely, however, rigid body translation is prevented. The user specified radius of the fibers is easily changed to simulate various void ratio, therefore, minimizing the effort required for re-analysis of the cube with different fiber to total volume ratios.

In Fig. 8.9.2 the effective coefficient of thermal expansions in the lateral and transverse directions are shown as a function of the fiber to total volume ratio for a fiber composite material with the following material properties:

$$E^{\text{matrix}} = 17.0 \times 10^6 \text{psi} \qquad E^{\text{fiber}} = 28.0 \times 10^6 \text{psi}$$

$$\nu^{\text{matrix}} = 0.24 \qquad \nu^{\text{fiber}} = 0.24$$

$$\alpha^{\text{matrix}} = 0.5 \times 10^{-6}/F \qquad \alpha^{\text{fiber}} = 2.1 \times 10^{-6}/F$$

Also shown are the predictions by Hopkins and Chamis (1985). The solutions of the two analysis are in good agreement at low fiber to total volume ratios and deviate slightly from one another as the fiber to total volume ratio is increased. A graph for a similar analysis is shown in Fig. 8.9.3 for a perfectly-bonded fiber composite material with the following material properties of aluminum and steel are used.

$$E^{\text{matrix}} = 10.0 \times 10^6 \text{ psi} \qquad E^{\text{fiber}} = 30.0 \times 10^6 \text{ psi}$$

$$\nu^{\text{matrix}} = 0.3 \qquad \nu^{\text{fiber}} = 0.3$$

$$\alpha^{\text{matrix}} = 12.0 \times 10^{-6}/F \qquad \alpha^{\text{fiber}} = 6.0 \times 10^{-6}/F$$

This time the coefficient of thermal expansion of the fibers is less than that of the matrix, and therefore, the effective coefficient of thermal expansion decreases with increasing fiber to total volume ratio. Once again good agreement is seen between the solutions of the two analyses.

8.10 Heat Conduction: Linear Thermal Resistant Fiber Interface

A cube with five fibers is used to demonstrate the linear thermal resistant interface relation between the matrix and the fiber. The boundary element mesh containing sixteen surface elements and five fiber elements is shown in Fig. 8.10.1. The radius of the fibers is 0.1. The conductivity of the fiber and matrix are both 100.0, however, the conductivity across the fiber-matrix interface is varied. The cube is subjected to a temperature of 100.0 on a face parallel to the fibers and a temperature of 0.0 on the opposite face. The other four sides are insulated.

A graph of the flux at the center of the zero temperature face versus the thermal conductivity of the interface is shown in Fig. 8.10.2. For very large values of the interface conductivity the interface connection approaches a perfect bond and the overall solution approaches the solution of a homogeneous cube with a conductivity of 100.0. As the interface conductivity decreases the flux decreases. For an interface conductivity of 0.0 the cube exhibits the solution of a cube with perfectly insulated holes.

8.11 Thermoelasticity: Linear Spring-Thermal Resistant Fiber Interface

The cooling of a cube containing five fibers is analyzed using the thermoelastic formulation. Shown in Fig. 8.10.1 is a boundary element model with sixteen surface elements and five fiber elements of radius 0.1. The fibers are assumed to be connected by a linear spring-thermal resistant interface. To demonstrate the effect of the interface connection, the fiber and the matrix are assumed to be constructed from the same material with an elastic modulus, a Poisson ratio, a thermal conductivity and a coefficient of thermal expansion of 100.0, 0.3, 100.0, and 0.01, respectively. The thermal conductivity across the fiber-matrix interface is held constant at 100.0, however, the spring constants between the fiber and the matrix are varied. A roller boundary condition is applied on two opposite faces of the cube and the other four sides are free to expand, however, rigid body translation is prevented. The cube is then subjected to a uniform decrease in temperature of 100.0.

A graph is shown in Fig. 8.11.1 of the resultant tractions at the center of the roller boundary condition faces versus the interface spring constants ($k_n = k_t$). For large spring constant values the interface connection approaches a perfect bond, and since the material properties of the fiber and matrix are equal, the overall solution approaches the solution of a homogeneous cube. As the spring constants decrease, the tractions at the roller boundary conditions decrease.

8.12 Nonlinear Fiber-Matrix Interface: Beam in Bending

A boundary element model of a 4x1x1 beam with four longitudinal fibers from example 8.6 is shown in Fig. 8.6.1. The effect of the ratio of the fiber modulus to matrix modulus (Ef/E) is studied for a range of values between 1.0 and 100.0. The Poisson ratio is 0.3 throughout. A nonlinear frictional interface between the fiber and matrix is assumed. The coefficient of friction is 0.2 and the normal tangential spring coefficients are both 1000.0 times the elastic modulus of the matrix.

The beam is completely fixed at one end and a downward shear traction of 100.0 is applied to the other end. The non-dimensional vertical displacement of the end obtained from the present analysis is shown in Fig. 8.12.1 as a function of Ef/E. The non-dimensional displacement is defined as the end displacement of the fiber composite beam divided by the displacement of a homogeneous beam subjected to the same boundary conditions. The plot of end displacement obtained in example 8.6 for a reinforced beam with perfectly bonded fiber-matrix interface connections is also displayed in Fig. 8.12.1. The beam with the perfectly-bonded fibers exhibits greater stiffness than the beam with the nonlinear fiber-matrix interface connections, as expected.

8.13 Effect of Poisson Ratio in Fiber Composites

The goal of the present five year project is to develop an accurate, yet practical boundary element program for the analysis of ceramic composite material. A conventional BEM approach is computationally expensive and mesh generation is tedious for an analysis of a

solid which may have hundreds of fibers. Therefore the challenge of the present work is to introduce certain approximations in the formulation which will produce an efficient BEM analysis and will not compromise accuracy. One approximation unique to this BEM implementation is the assumption that boundary quantities vary as a trigonometric function around the circumference of the fiber and hole. This was shown to be an accurate approximation through the numerical applications of this section. Secondly, the steady-state BEM formulations derived in Chapters 2-4 assume that the Poisson ratio of the fiber is equal to the Poisson ratio of the matrix. (This limitation was removed in the formulations of Chapters 5, however, these formulations are more expensive.) This second assumption is investigated in this example using a two-dimensional BEM analysis.

A boundary element model of a cube with a single fiber is shown in Fig. 8.13.1. Sixteen quadratic boundary elements are used to model the outer boundary and eight elements are used to model both the hole and fiber. The modulus of elasticity of the matrix is 10^6 and the Poisson ratio is 0.25. The elastic modulus of the fiber is assumed to range from 10^4 to 10^8 and the Poisson ratio from 0.0 to 0.5. The cube is secured by roller boundary conditions on two adjacent sides, a traction of 10^5 is applied on a third side, and the normal displacement is measured at the center of the remaining face. The ratio of fiber diameter to side of cube is 0.2 for the volume of fiber to total volume ratio of 0.031. The displacement versus the variation in Poisson ratio (ν^F/ν^M) is shown in Fig. 8.13.2 for the elastic modulus ratios (E^F/E^M) of 0.01, 0.1, 1.0, 10.0, and 100.0. The displacement in these curves are normalized by the displacement obtained for the respective elastic modulus ratios when the Poisson ratio of the fiber and matrix are the same ($\nu^F/\nu^M = 1.0$). The displacement is observed to be minimal in all cases. The effect is greatest for the modulus ratio E^F/E^M of 1.0 at the extreme values of ν^F/ν^M. The maximum error, however, is less than 4.5%.

This same problem is analyzed for the fiber diameter to side of cube ratio of 0.6 for a fiber volume to total volume ratio of 0.283 as shown in Fig. 8.13.3. The normalized displacement versus ν^F/ν^M for five modulus ratios is shown in Fig. 8.13.4. A very minute

change with variation of ν^F/ν^M is observed for modulus ratios of 0.01 and 100.0 which are almost indistinguishable from one another on the graph. The variation in Poisson ratio is seen to have a modest effect on the displacement values for modulus ratios of 0.1 and 10.0. For an elastic modulus of 1.0, the effect of Poisson ratio is somewhat tolerable for the midrange values of ν^F/ν^M, however, it has a strong effect for extreme values of ν^F/ν^M.

Next the effect of the Poisson ratio in a cube with multiple fibers interacting with one another is investigated. A cube with nine fibers (Fig. 8.13.5) is analyzed under similar conditions as the analyses of a cube with a single fiber. The volume of fiber to total volume ratio is again 0.283. In Fig. 8.13.6 the displacement versus ν^F/ν^M is shown for the multiple fiber composite for a modulus ratio E^F/E^M of 1.0. For comparison, the curve for a cube with a single fiber with the same modulus and fiber to total volume ratio is shown. The effect with the multiple fibers is just slightly less than the effect with a single fiber.

In conclusion, we note that a difference in Poisson ratio between a fiber and a matrix should not be ignored if the difference in the modulus of elasticity is small and the volume of fiber to total volume is large. Nevertheless, fibers are generally added to material in order to strengthen the material, and the elasticity modulus ratio (E^F/E^M) is usually greater than five. Furthermore, many composite constituents often have comparable Poisson ratio values. Therefore, the assumption that the Poisson ratio of the fiber must be equal to the Poisson ratio of the matrix is not very limiting.

8.14 Composite with Fifty-one Fibers

In Fig. 8.14.1 a boundary element mesh is shown for the outer surface of a rectangular block containing fifty small fibers and one large fiber (fiber elements not shown). The fibers are aligned parallel to one another in the arrangement shown in Fig. 8.14.2. Due to the relative size of the large central fiber, this fiber is explicitly modeled as a separate region in the conventional boundary element sense. The other fifty fibers are each modeled with one quadratic fiber element. The total number of nodes in the problem is five-hundred and ninety-eight. The material properties of the composite constituents are

Matrix	Fiber Type 1	Fiber Type 2
$E^M = 17.2 \times 10^6$ psi	$E^{F1} = 60.0 \times 10^6$ psi	$E^{F2} = 28.0 \times 10^6$ psi
$\nu^M = 0.24$	$\nu^{F1} = 0.24$	$\nu^{F2} = 0.24$
$\alpha^M = 0.5 \times 10^6/\mathrm{F}$	$\alpha^{F1} = 4.0 \times 10^{-6}/\mathrm{F}$	$\alpha^{F2} = 2.1 \times 10^{-6}/\mathrm{F}$

In Fig. 8.14.3 through 8.14.9 displacement contours are shown for a model constrained with roller boundary conditions on three adjacent sides (bottom, left, and back faces) and subjected to a normal traction of 10^5 on the small (right side) face perpendicular to the fibers. In. Figs. 8.14.4, 8.14.6, 8.14.8 and 8.14.9 a uniform temperature decrease of 2400°F has also been applied in addition to the normal traction. Contours for displacement (of the top, traction free face) in the direction parallel to the normal traction is shown in Figs. 8.14.3 and 8.14.4. In Fig. 8.14.5 and Fig. 8.14.6 the contours are shown for the displacement (of the top face) in the direction perpendicular to the normal traction and the fibers. In Fig. 8.14.7 and Fig. 8.14.8 the contours are shown for the displacement (of the top face) parallel to the fibers. Fig. 8.14.9 displays a three-dimensional view of 8.14.8.

In Fig. 8.14.10 a contour plot of displacement is shown for a model subjected to a normal traction on the top face perpendicular to the fibers. The displacement shown is of the top face in the direction parallel to the loading. The opposite face is fixed on rollers, and the lateral faces are traction free (rigid body translation is prevented). The fifty small fibers primarily strengthen the matrix uniformly, and the large fibers interacts with the strengthened matrix resulting in the deformation displayed in the figures.

8.15 Transient Thermoelastic Analysis of a Cube with Fibers

An uncoupled thermoelastic analysis of a cube with one and nine fibers is studied. A unit cube is discretized with six quadratic boundary elements on the surface of the cube and one fiber element per fiber. The radius of the fiber is 0.2 for the cube with a single fiber and 0.1 for the cube with nine fibers. The material properties, given in consistent

units are

$$E^{\text{fiber}} = 100.0 \qquad E^{\text{matrix}} = 1.0$$

$$\nu^{\text{fiber}} = 0.3 \qquad \nu^{\text{matrix}} = 0.3$$

$$k^{\text{fiber}} = 1000.0 \qquad k^{\text{matrix}} = 1.0$$

$$\rho c_e^{\text{fiber}} = 1.0 \qquad \rho c_e^{\text{matrix}} = 1.0$$

The temperature of the cube is initially at zero degrees. On a face parallel to the length of the fiber, the temperature is held at 0^o degrees and the face is supported by rollers. On the opposite face the temperature is suddenly raised to 100^o. All other sides are insulated and rigid body translation is prevented. The results of the flux and end displacement versus nondimensionalized time for the traction-free face is given in Fig. 8.15.1 through 8.15.4.

The three-dimensional fiber composite BEM results are compared with conventional, two-dimensional BEM results. In Figs. 8.15.1 and 8.15.2 the flux on the free face is shown for a cube with a single fiber and a cube with nine fibers, respectively. Similarly, Figs. 8.15.3 and 8.15.4 display the results for end displacement versus time. The fiber composite analysis is in good agreement with the conventional, two-dimensional results. Slight deviation is expected due to the 2-D assumption and the use of a somewhat crude 3-D discretization.

8.16 Transient Heat Conduction Analysis of a Turbine Blade

A boundary element discretization of a turbine blade is shown in Fig. 8.16.1. Half symmetry is employed in this model which consists of a single region with ninety-two quadratic boundary elements. The model is 58.2 mm long, 13.9 mm wide, the radius of the base is 6.95 mm, and the tip is 1.98 mm (from the plane of symmetry) in thickness at the largest point.

A transient heat conduction analysis is first carried out on a homogeneous blade with a conductivity of $k = 0.0216$. The blade initially rests in thermodynamic equilibrium at zero temperature. Then, a gas at a temperature of 1200^o is assumed to flow over the blade

while a gas at a temperature of 500° surrounds the base of the blade. At the leading edge of the blade the film coefficient is $h = 0.003395$ and tapers off to $h = 0.00064$ at the trailing edge. At the base of the blade the film coefficient of $h = 0.00005$ is assumed. Figures 8.16.3a through 8.16.7a contain contour plots describing the temperature flow through the blade at 1.0, 2.0, 4.0, 6.0, and 8.0 seconds.

The blade is reanalyzed, this time with eight fibers (four fibers per side) running from the tip of the blade to half way through the base. The radius of the fibers is 0.15 mm and their cross-sectional locations are shown in Fig. 8.16.2. Five (9-noded) fiber elements are used to model each fiber. The conductivity of the fibers is 100 times the conductivity of the blade. In Figs. 8.16.3b through 8.16.7b the resulting temperature distributions are shown in contour plots. Overall, the higher conductivity of the fibers increases the heat flow through the blade. Hence, the heat at the tip of the blade is carried to the base faster than in the homogeneous blade. This results in a temperature distribution which is lower than the homogeneous blade near the tip and higher near the base.

8.17 Heat Flow in a Cube with Multiple Fibers

The steady-state heat flow through a unit cube with one, five, and nine fibers is analyzed. The radii of the fibers is 0.1 and the arrangement of the fibers is shown in Figure 8.17.1. The conductivity of the fibers is assumed to be 10 times the conductivity of the composite matrix. A uniform flux of 100 is applied to a side of the cube parallel to the fibers. The opposite side is maintained at a temperature of 0°. The remaining four sides are insulated.

The resulting temperature profiles on the face subjected to the flux is shown in Figure 8.17.2 for the three fiber arrangements. Note, the effect of the number of fibers on the temperature profile. As the number of fibers are increased, the overall conductivity of the cube is increased. Hence, the heat from the applied flux is carried away (to the face which is maintained at 0°) at a higher rate, resulting in lower temperatures. Also note, the local temperature minimums in the temperature profiles are associated with the close proximity

of the fibers near the flux boundary.

8.18 Effective Conductivity in a Fiber Composite

In problem 8.9, the effective coefficient of thermal expansion was calculated for a fiber composite with nine fibers. In the present example, the conductivity of heat flow in a similar specimen is examined. The boundary element model is shown in Figure 8.9.1. The fibers are assumed to be perfectly bonded to the composite matrix so that the resistance of the heat flow across the interface is zero. Twenty-four boundary elements are used to model the outer surface of the cube and one fiber element is used to model each of the nine fibers. The cube is subjected to a temperature of 0°F on a face perpendicular to the fibers and 100°F on the opposite face. The remaining four faces are insulated. The total heat flux through the cube is calculated and the effective conductivity in the direction parallel to the fibers can be found. When the boundary conditions are rearranged to produce heat flow perpendicular to the fibers, the effective conductivity in the transverse direction can be determined.

In figure 8.18.1, the effective conductivity in both the lateral and transverse directions are shown as a function of the ratio of the fiber volume to the total volume of the specimen. The fiber composite has the following conductivities:

$$k^{\text{matrix}} = 8.2 \text{ Btu/hr ft F} \qquad k^{\text{fiber}} = 32.0 \text{ Btu/hr ft F}$$

The solutions are in good agreement with the approximate solutions by Hopkins and Chamis (1985) at low fiber to total volume ratios and deviates slightly from one another when the fiber to total volume ratio is increased.

A similar analysis was carried out for a fiber composite with the following conductivities:

$$k^{\text{matrix}} = 25.0 \text{ Btu/hr ft F} \qquad k^{\text{fiber}} = 5.8 \text{ Btu/hr ft F}$$

Once again, the results shown in Figure 8.18.2 are in good agreement with the solutions obtained with the formulas given by Hopkins and Chamis (1985).

8.19 Effective Modulus of Elasticity

In problem 8.9, the effective coefficient of thermal expansion was calculated for a fiber composite, and in the above example (8.18) the effective conductivity was determined. In the present example, the effective modulus of elasticity will be calculated for a similar specimen with 9 perfectly bonded fibers. The effective modulus of elasticity can be calculated in both the longitudinal and transverse directions by subjecting the cube to tension in the directions parallel and perpendicular to the fibers, respectively.

In Figure 8.19.1, the effective modulus of elasticity in the longitudinal and transverse directions are shown as a function of the ratio of the fiber volume to the total volume of the specimen. The fiber composite has the following material properties:

$$E^{\text{matrix}} = 17.0 \times 10^6 \text{ psi} \qquad E^{\text{fiber}} = 28.0 \times 10^6 \text{ psi}$$

$$\nu^{\text{matrix}} = 0.24 \qquad \nu^{\text{fiber}} = 0.24$$

The solutions are again in good agreement with the approximate solutions by Hopkins and Chamis (1985) for the low fiber to total volume ratios, and deviates slightly from one another when the volume ratio is increased.

A similar analysis is also carried out for the aluminum-steel composite matrix of example 8.9.

$$E^{\text{matrix}} = 10.0 \times 10^6 \text{ psi} \qquad E^{\text{fiber}} = 30.0 \times 10^6 \text{ psi}$$

$$\nu^{\text{matrix}} = 0.3 \qquad \nu^{\text{fiber}} = 0.3$$

Once again, good agreement is seen between the solutions as displayed in Figure 8.19.2.

8.20 Elastoplasticity: Cube with a Single Fiber

The elastoplastic analysis of a unit cube with a single fiber of diameter 0.6 is analyzed using the fiber element approach developed in Chapter 6. In order to gage the accuracy of the formulation, a von Mises constitutive model was employed and the solution was compared to a two-dimensional plane stress boundary element analysis. The discretization of the fiber element model is shown in Figure 8.20.1. Six quadratic boundary elements are used to model the outer surface of the composite. Three fiber elements (with cylindrical volume cells of diameter 0.98) were used to model the fiber. The two-dimensional

discretization is shown in Figure 8.20.2. Three regions modeled with quadratic boundary elements and volume cells were used. The first region contains twelve boundary elements and is used to model the fiber. A second region (surrounding the fiber) contains twenty-four boundary elements and twelve volume cells and a third region contains twenty-four boundary elements and sixteen volume cells and is used to model the matrix. The elastic modulus of the fiber and the matrix are 60×10^6 psi and 15.0×10^6 psi., respectively, and the Poisson's ratio is assumed to be 0.25 in both materials. The fiber is assumed to remain elastic and the matrix is assumed to have a yield strength of 10.0×10^4 psi.

Two different analyses were carried out. In the first case the matrix is assumed to have a strain hardening parameter of 15.0×10^6 psi, and in the second case zero strain hardening is assumed. The cube is subjected to a normal traction on a side of the cube parallel to the fiber and a roller boundary condition is applied to the opposite face. In figure 8.20.3, the results of the end displacement vs. traction is shown for the two analyses. The 3D strain hardening iterative solution is stiffer than the 2D results. The difference in the solution is partly contributed to the plane stress assumption and to the fact that a finer discretization is used in the 2D analysis. Also, the cylindrical volume cell of the fiber element approach does not completely cover the entire volume of the composite matrix, and therefore, some of the nonlinear behavior is not accounted for.

As a check of the iterative algorithm, the 3D fiber element analysis with strain hardening was conducted using the variable stiffness plasticity algorithm [Henry and Banerjee, 1988b]. The variable stiffness solution is in excellent agreement with the iterative solution (Figure 8.20.3). The analysis with zero strain hardening is also shown in Figure 8.20.3. Once again the 3D solution is stiffer than the 2D results, however, both solutions collapse close to the same load level.

It is important to note that even though the fiber element analysis is three-dimensional, the computational time was slightly less than the solution time of the 2D approach. For problems with additional fibers, the fiber element approach will produce even greater

savings!

8.21 Elastoplasticity: Cube with a Thin Fiber

An analysis similar to the previous example is carried out for a unit cube with a fiber of diameter 0.2. The material properties from the previous example are used. The model shown in Figure 8.20.1 is employed with a cylindrical volume cell of diameter 0.98.

A fiber composite analysis is carried out for four different hardening parameters: 15.0×10^6 psi, 8.0×10^6 psi, 2.0×10^6 psi, and 0.0 psi. Figure 8.21.1 displays the end displacement vs. traction results for a cube subjected to a normal traction on a face parallel to the fibers with the opposite face constrained against normal displacement. The thin fiber strengthens the composite to a lesser degree than the larger fiber in the previous problem, resulting in a softer elastic and nonlinear solution and a lower collapse load for the zero hardening case.

8.22 Elastoplasticity: Cube with Multiple Fibers

An elastoplastic analysis of a cube with 9 fibers in a square packing arrangement is analyzed. The discretization of the fiber element model is shown in Figure 8.22.1. Six quadratic boundary elements are used to model the outer surface of the unit cube and one fiber element is used to model each fiber. The fibers have a diameter of 0.2 and a volume cylinder diameter of 0.32. The elastic modulus of the fiber and matrix is 60.0×10^6 psi and 15.0×10^6 psi, respectively, and the Poisson's ratio is assumed to be 0.25 in both materials. The fibers are assumed to remain elastic and the matrix is assumed to have a yield strength of 10.0×10^4 psi.

The analysis was carried out for a number of different hardening parameters. The cube is subjected to a normal traction on a face parallel to the fibers and a roller boundary condition is applied on the opposite face. In Figure 8.22.2, the end displacement vs. traction is shown. It is interesting to compare these results to the solution of the single fiber in problem 8.20 (Figure 8.20.3) which involved similar material properties, similar

loading, and had the same volume of fiber to total volume ratio. The analysis of the specimen with 9 fibers yields at a slightly lower stress level, however, exhibits a greater stiffness in both the elastic and nonlinear solution, than the analysis of the single fiber. The results of the zero hardening case indicate a lower collapse load in the present analysis than in example 8.20.

8.23 Elastoplastic-Fracture: Cube with a Fiber

The elastoplastic fracture model described in Section 6.5 is used to model the constitutive behavior of a unit cube with a fiber of diameter 0.6. The modulus of elasticity of the fiber and the matrix are 1000.0 psi and 100.0 psi, respectively, and the Poisson's ratio is 0.3 for both materials. The parameters associated with the elastoplastic-fracture model are given below in units of psi:

Compression Zone:

$$\tau_y = 1000.0 \quad \tau_{ult} = 10,000.0 \qquad A_y = 1000.0 \quad A_{ult} = 2000.0 \qquad H = 1000.0$$

Tension Zone:

$$\tau_y = 100.0 \quad \tau_{ult} = 5000.0 \qquad A_y = 100.0 \quad A_{ult} = 200.0 \qquad H = 100.0$$

Two analyses are carried out. In the first analysis, the cube is subjected to a normal tensile traction on a face parallel to the fiber and roller boundary conditions are applied on the opposite face. In the second analysis, a normal compressive traction is applied in a similar manner. 2D and 3D approaches are used in both analyses. The discretization shown in Figure 8.20.1 is used for the 3D case and the discretization of Figure 8.20.2 is employed for the 2D approach.

The results of both analyses are shown in Figure 8.23.1. In Figure 8.23.2, a close up view is shown for the tension case. The results of the 2D and 3D approaches agree quite well in both the tension and compression analyses.

8.24 Elastoplastic-Fracture: Fiber Composite under Axial Loading

A 1 x 1 x 4 rectangular block has a single fiber at its center running through its length (Figure 8.24.1). The elastic and inelastic material properties of the composite of example 8.23 are assumed in the present analysis. The effect of the fiber radius on the deformation of the composite is carried out. Three cases were examined in which the radius of the fiber is 0.3, 0.2 and 0.0 (homogeneous case).

In Figure 8.24.2, the axial strain at the center of the specimen (inside the fiber) is shown for the three cases under both tension and compression loading. Significant stiffening is observed in both loading configurations as the radius is increased. In previous examples (8.20-8.23) it was observed that the presence of the fibers resulted in a significant loss of strength when the composite was loaded perpendicular to the fibers beyond its elastic limit. In the present analysis, a specimen loaded in tension yields at a very low level. For a specimen in compression the yield is higher and the hardening parameter is greater resulting in a very slight deviation from the elastic solution. Since the fiber remains elastic and the strain hardening is constant, the inelastic deformation is relatively linear once yielding occurs.

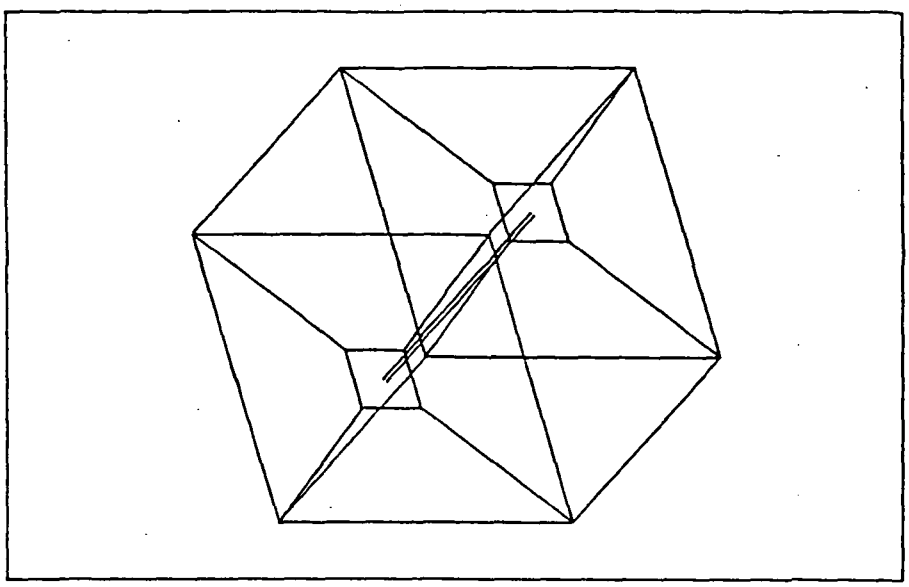

Fig. 8.2.1 Discretization of a Fiber in a Unit Cube Utilizing Quadratic Fiber Elements

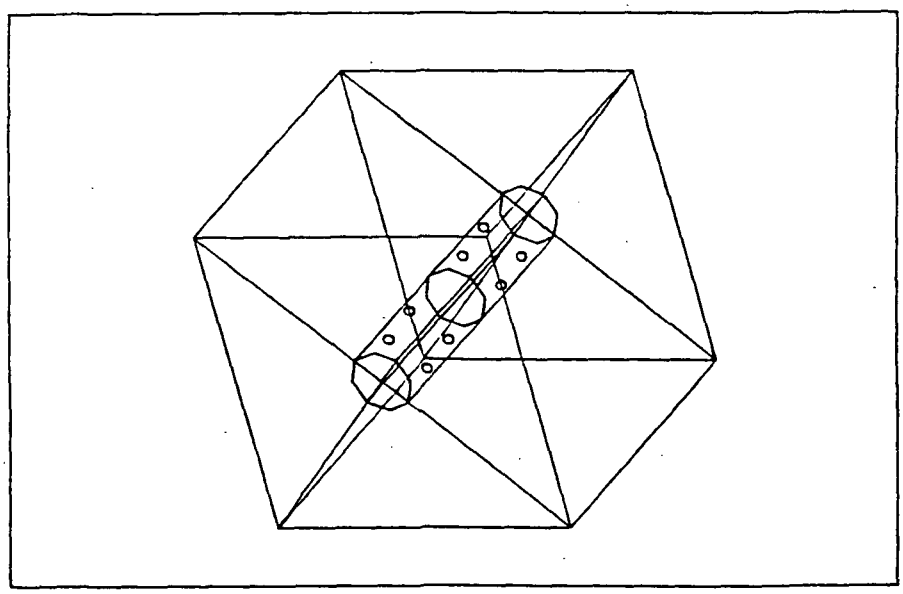

Fig. 8.2.2 Full Three-dimensional, Multi-region Discretization of a Fiber in a Unit Cube

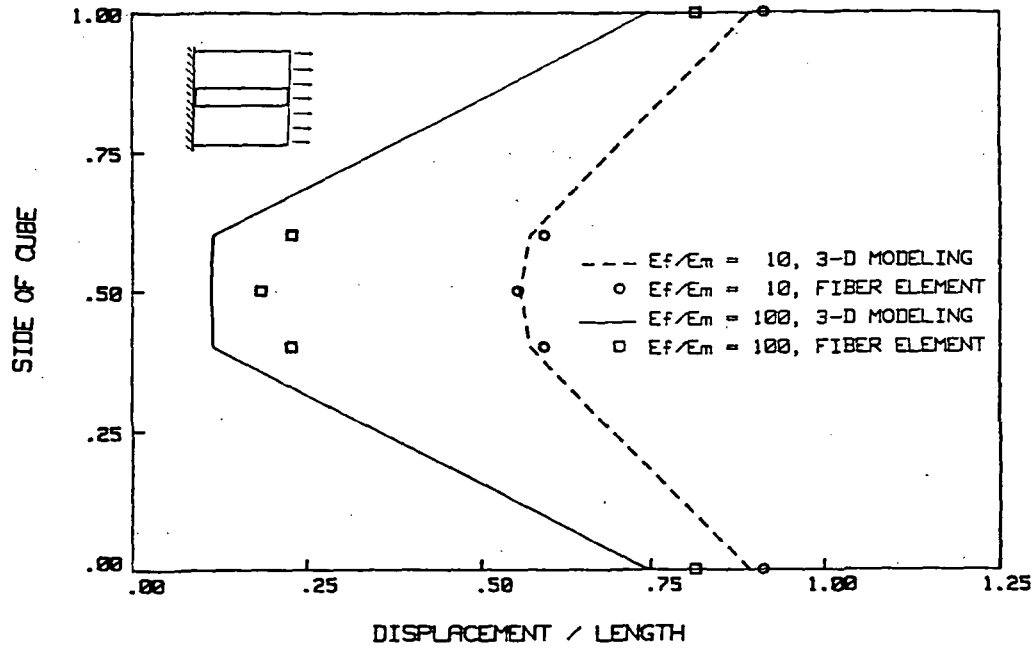

Fig. 8.2.3 Comparison of Displacement Profiles Between the Full 3-D Model and the Fiber Element Model for the End of a Cube in Tension

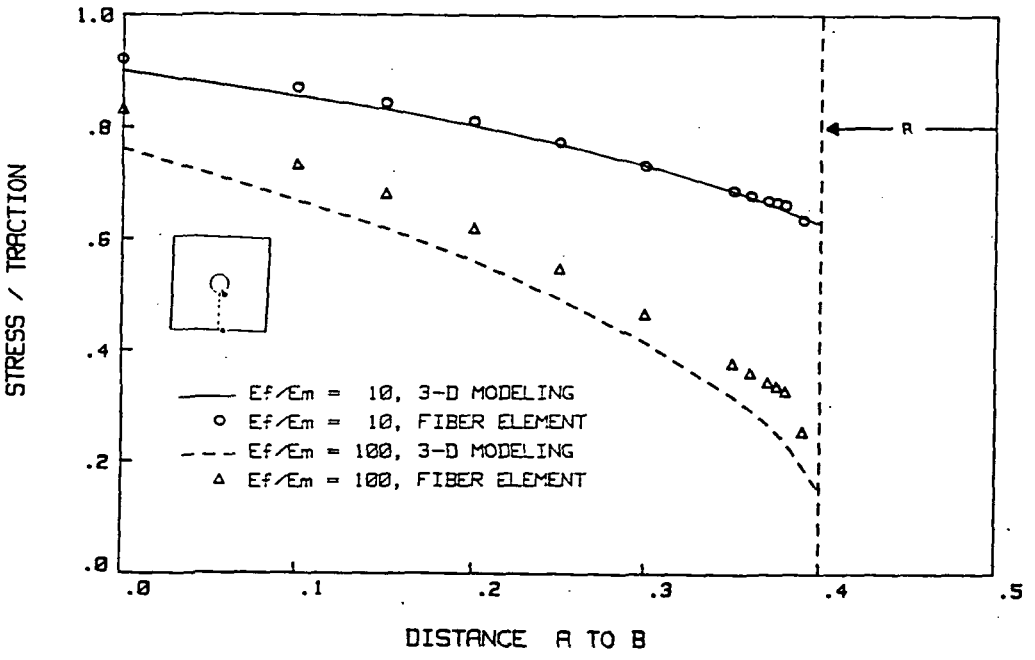

Fig. 8.2.4 Axial Stress Through the Cross Section of a Unit Cube in Tension with a Single Fiber in Parallel with the Loading

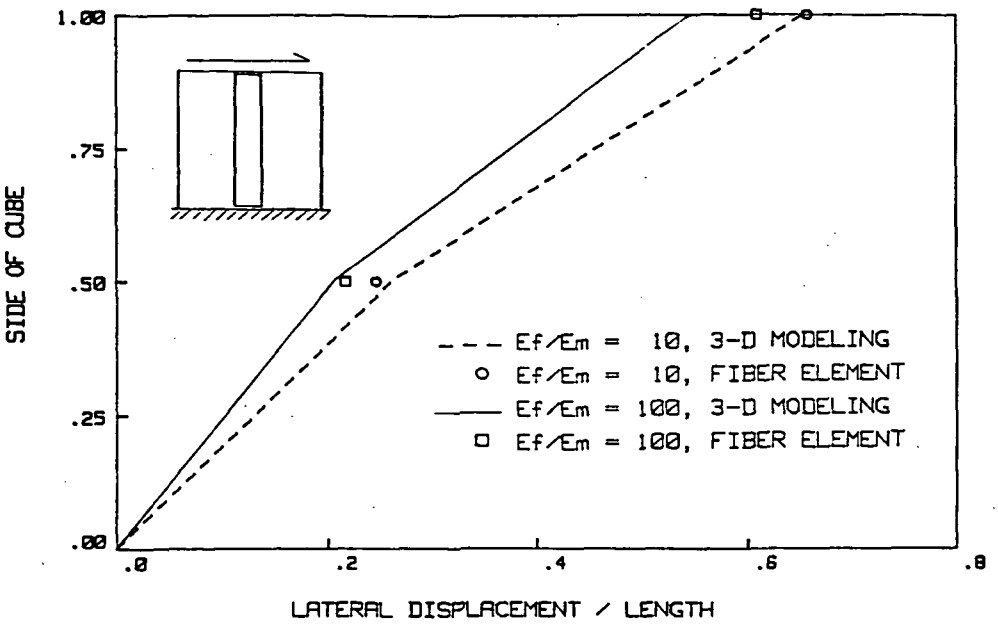

Fig. 8.2.5 Lateral Displacement Along a Side of a Cube Subjected to a Shear Force Perpendicular to the Fiber

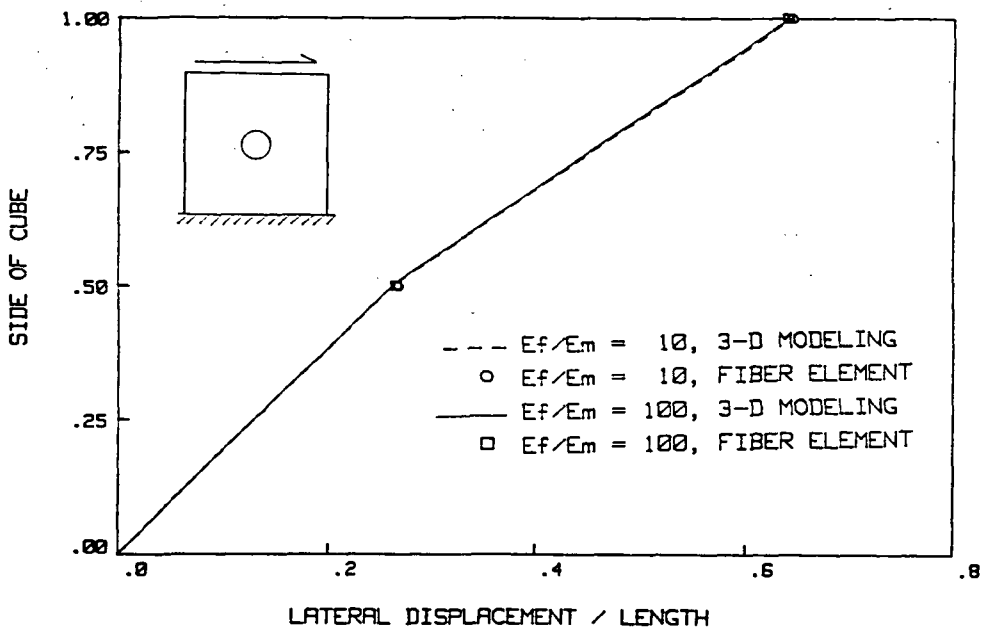

Fig. 8.2.6 Lateral Displacement Along a Side of a Cube Subjected to a Shear Force in the Cross-Plane of the Fiber

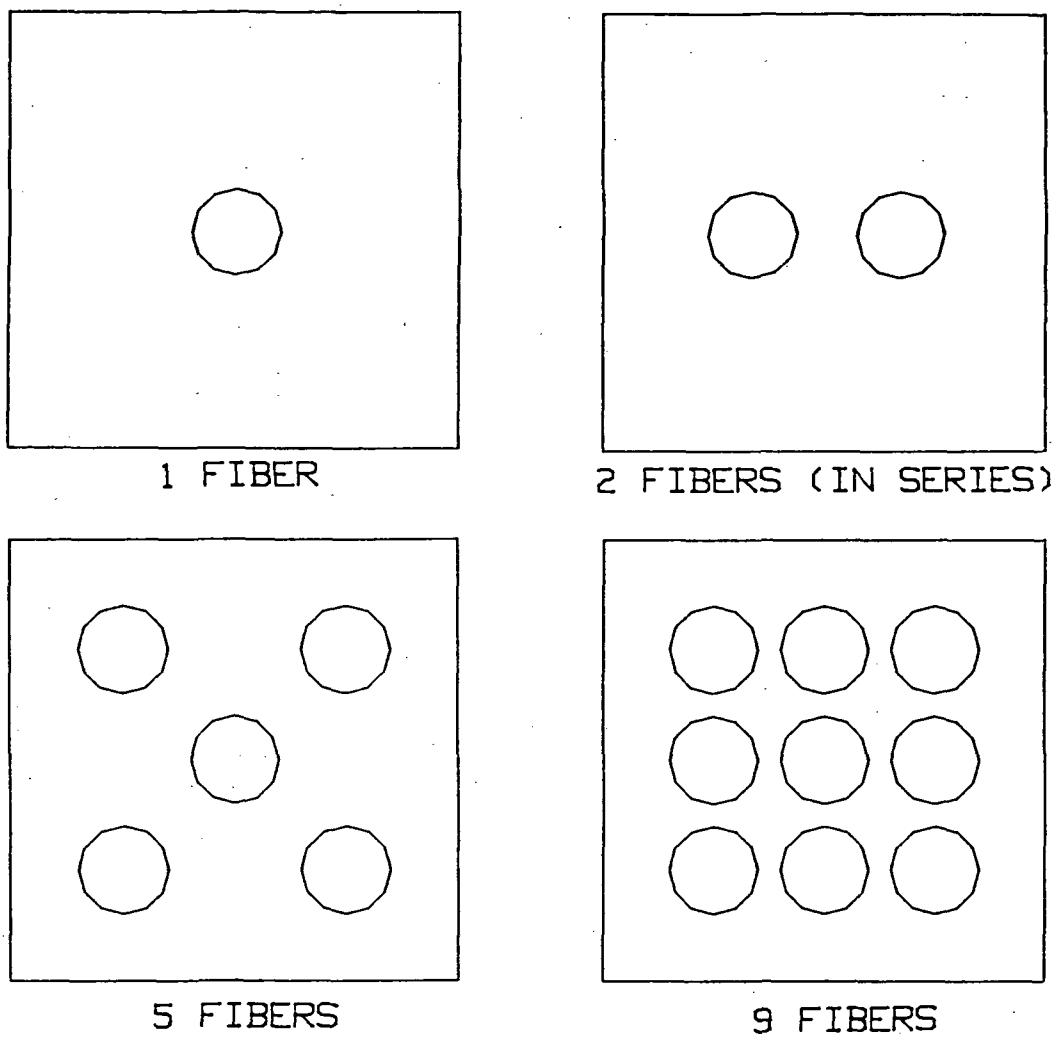

Fig. 8.3.1 Arrangement of Multiple Fibers in a Unit Cube Subjected to Lateral Tension

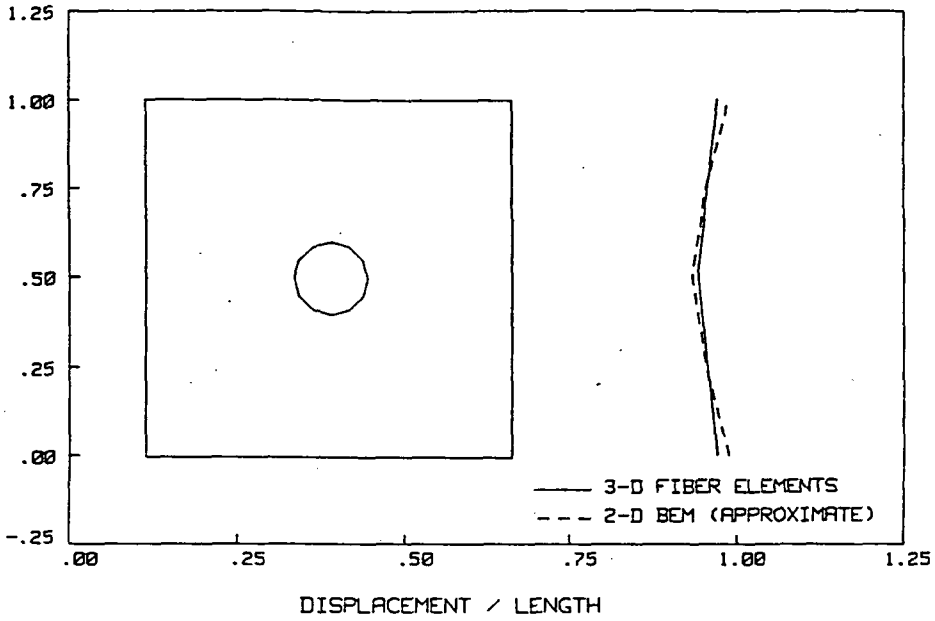

Fig. 8.3.2 Displacement Profile of a Cube with a Single Fiber Under Lateral Tension

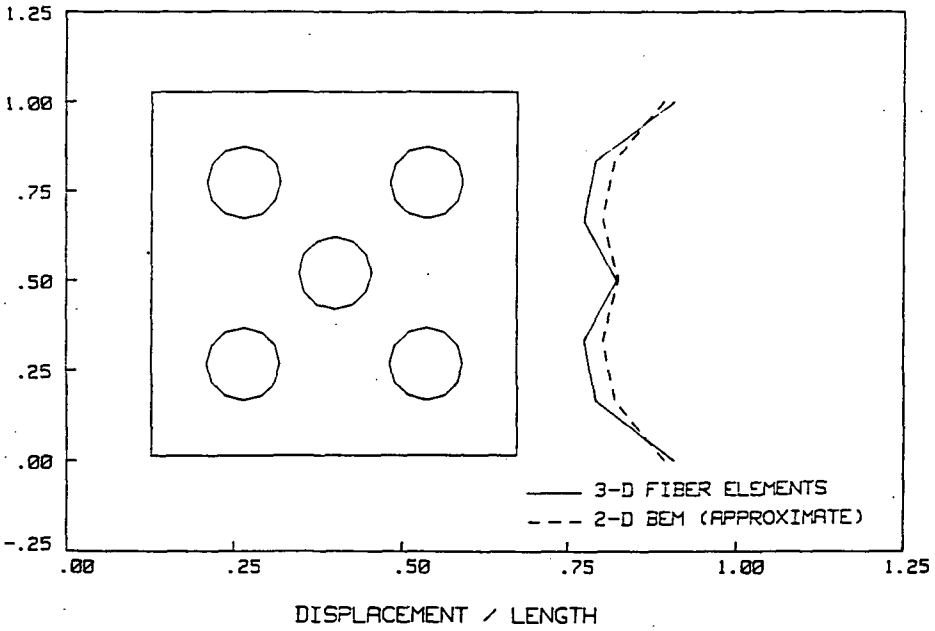

Fig. 8.3.3 Displacement Profile of a Cube with Five Fibers Under Lateral Tension

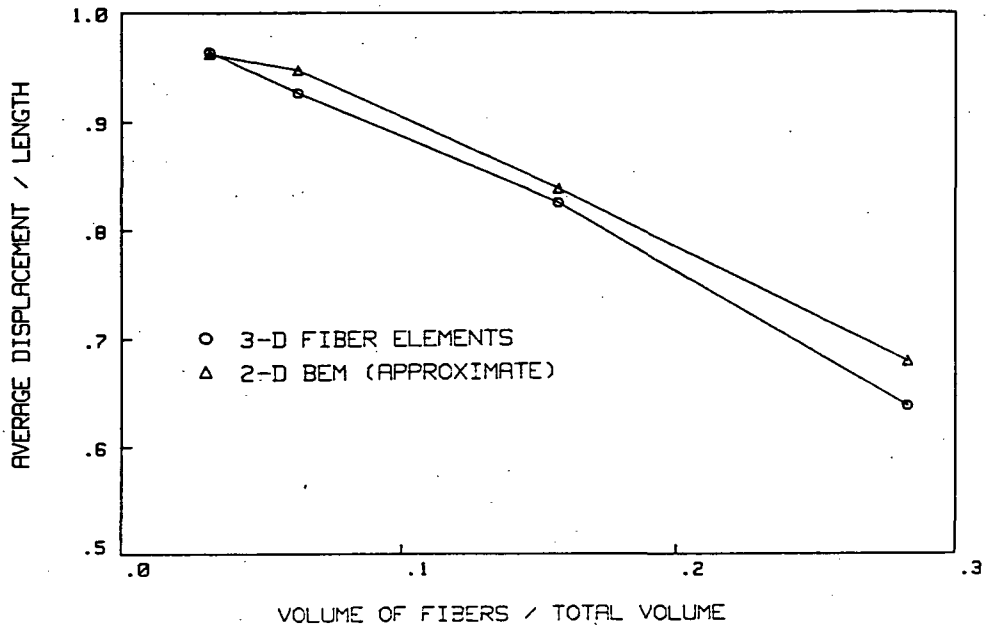

Fig. 8.3.4 Average End Displacement of a Cube Under Tension vs. the Volume of Fiber to Total Volume Ratio

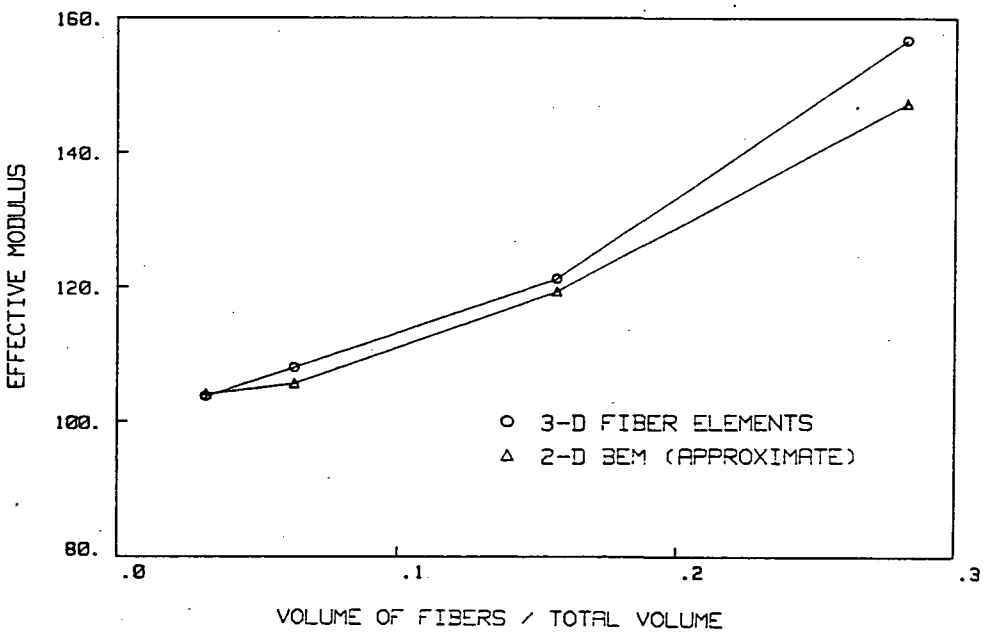

Fig. 8.3.5 Effective Transverse Modulus of a Cube as a Function of Fiber Volume to Total Volume

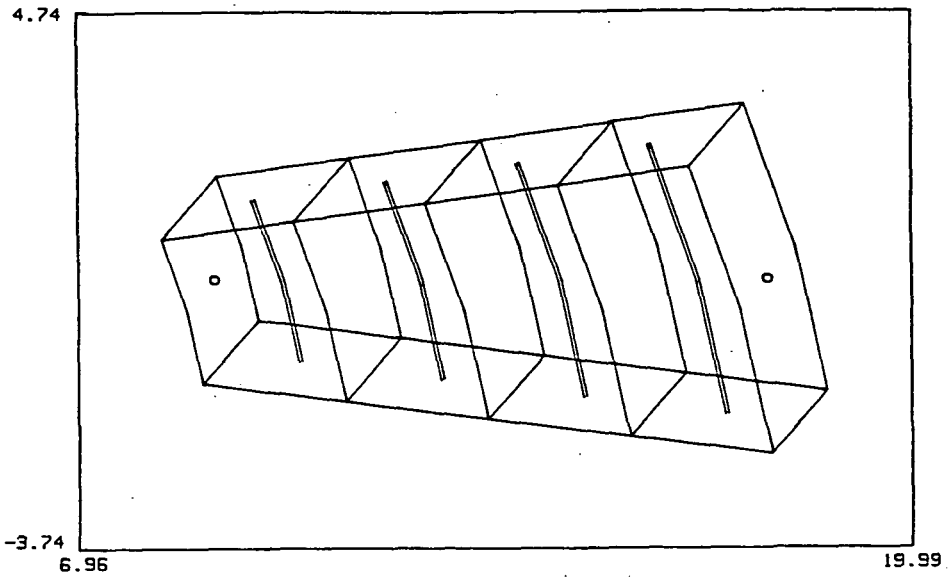

Fig. 8.4.1 Discretization of a Thick Cylinder with Four Fibers Utilizing Fiber Elements

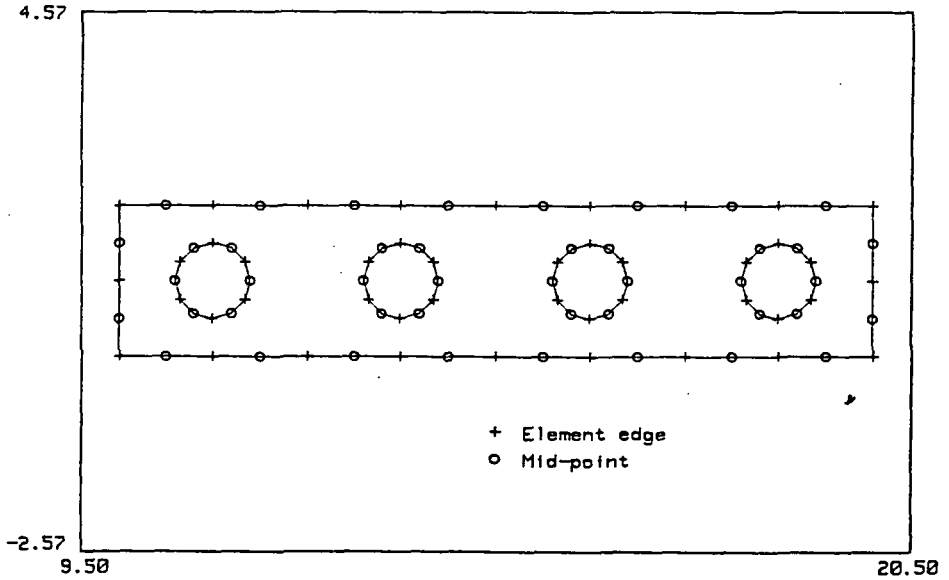

Fig. 8.4.2 Axisymmetric Multi-region, Discretization of a Thick Cylinder with Four Fibers

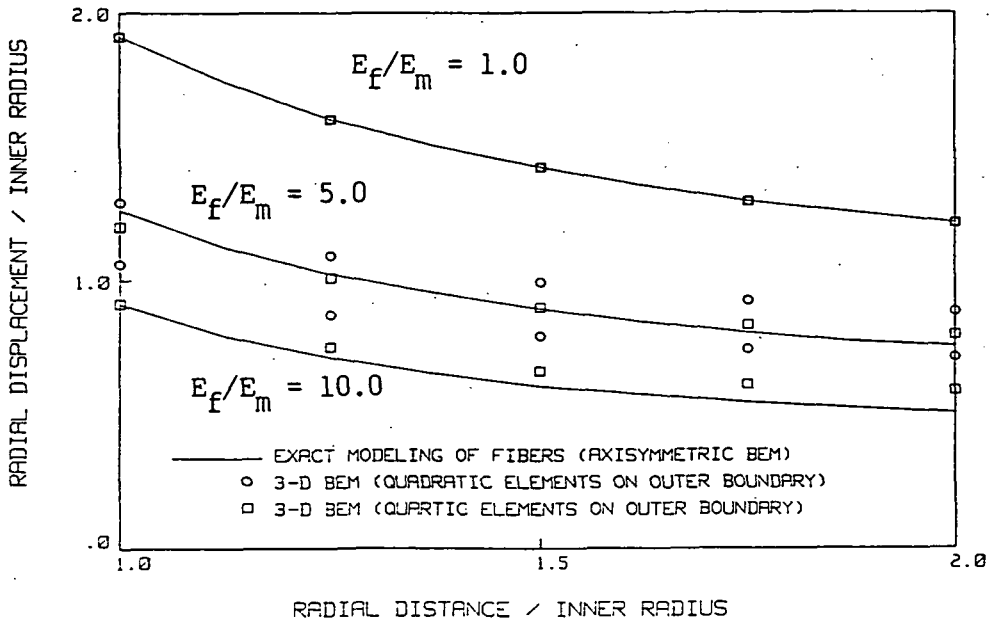

Fig. 8.4.3 Radial Displacement Through a Pressurized Thick Cylinder with Circumferential Fibers

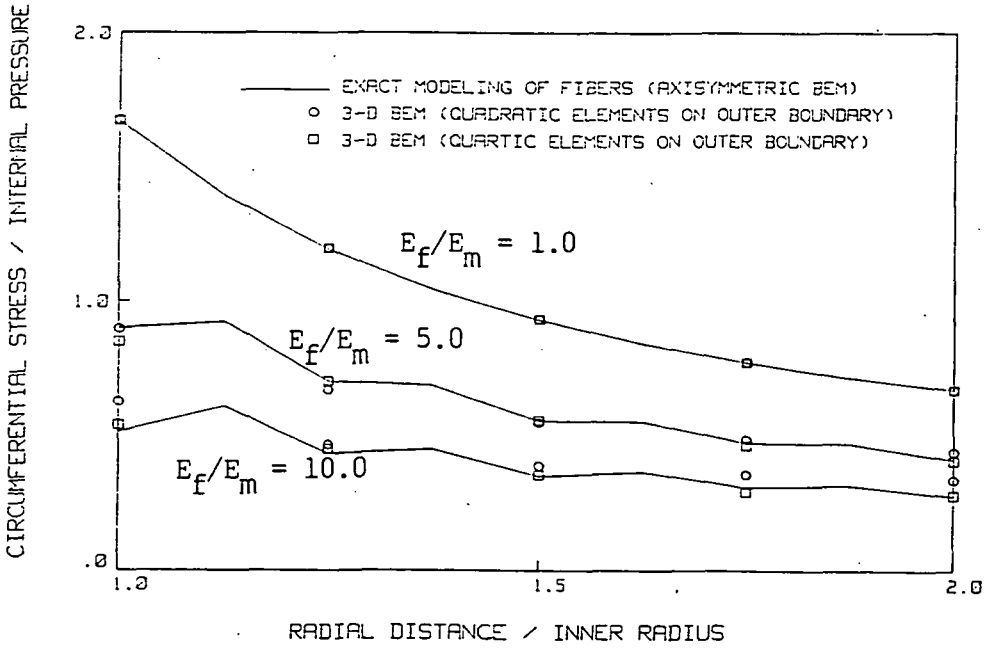

Fig. 8.4.4 Circumferential Stress Through a Pressurized Thick Cylinder with Circumferential Fibers

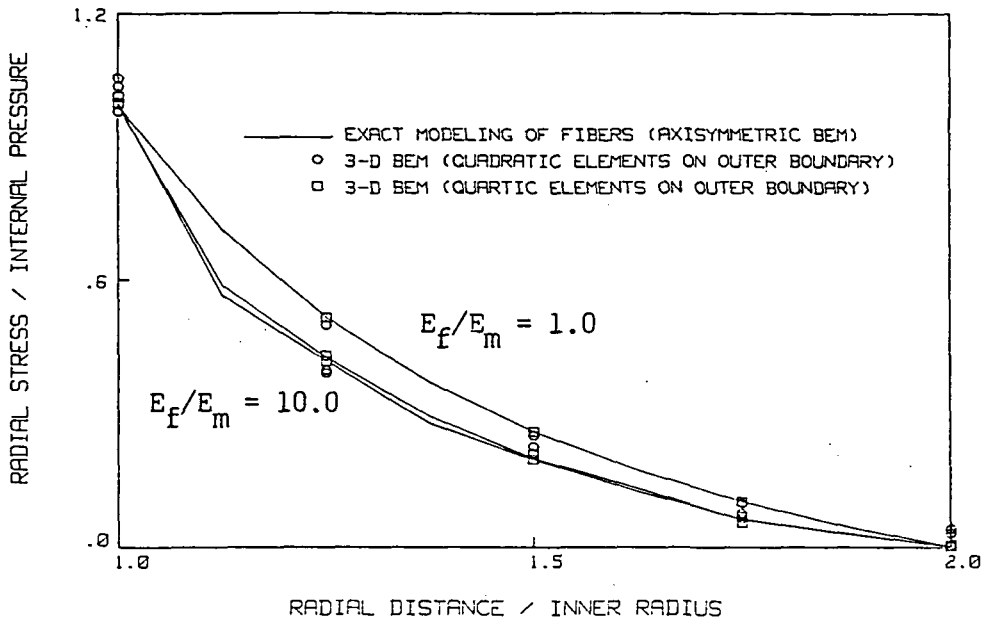

Fig. 8.4.5 Radial Stress Through a Pressurized Thick Cylinder with Circumferential Fibers

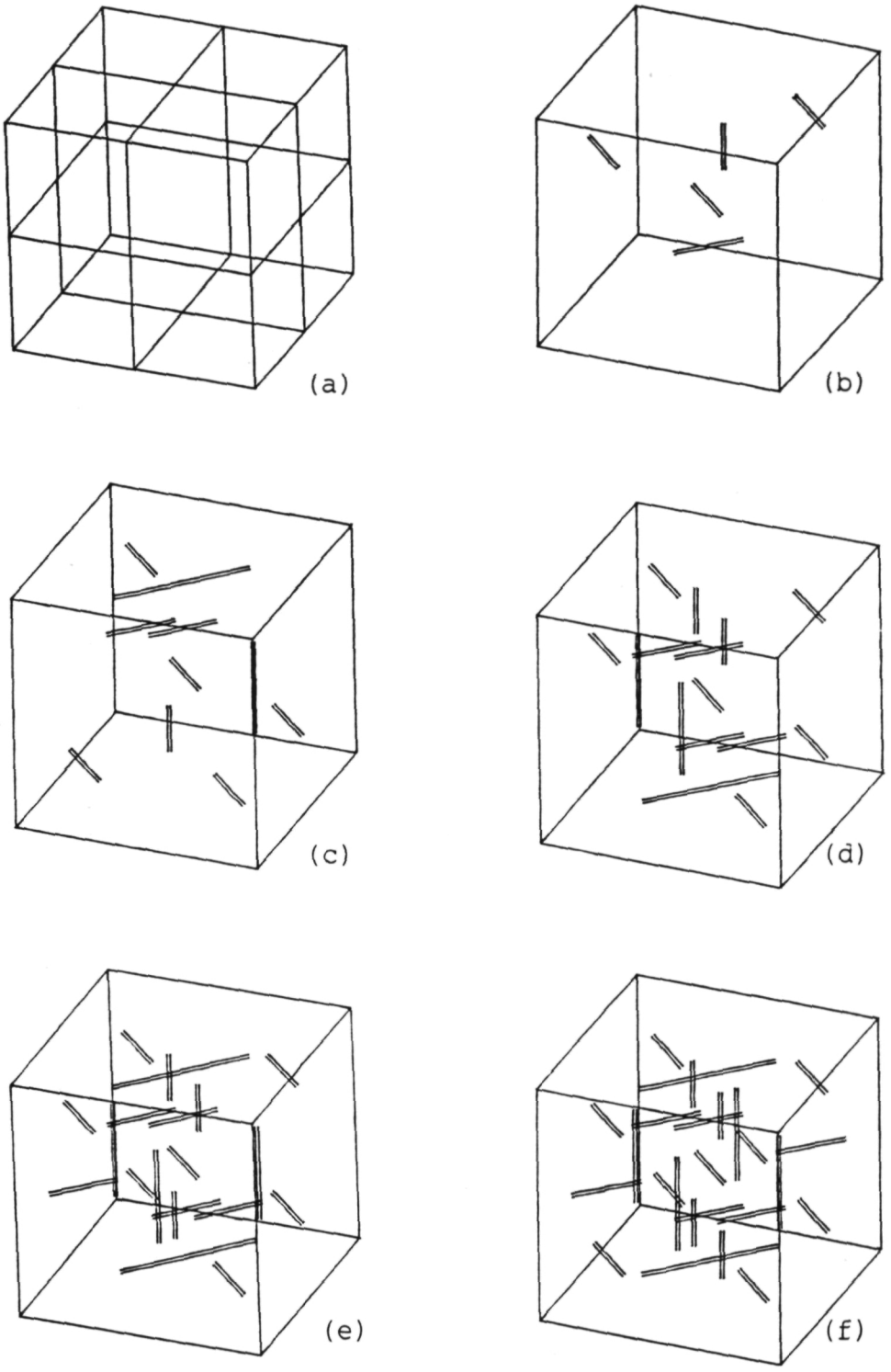

Fig. 8.5.1 (a) Surface Discretization of a Unit Cube Used in the Study of Random Oriented Fibers , (b-f) Orientation of Variable Length Fibers Within Unit Cubes Containing 5, 10, 15, 20, and 25 Fibers , respectively

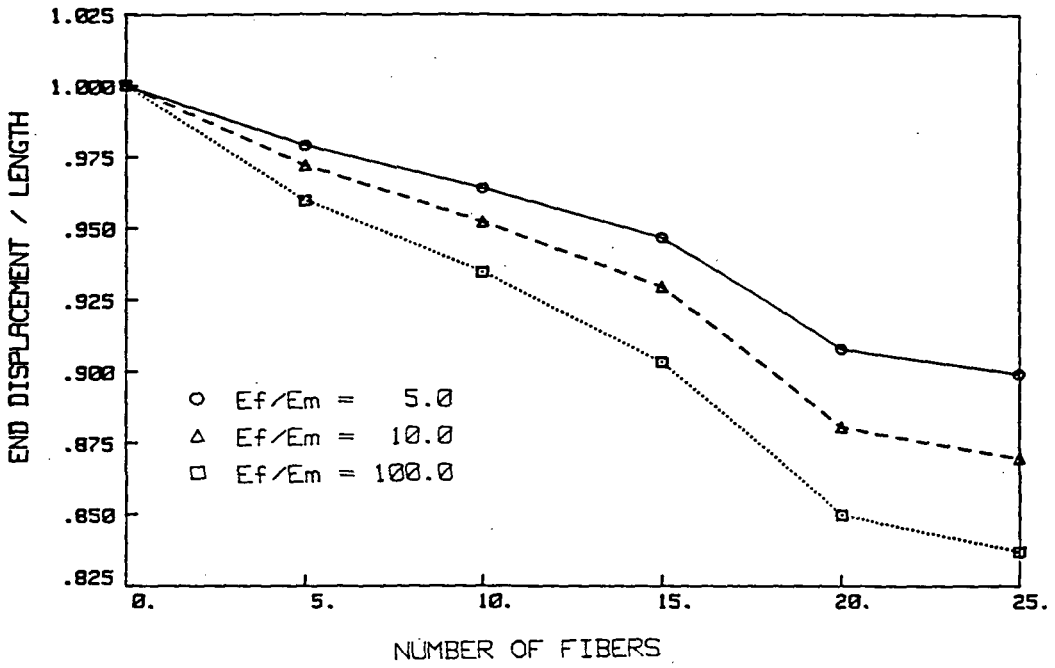

Fig. 8.5.2 End Displacement of a Unit Cube With Random Oriented Fibers of E_f/E_m = 5.0, 10.0 and 100.0

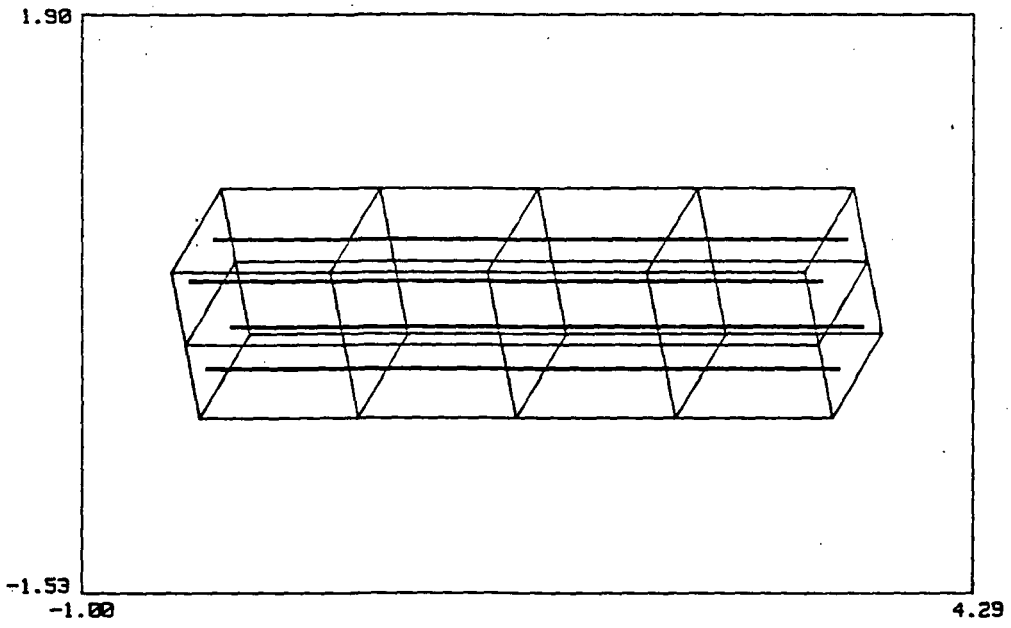

Fig. 8.6.1 Discretization of a Reinforced Beam Utilizing Quadratic Fiber Elements to Model the Four Fibers

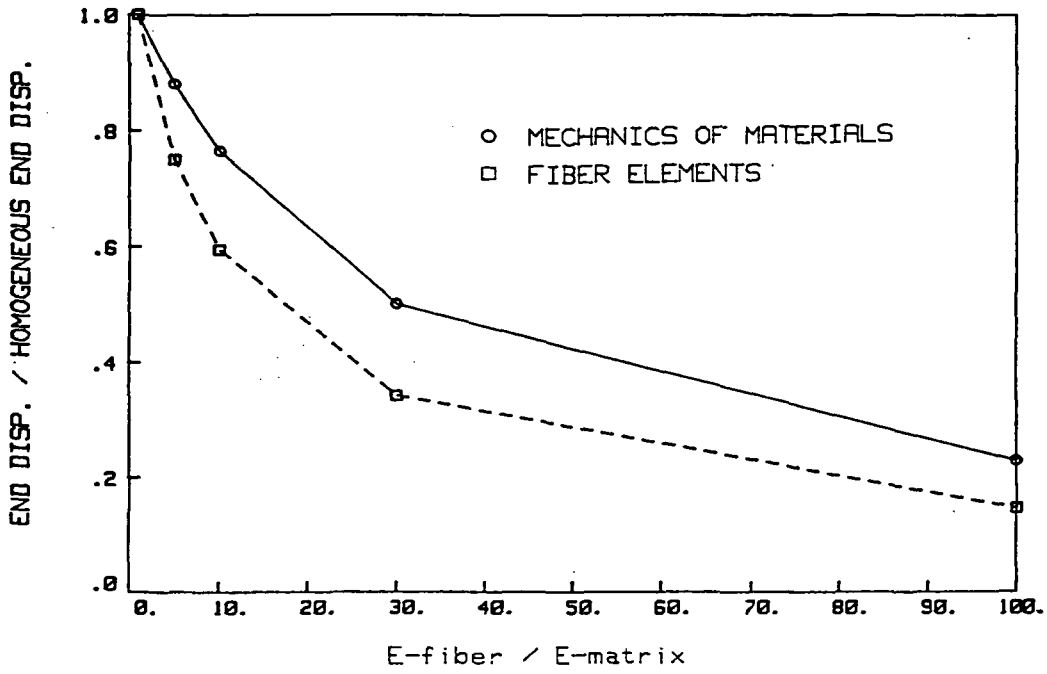

Fig. 8.6.2 Non-dimensionalized Vertical End Displacement of a Reinforced Beam in Bending vs. the Modulus of the Fiber Over Modulus of the Beam

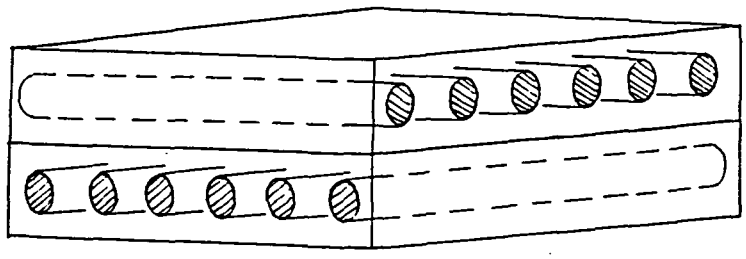

Fig. 8.7.1 Laminate-Fiber Composite

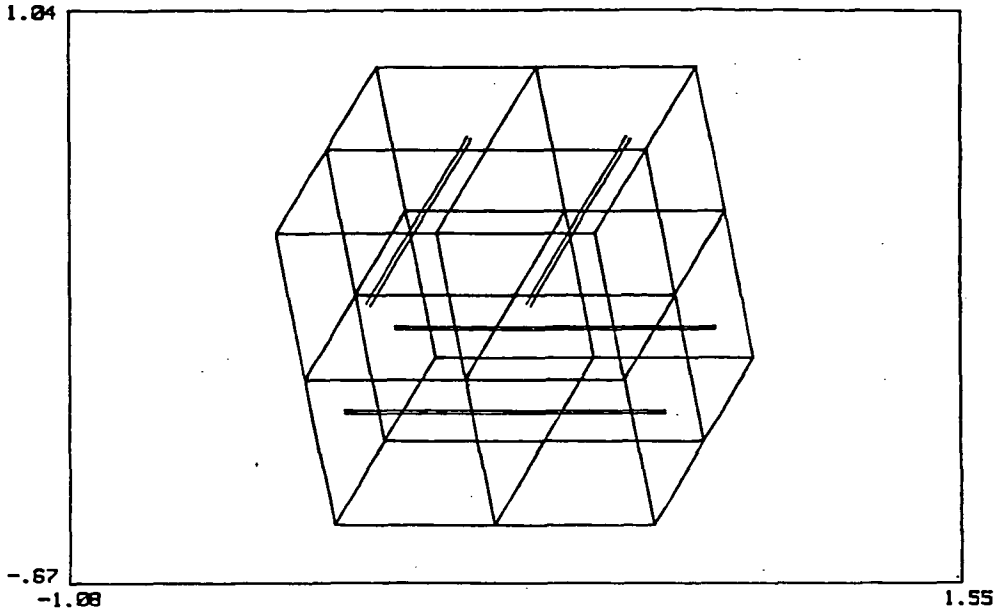

Fig. 8.7.2 BEM Discretization of a Laminate-Fiber Composite

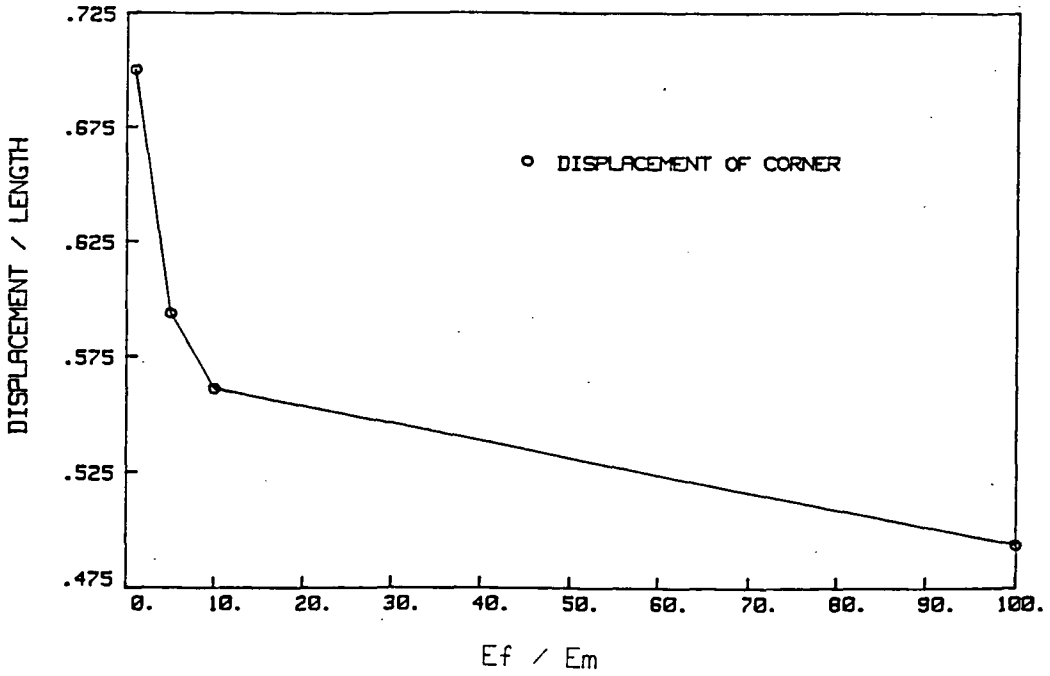

Fig. 8.7.3 Lateral Displacement of a Point at the Corner of the Interface of a Laminate-Fiber Composite Under Bi-axial Tension

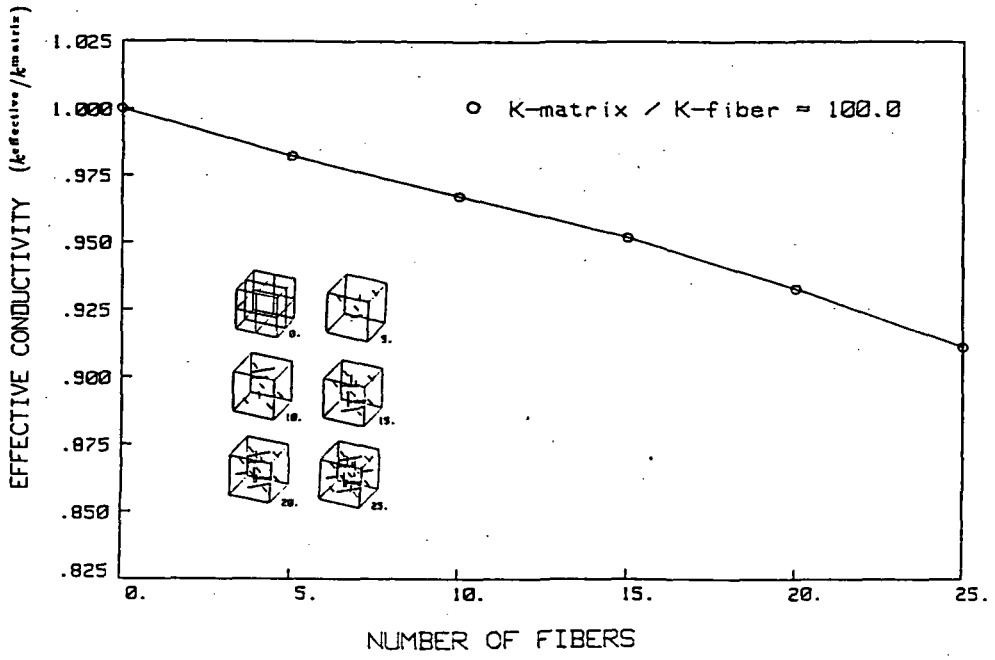

Fig. 8.8.1. Effective Conductivity of a Unit Cube with Random Oriented Fibers

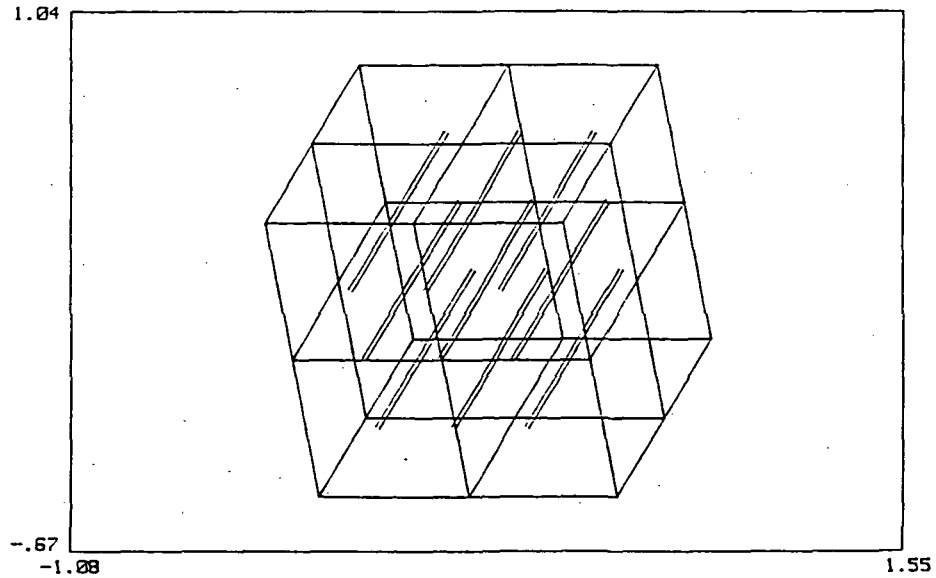

Fig. 8.9.1. Discretization of a Cube with Nine Quadratic Fiber Elements

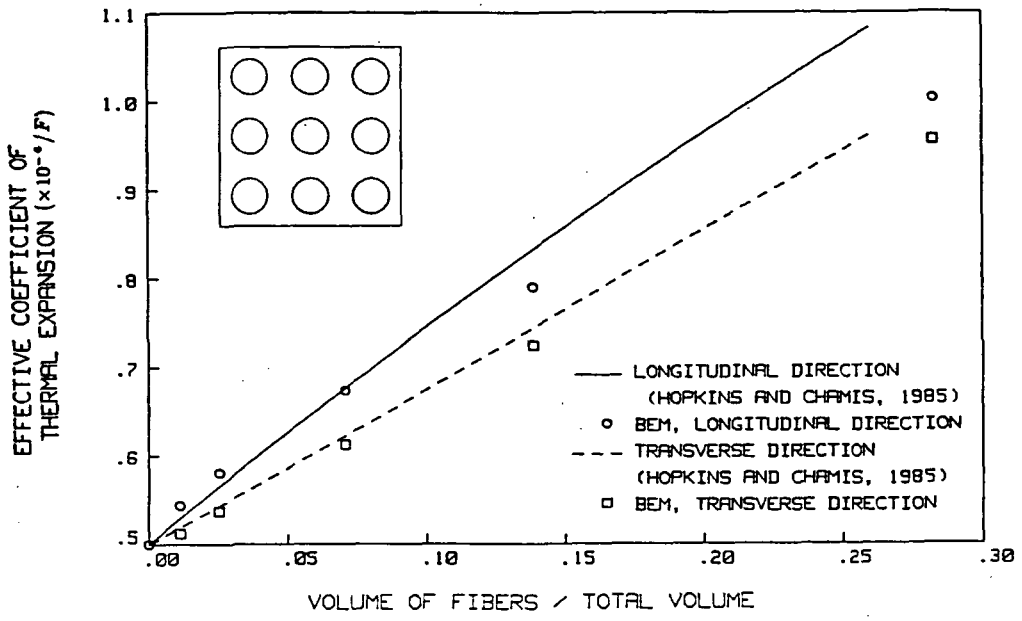

Fig. 8.9.2 Effective Coefficient of Thermal Expansion in a Cube for Various Fiber Diameters

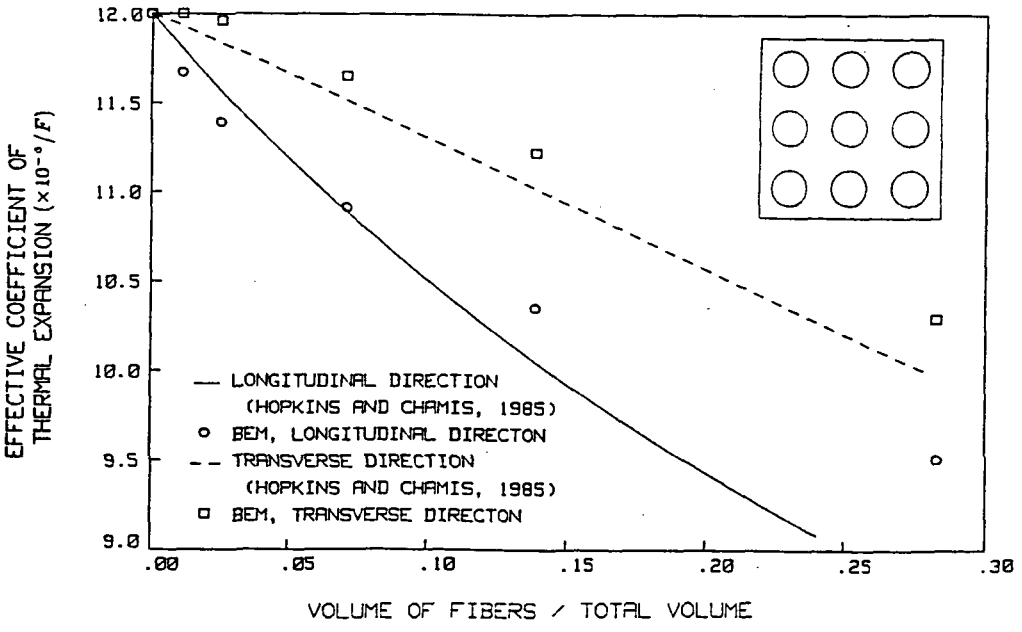

Fig. 8.9.3 Effective Coefficient of Thermal Expansion (in a Model of an Aluminum Cube with Nine Perfectly-bonded Steel Fibers) for Various Fiber Diameters

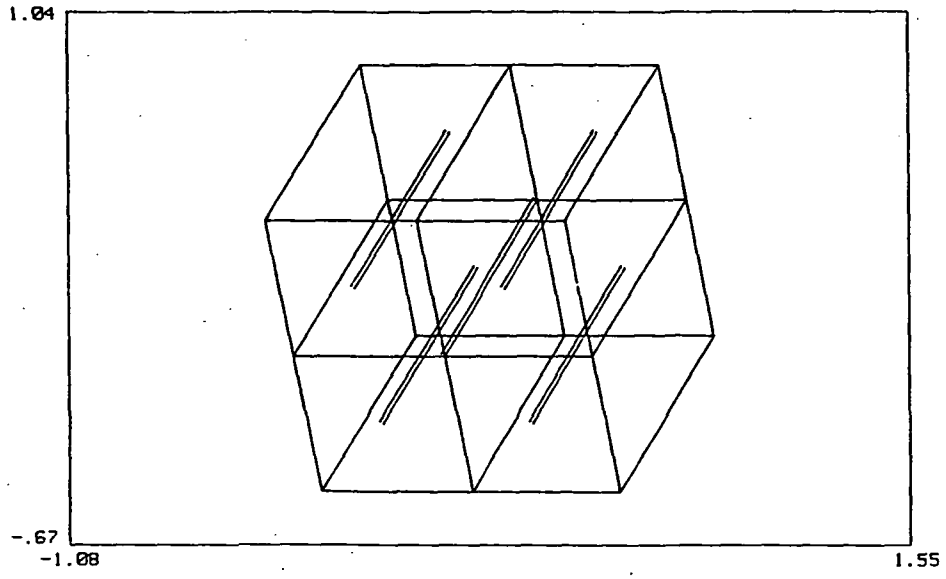

Fig. 8.10.1. Discretization of a Cube with Five Fibers Connected to the Matrix Through a Linear Constitutive Model

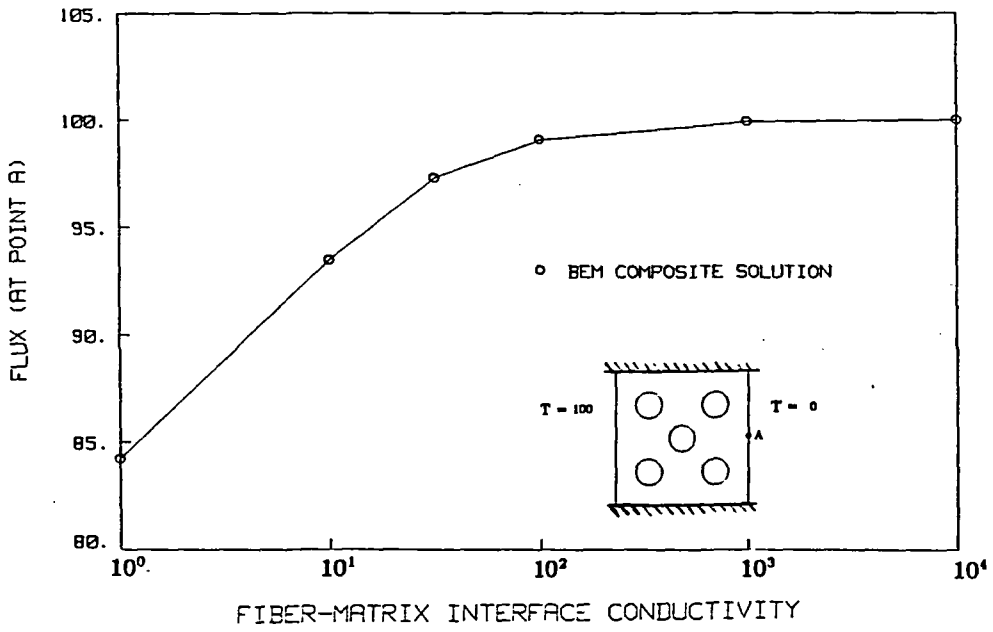

Fig. 8.10.2 Effect of a Thermal Resistant Fiber-matrix Interface on the Flux Through a Fiber Composite

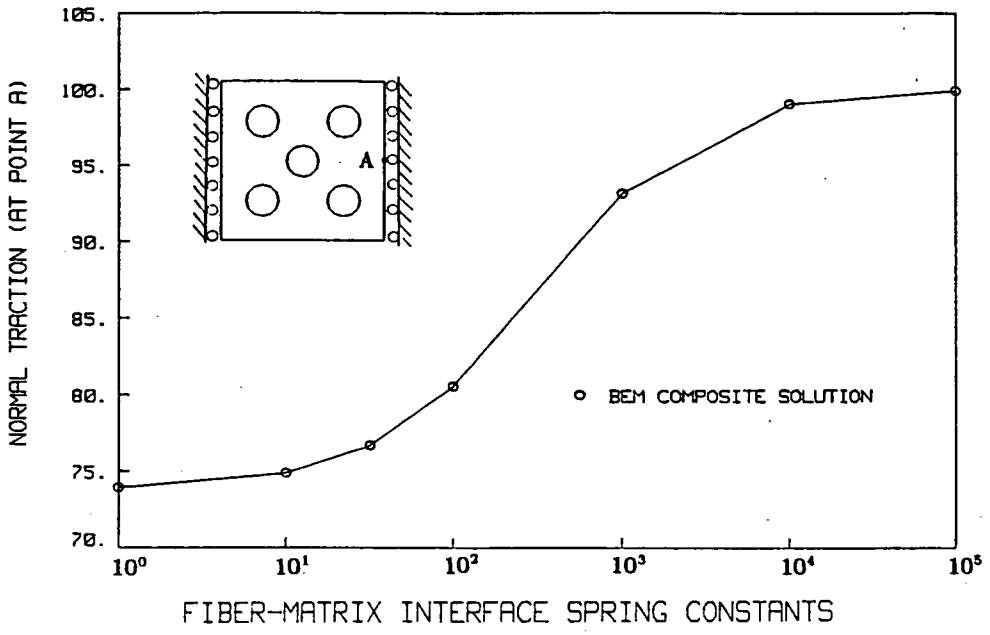

Fig. 8.11.1 Effect of a Spring Interface Between the Matrix and Fiber in a Cube Subjected to a Uniform Temperature Decrease

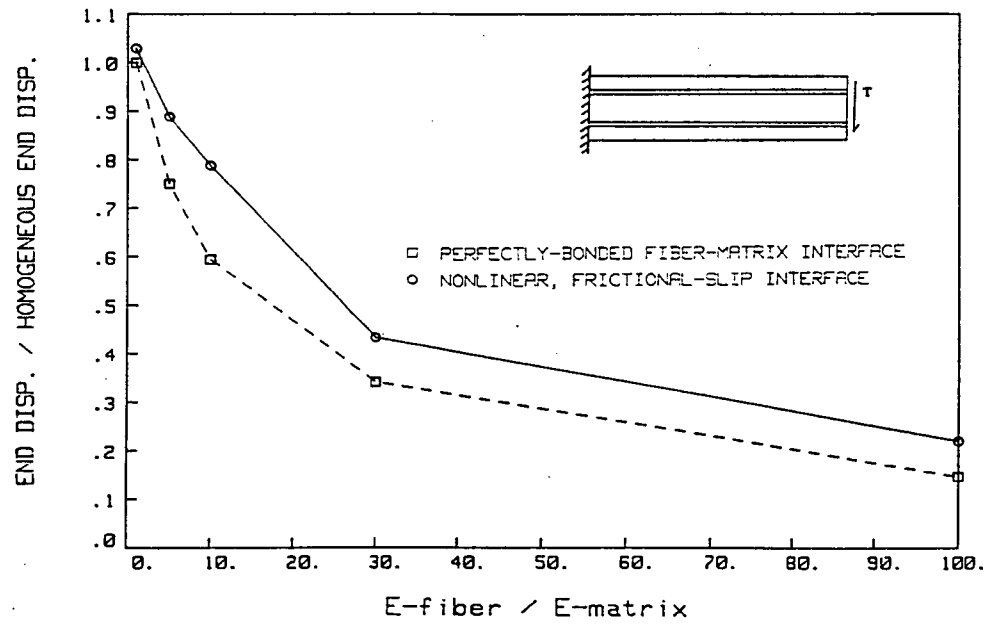

Fig. 8.12.1 Vertical End Displacement of a Beam in Bending with a Nonlinear, Frictional Interface Between the Four Fibers and the Matrix

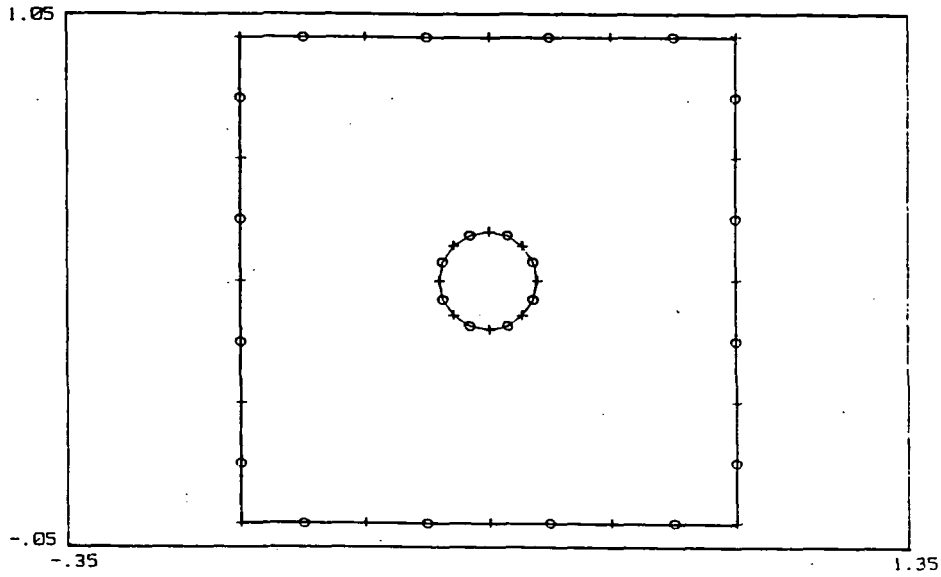

Fig. 8.13.1. Two-dimensional, Multi-region BEM Model of a Cube with a Single Fiber. (Fiber Volume/Total Volume = 0.031)

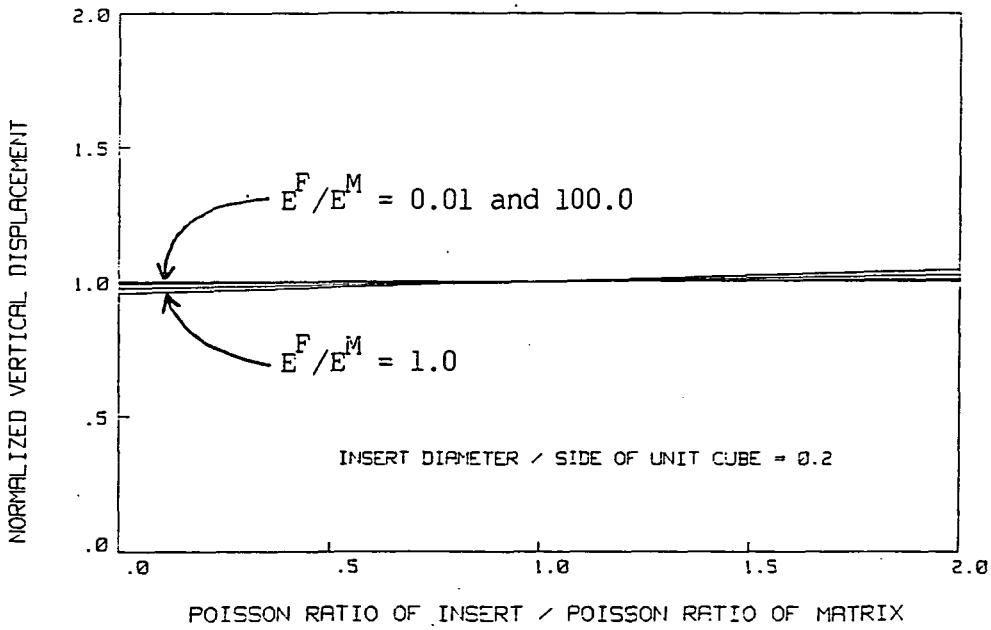

Fig. 8.13.2. Effect of Poisson Ratio on the Lateral Displacement of a Single-fiber Composite in Tension for Values of E^F/E^M of 0.01, 0.1, 1.0, 10.0, and 100.0

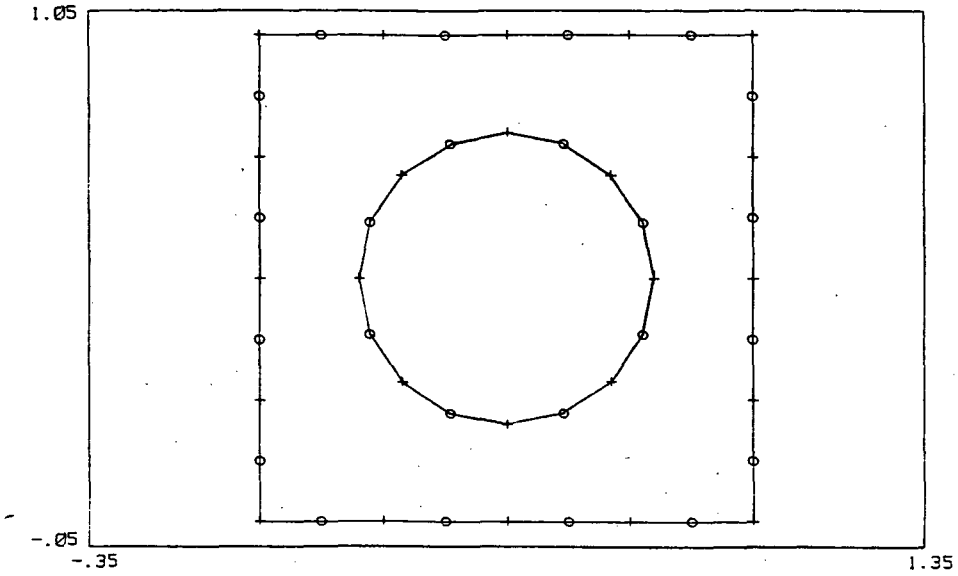

Fig. 8.13.3. Two-dimensional, Multi-region BEM Model of a Cube with a Single Fiber
(Fiber Volume/Total Volume = 0.283)

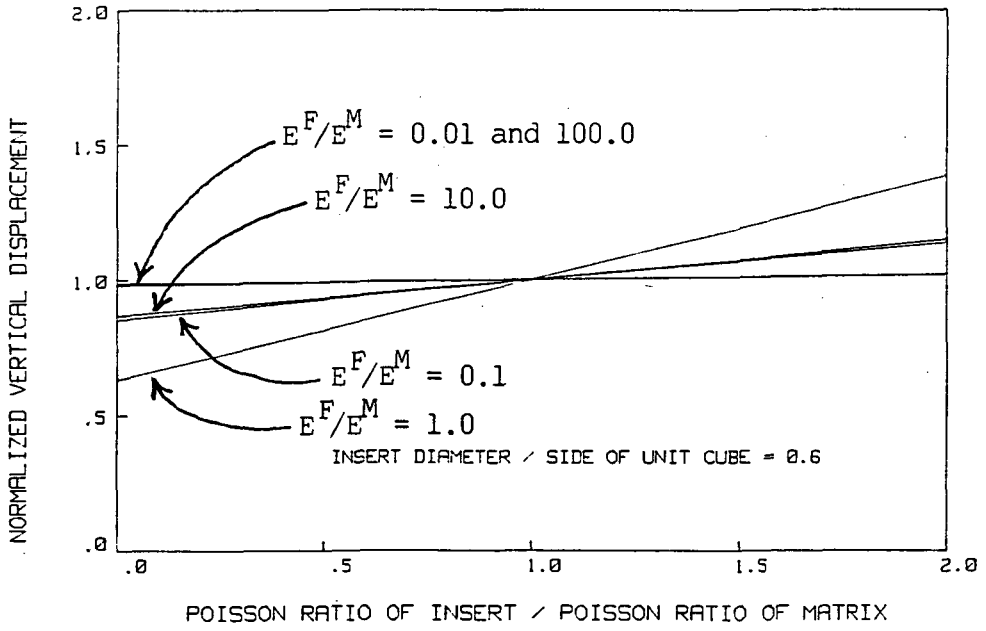

Fig. 8.13.4. Effect of Poisson Ratio on the Lateral Displacement of a Single-fiber Composite in Tension for values of E^F/E^M of 0.01, 0.1, 1.0, 10.0, and 100.0

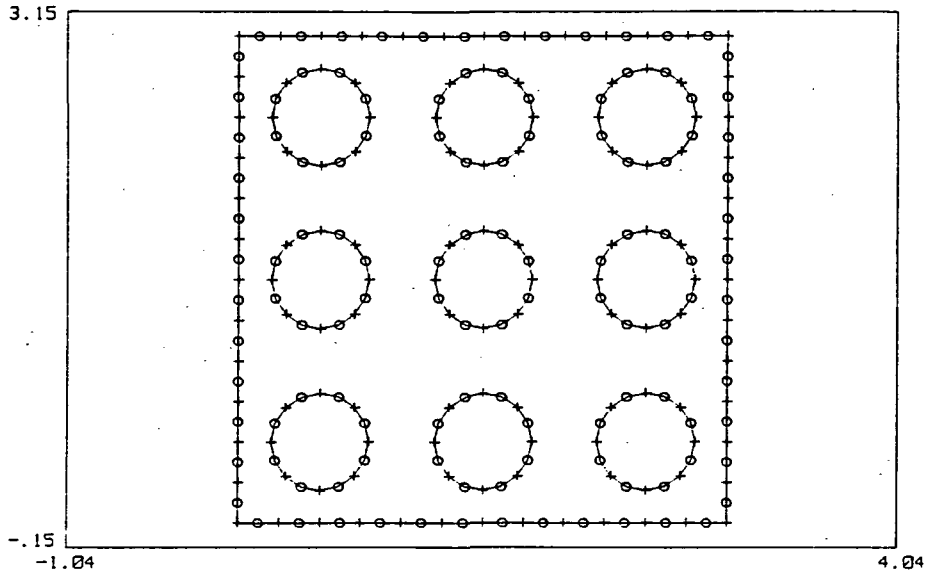

Fig. 8.13.5. Two-dimensional, Ten Region BEM Model of a Cube with Nine Fibers
(Fiber Volume/Total Volume = 0.283)

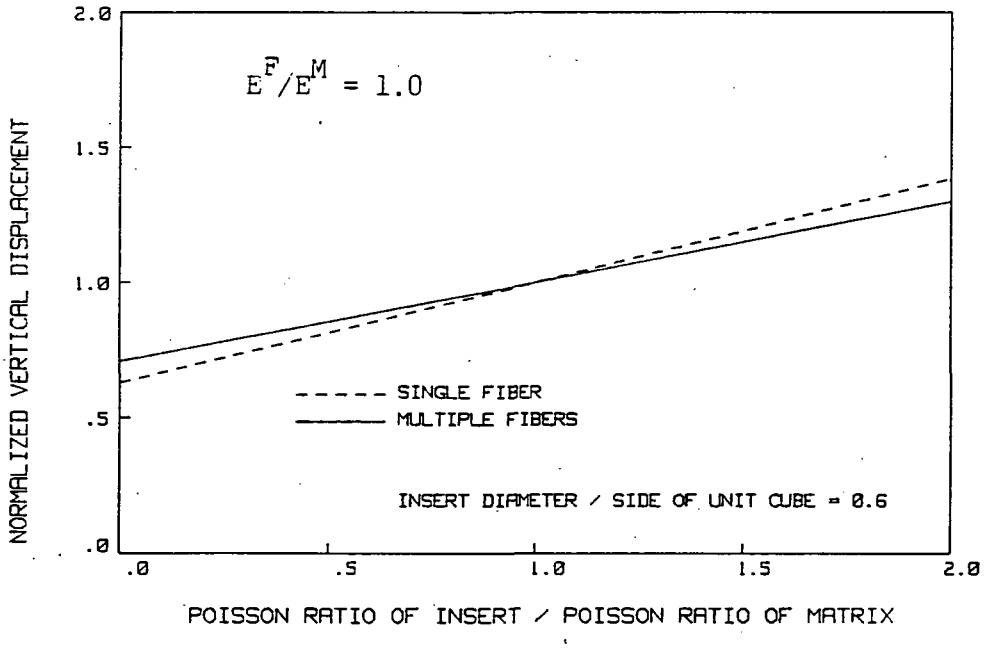

Fig. 8.13.6. Effect of Poisson Ratio on the Lateral Displacement of a Single-fiber Versus a Multi-fiber Composite in Tension with E^F/E^M = 1.0

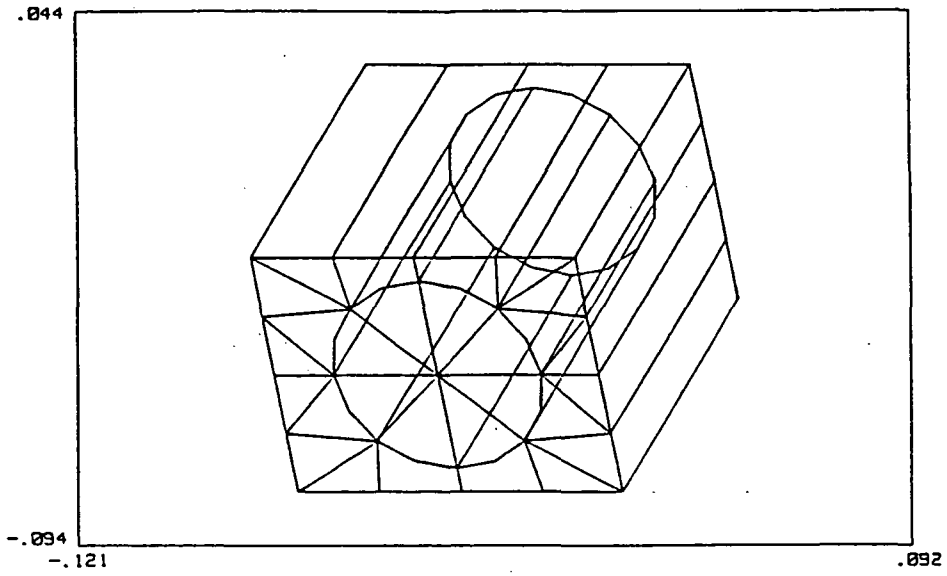

Fig. 8.14.1 Discretization of the Outer Surface of a Two-region Model Containing 50 Small Fibers (Small Fibers not shown)

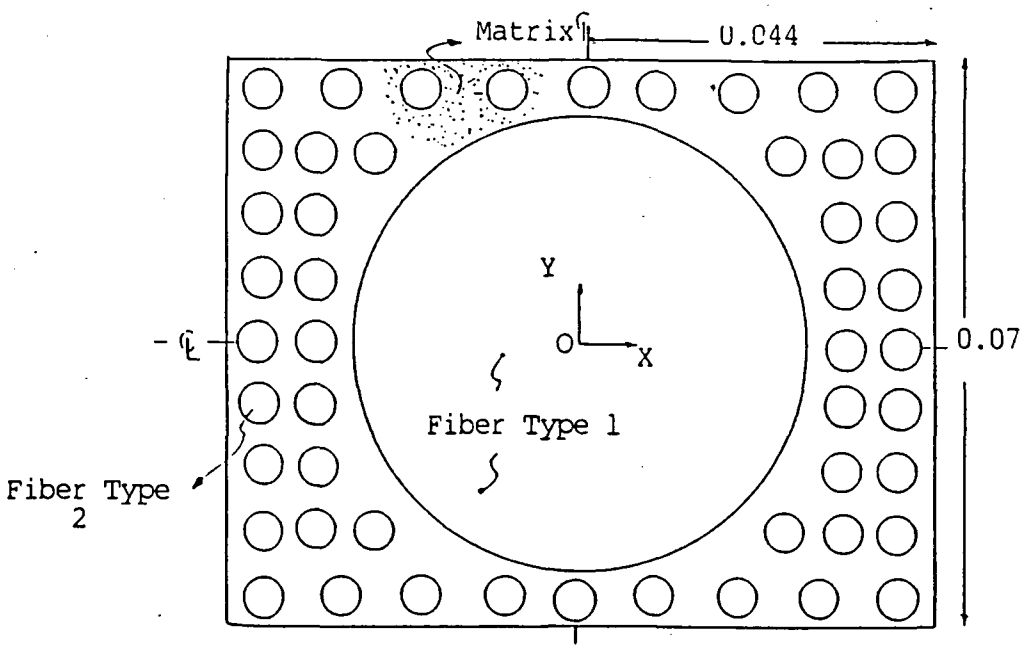

Fig. 8.14.2 Cross-section of the Composite Displaying the Arrangement of One Large (Type 1) Fiber and Fifty Small (Type 2) Fibers

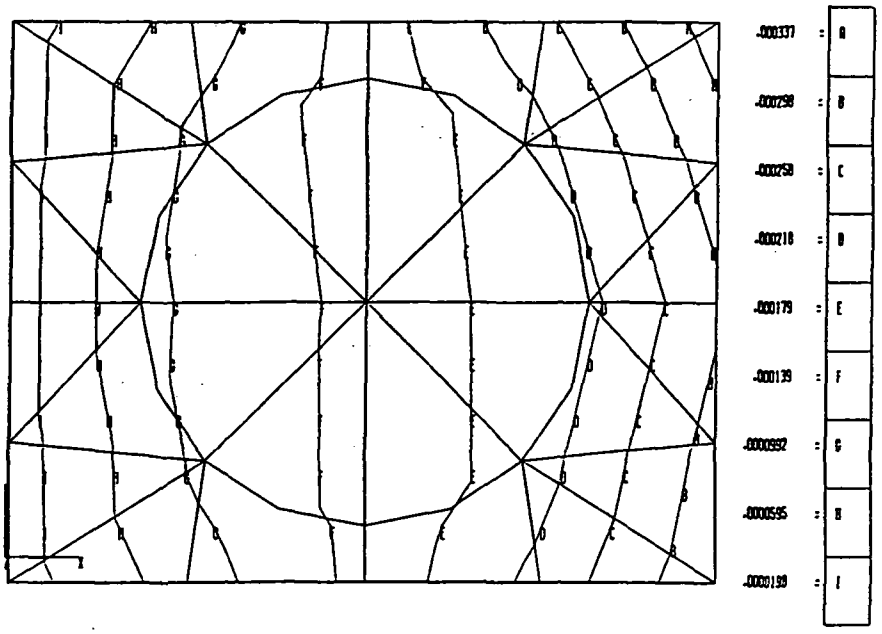

Fig. 8.14.3. Contours of Displacement in the Horizontal Direction Relative to the Page Due to a (Horizontal) Traction Loading

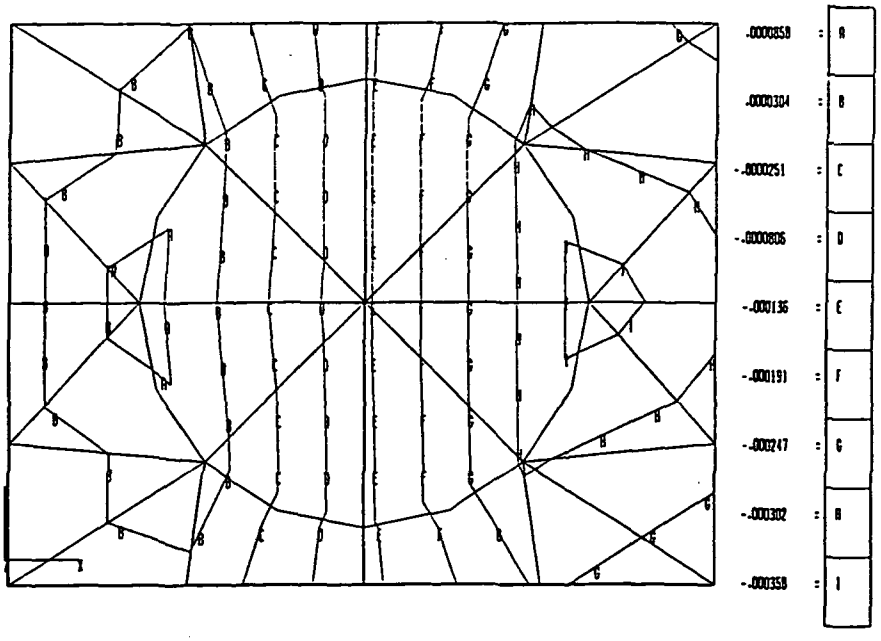

Fig. 8.14.4 Contours of Displacement in the Horizontal Direction Relative to the Page Due to a (Horizontal) Traction and Temperature Loading

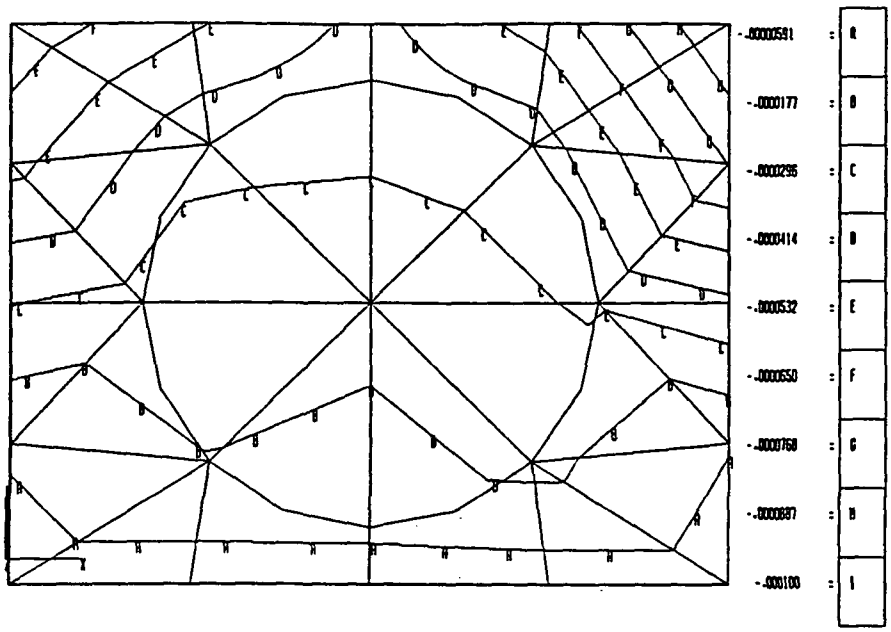

Fig. 8.14.5. Contours of Displacement in the Vertical Direction Relative to the Page Due to a (Horizontal) Traction Loading

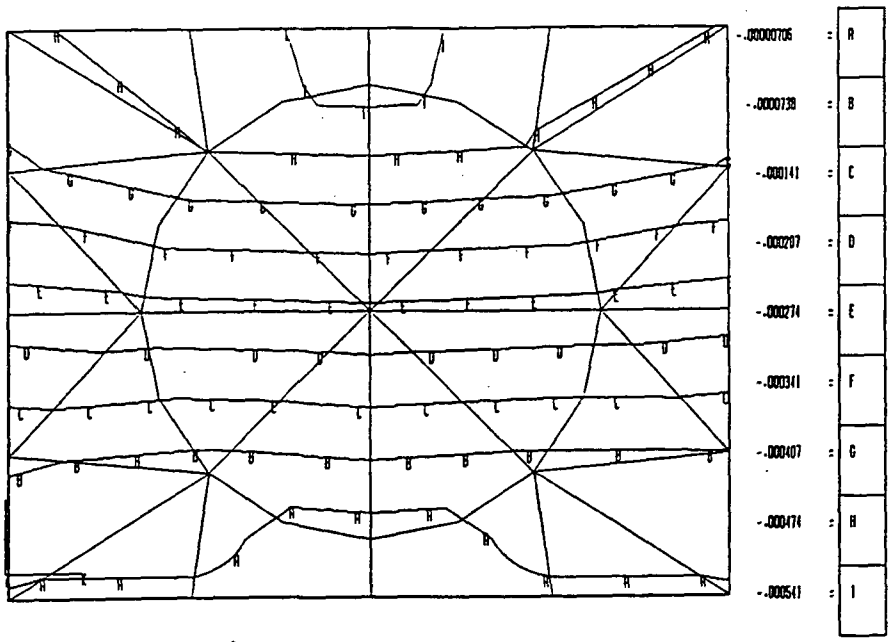

Fig. 8.14.6. Contours of Displacement in the Vertical Direction Relative to the Page Due to a (Horizontal) Traction and Temperature Loading

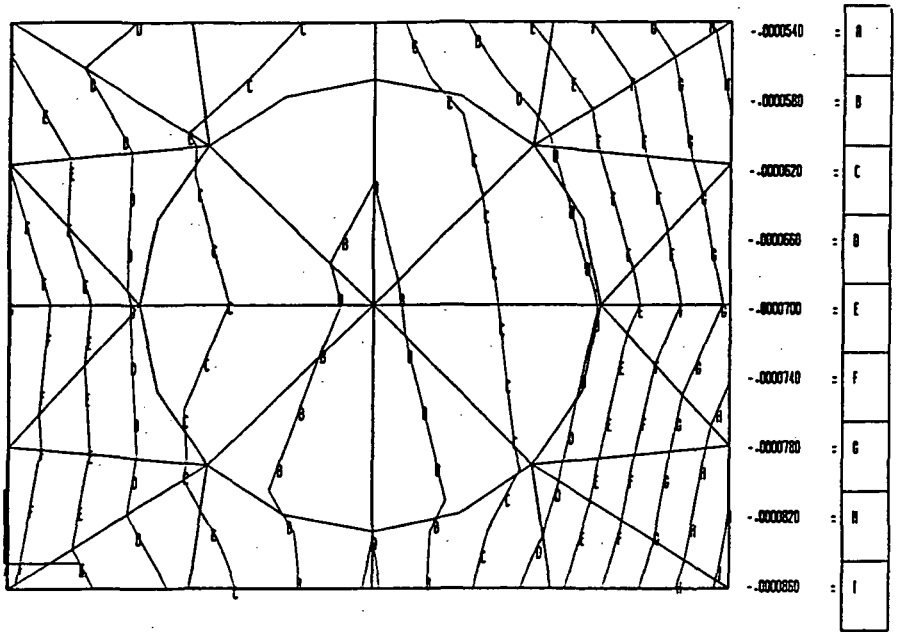

Fig. 8.14.7. Contours of Displacement in the Out of Plane Direction Due to a (Horizontal) Traction Loading

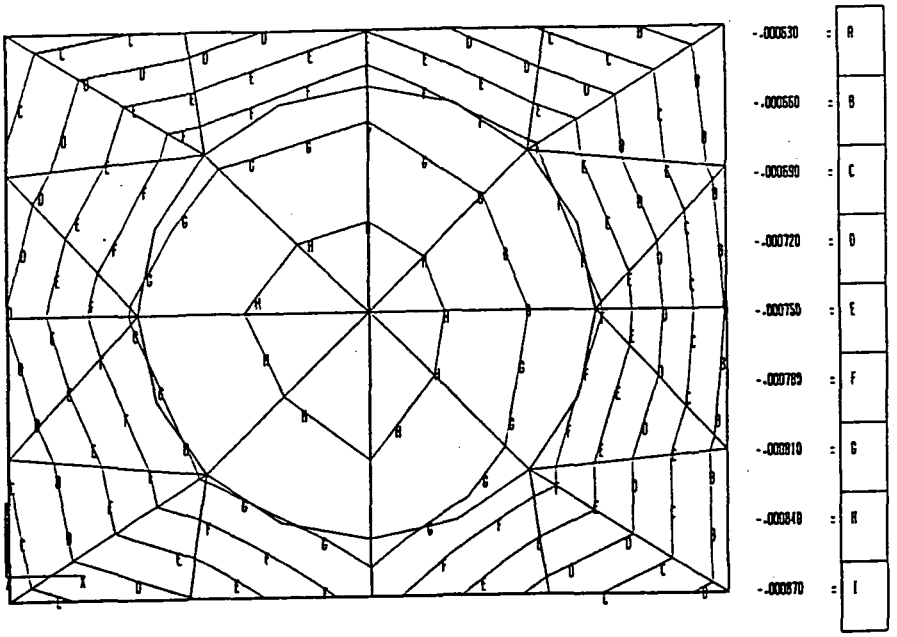

Fig. 8.14.8. Contours of Displacement in the Out of Plane Direction Due to a (Horizontal) Traction and Temperature Loading

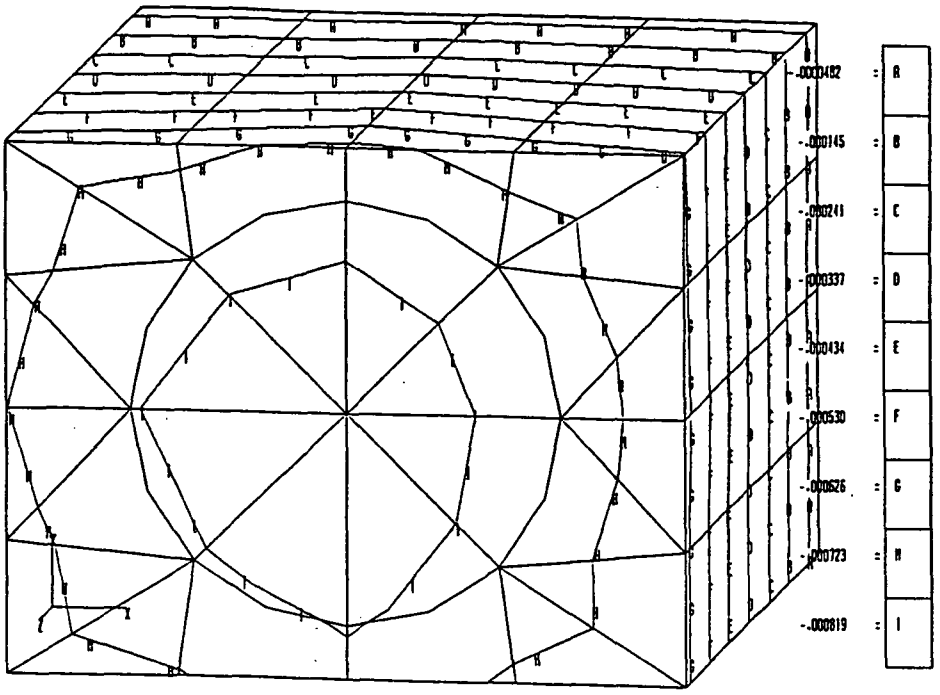

Fig. 8.14.9 Three-dimensional View: Contours of Displacement in the Out-of-Plane (z) Direction Due to a Traction (x-direction) and Temperature Loading

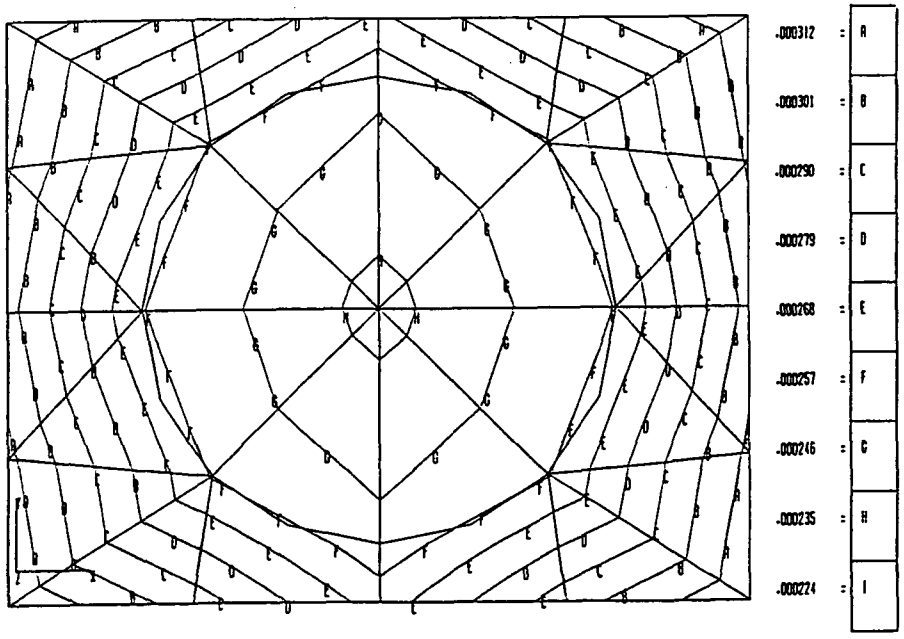

Fig. 8.14.10. Contours of Displacement in the Out-of-Plane Direction Due to a Traction in the Out-of-Plane Direction (Symmetric Boundary Conditions)

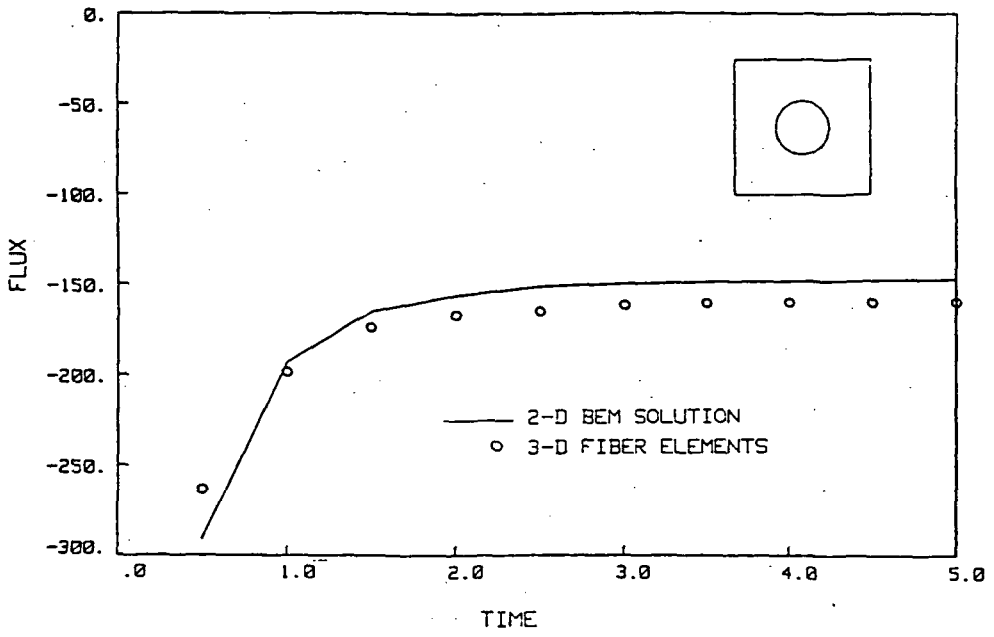

Fig. 8.15.1 Flux vs. Time: Transient Thermoelastic Analysis of A Cube with One Fiber

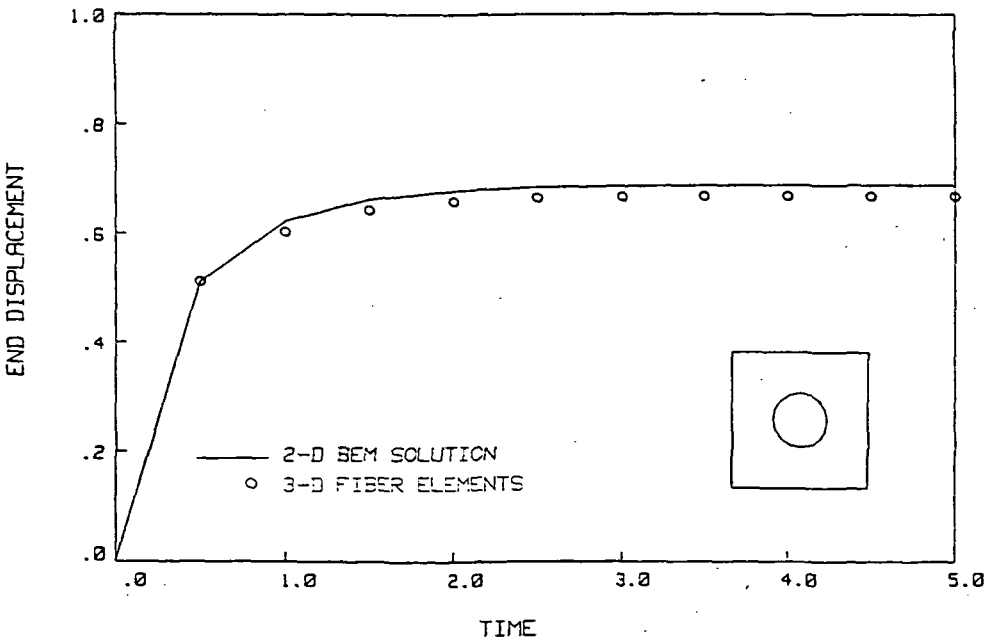

Fig. 8.15.2 End Displacement vs. Time: Transient Thermoelastic Analysis of a Cube with One Fiber

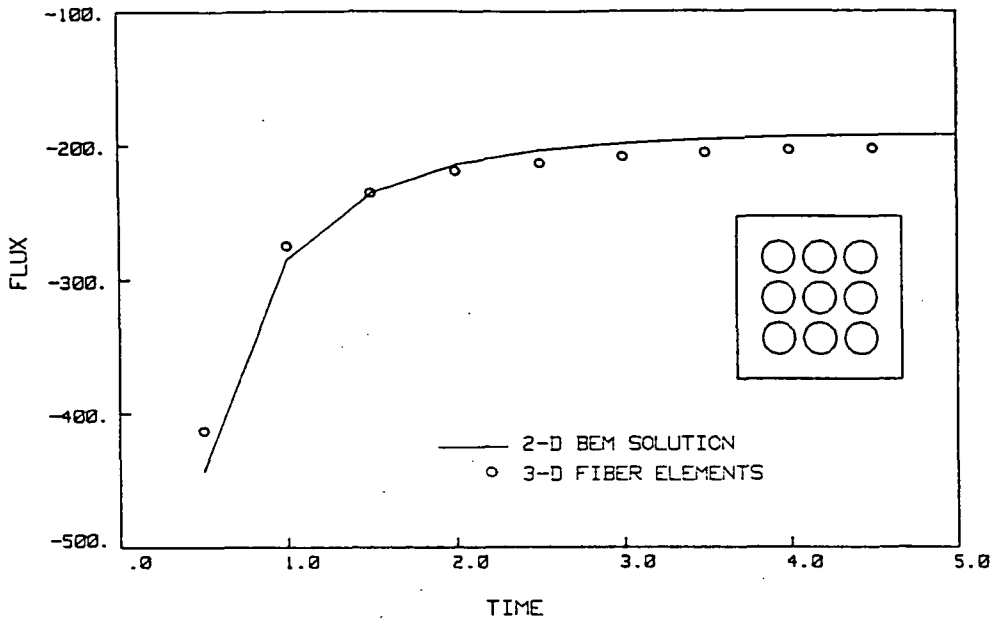

Fig. 8.15.3 Flux vs. Time: Transient Thermoelastic Analysis of a Cube with Nine Fibers

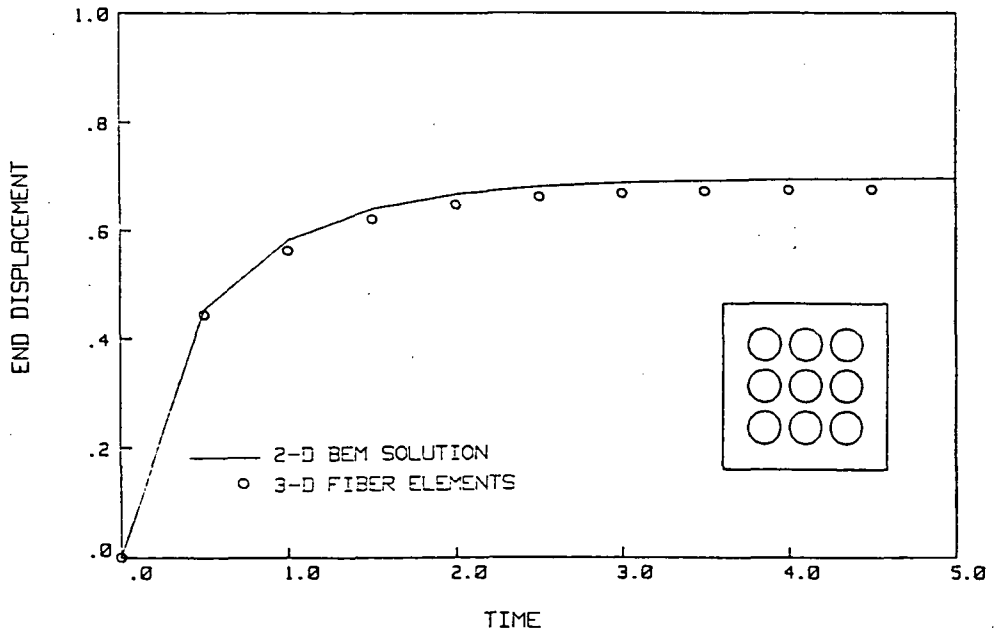

Fig. 8.15.4 End Displacement vs. Time: Transient Thermoelastic Analysis of a Cube with Nine Fibers

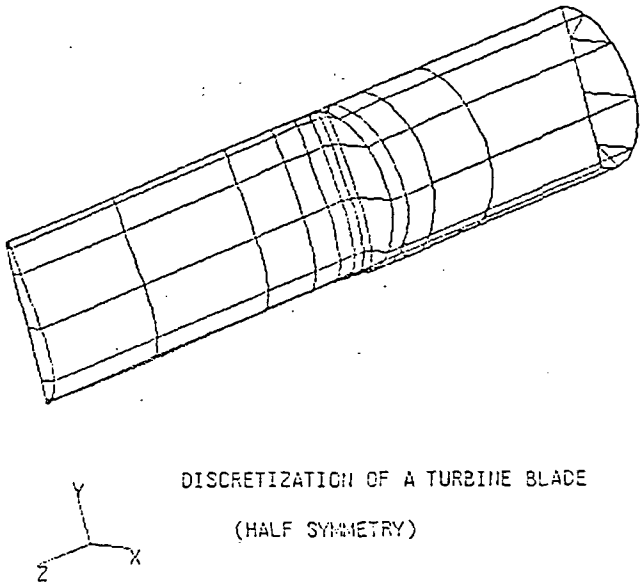

Fig. 8 .16.1 Discretization of a Turbine Blade
(Fiber Elements Not Shown)

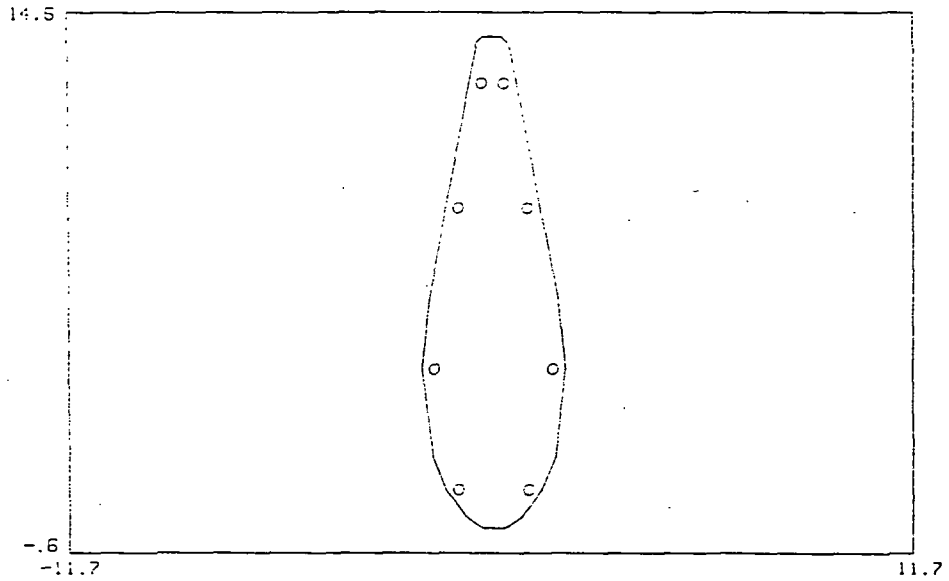

Fig. 8.16.2 Cross-Sectional View of the Turbine Blade
Displaying the Location of the Eight Fibers

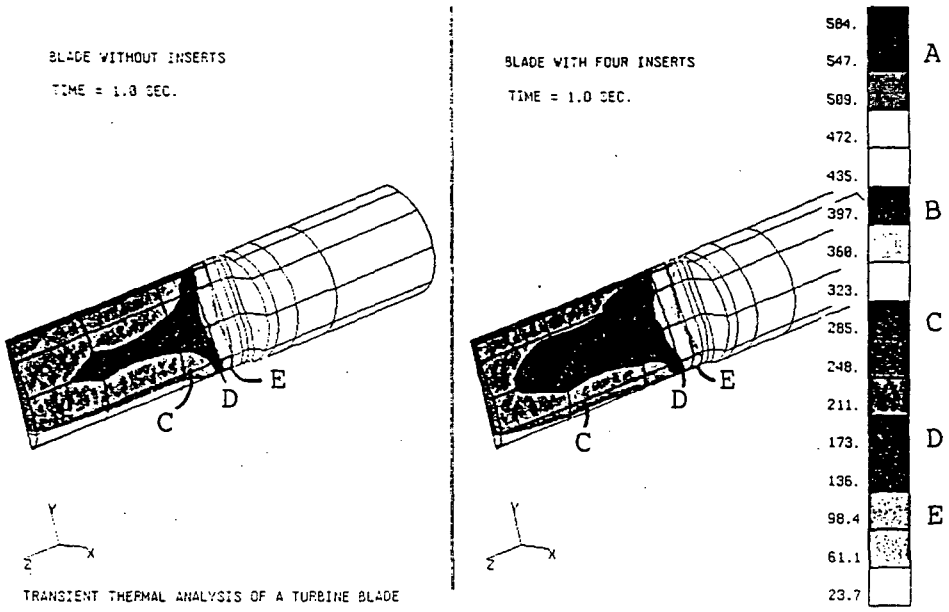

Fig. 8.16.3 Transient Heat Conduction Analysis of a Turbine Blade at 1 Second (Contour Plots of Temperature)

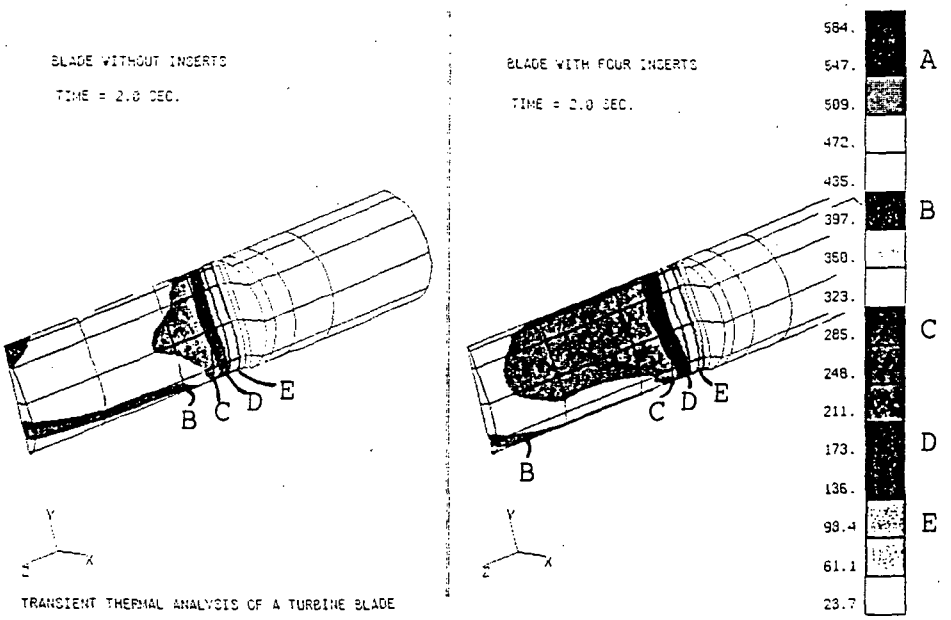

Fig. 8.16.4 Transient Heat Conduction Analysis of a Turbine Blade at 2 Seconds (Contour Plots of Temperature)

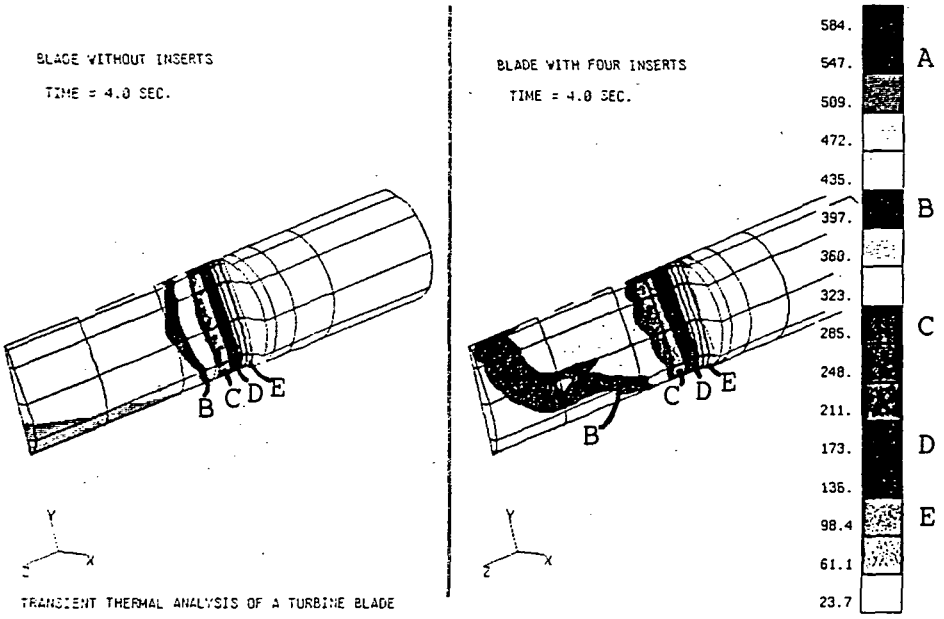

Fig. 8.16.5 Transient Heat Conduction Analysis of a Turbine Blade at 4 Seconds (Contour Plots of Temperature)

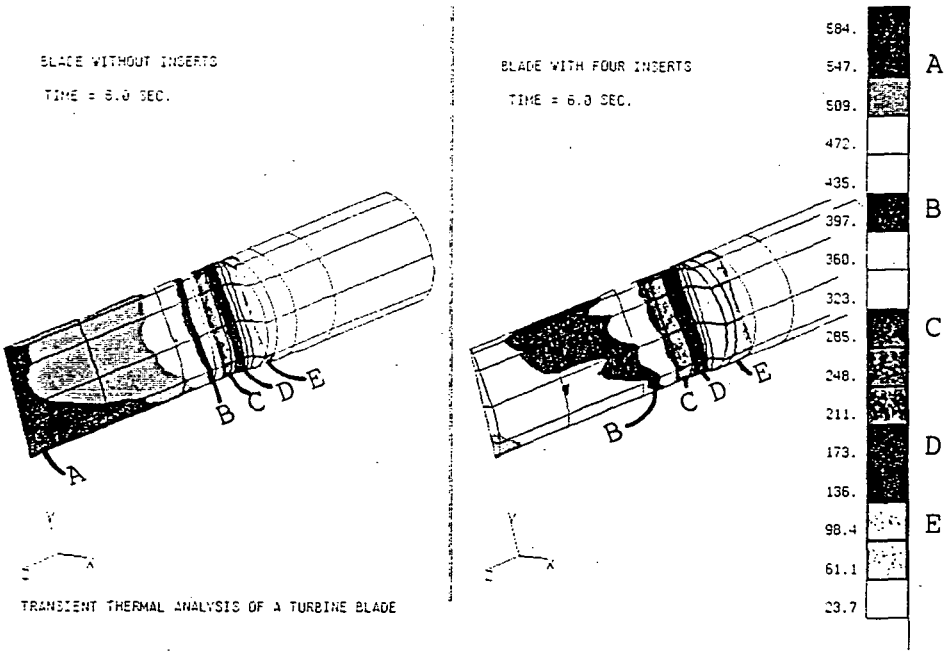

Fig. 8.16.6 Transient Heat Conduction Analysis of a Turbine Blade at 6 Seconds (Contour Plots of Temperature)

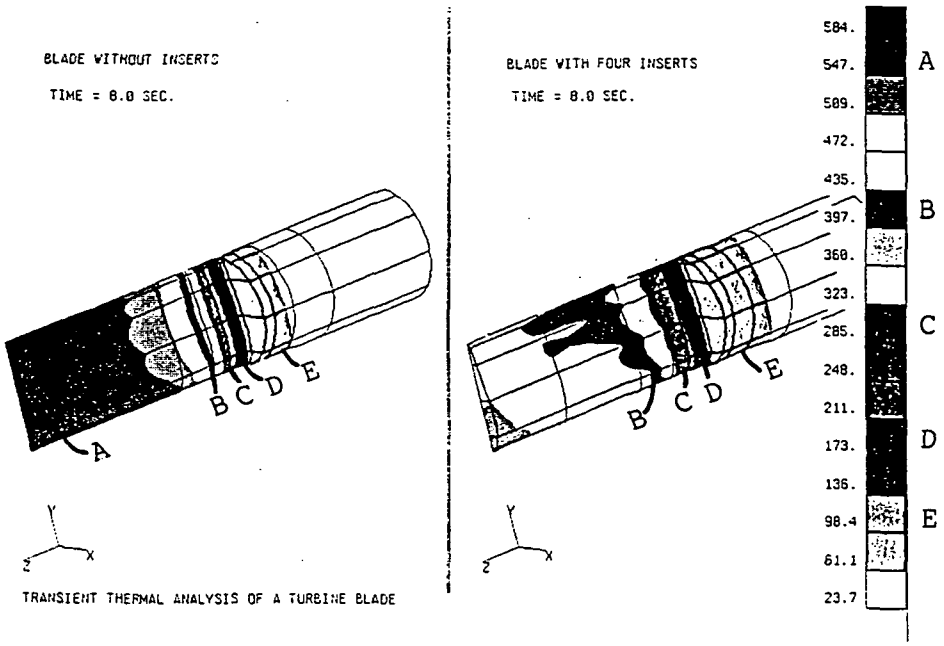

Fig. 8.16.7 Transient Heat Conduction Analysis of a Turbine Blade at 8 Seconds
(Contour Plots of Temperature)

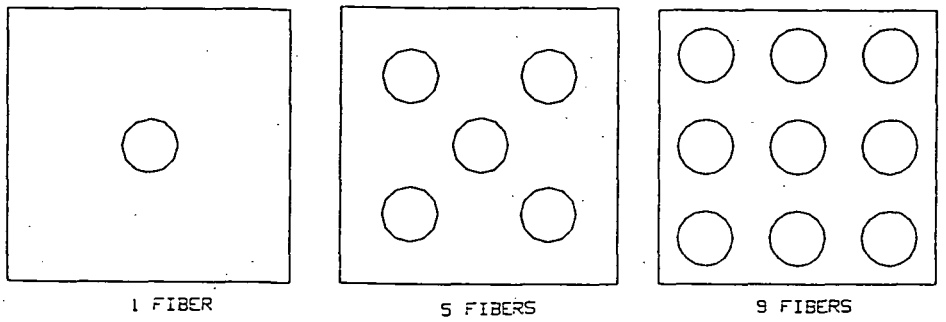

Fig. 8.17.1 Arrangement of Multiple Fibers in a Unit Cube

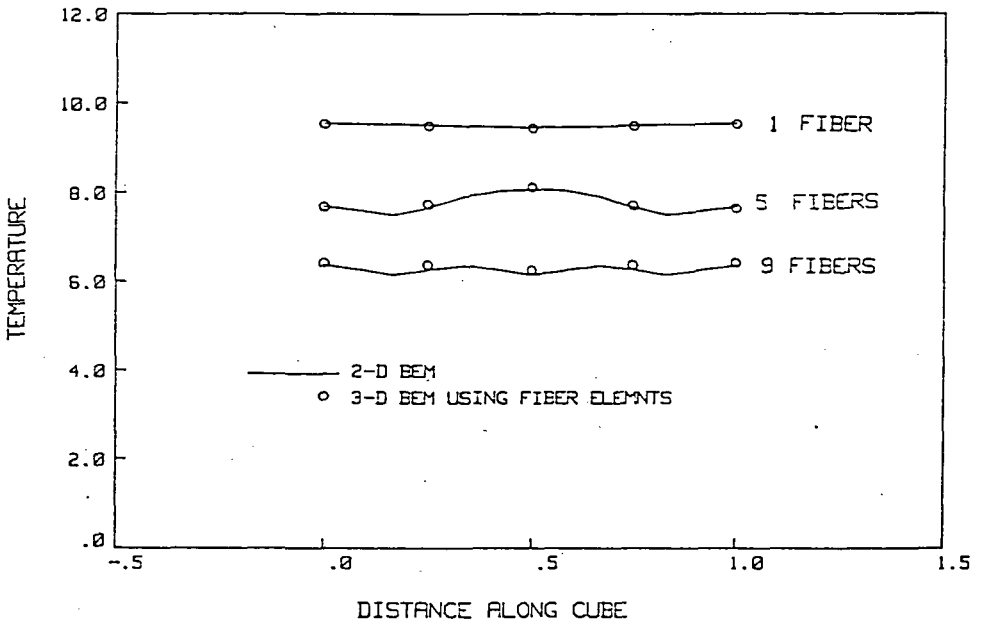

Fig. 8.17.2 Temperature Profile in a Cube for Multiple Fiber Arrangements

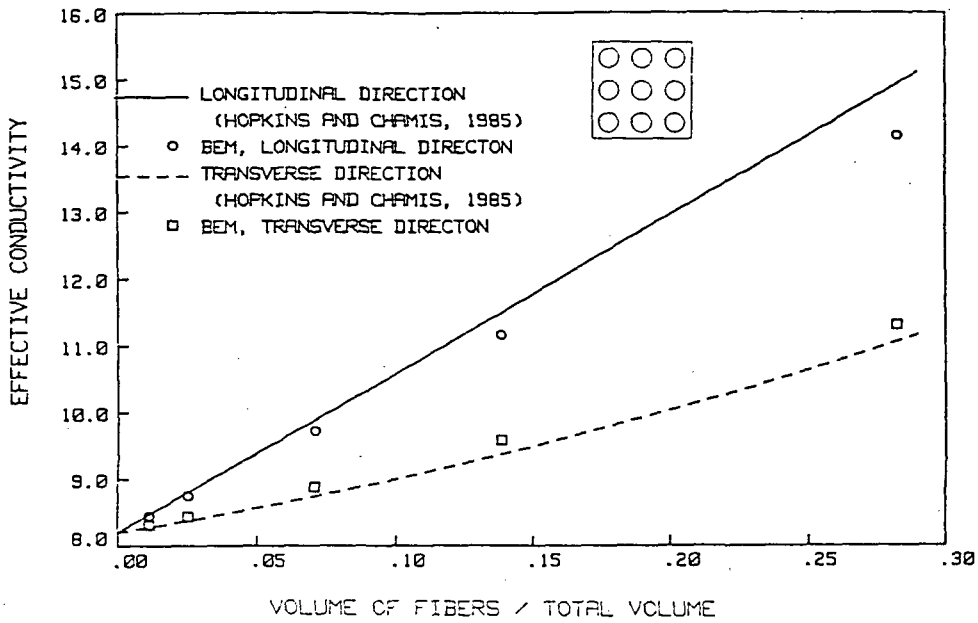

Fig. 8.18.1 Effective Conductivity in a Cube for Various Fiber Diameters

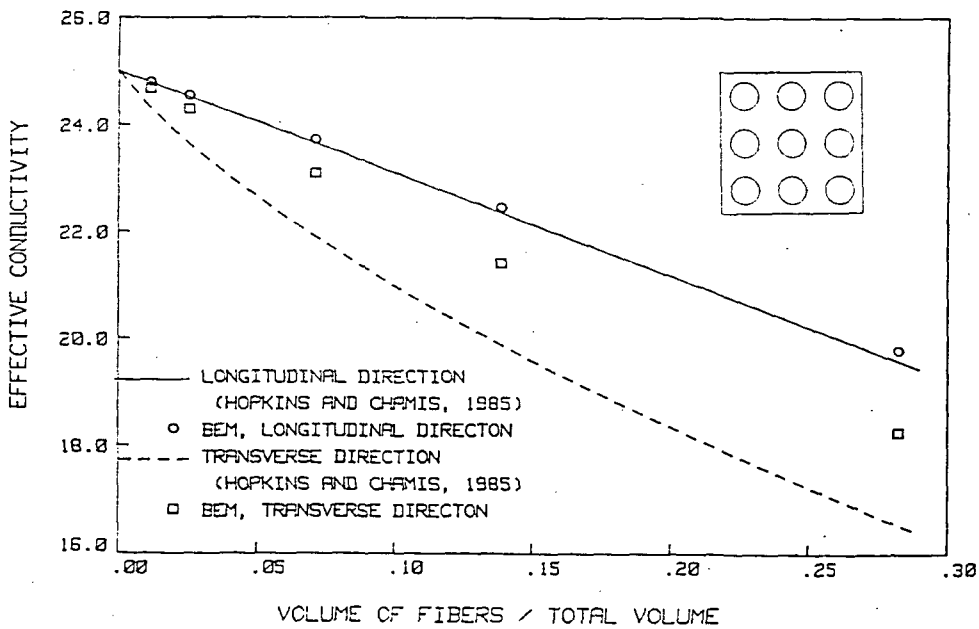

Fig. 8.18.2 Effective Conductivity in a Cube for Various Fiber Diameters

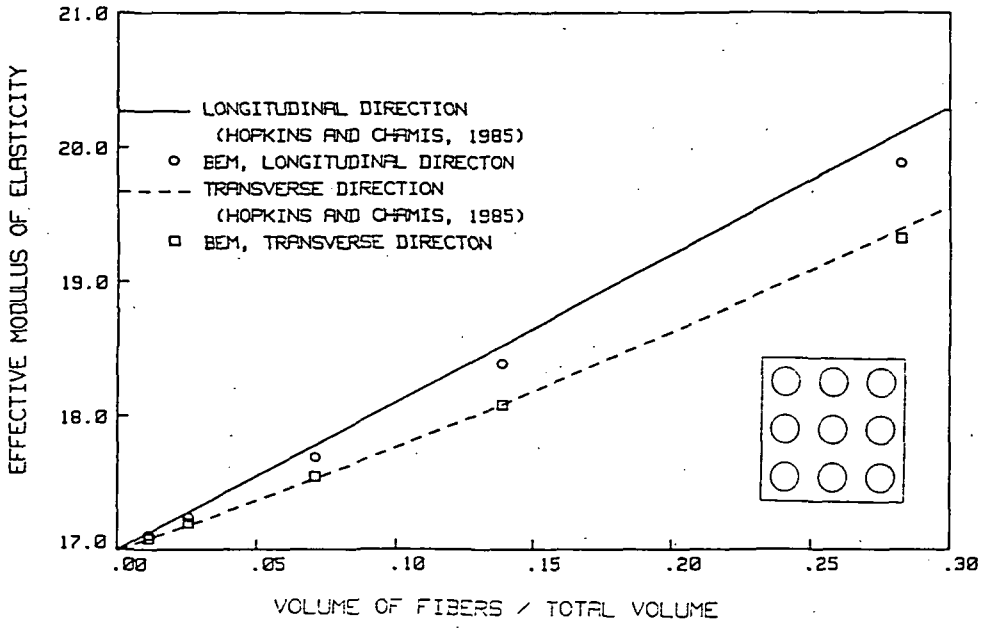

Fig. 8.19.1 Effective Modulus of Elasticity in a Cube for Various Fiber Diameters

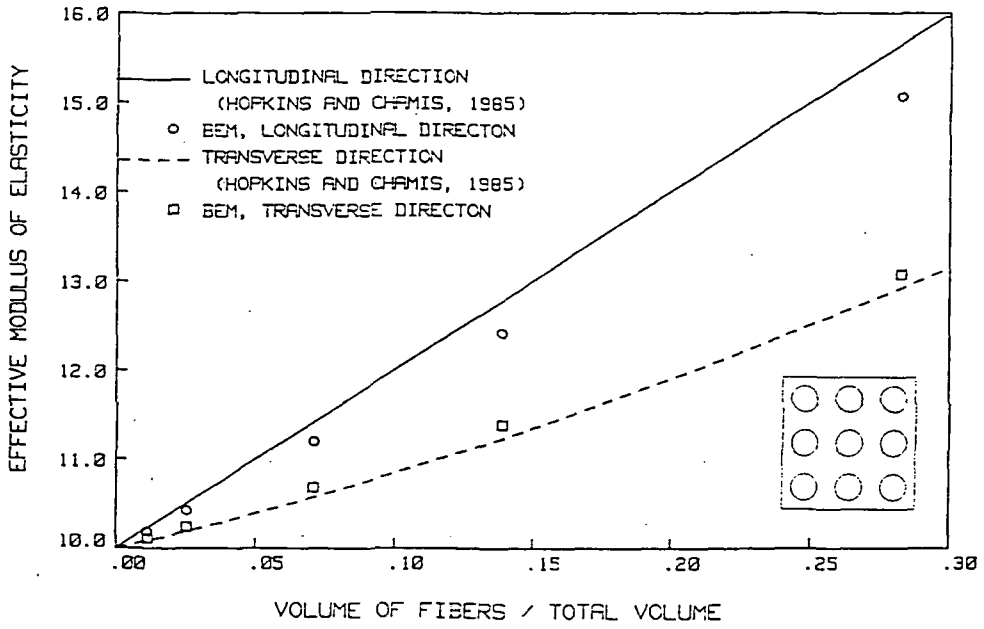

Fig. 8.19.2 Effective Modulus of Elasticity in a Cube for Various Fiber Diameters

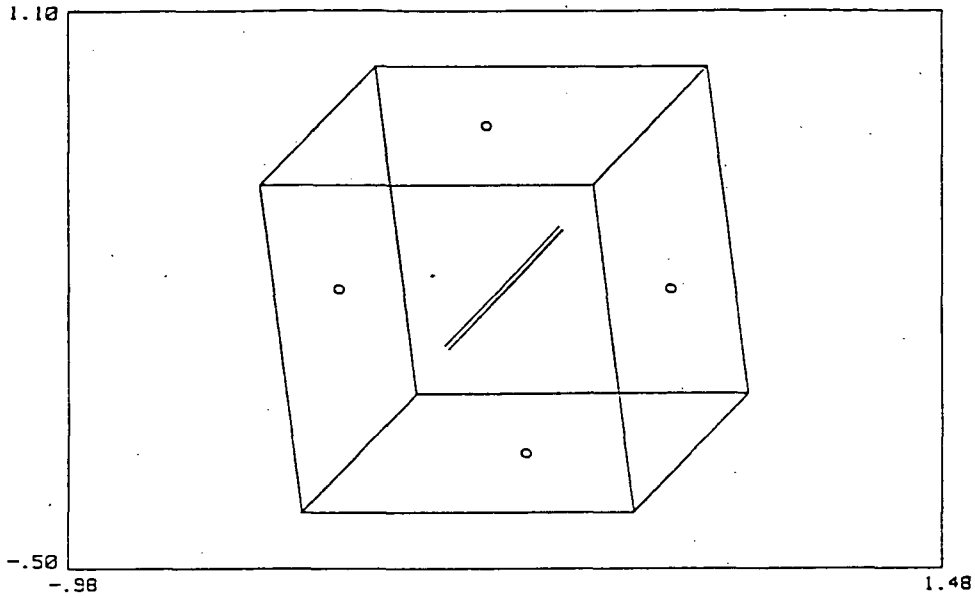

Fig. 8.20.1 Discretization of a Fiber in a Unit Cube Using Fiber Elements (includes a cylindrical volume cell not shown)

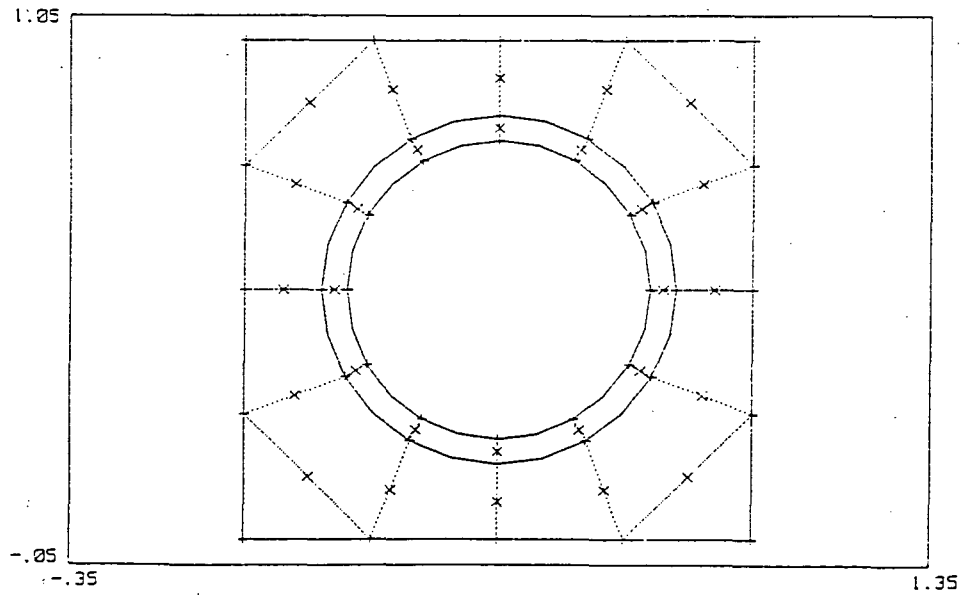

Fig. 8.20.2 Two-dimensional Discretization of a Cube with a Fiber; Two-dimensional Volume Cells are Shown

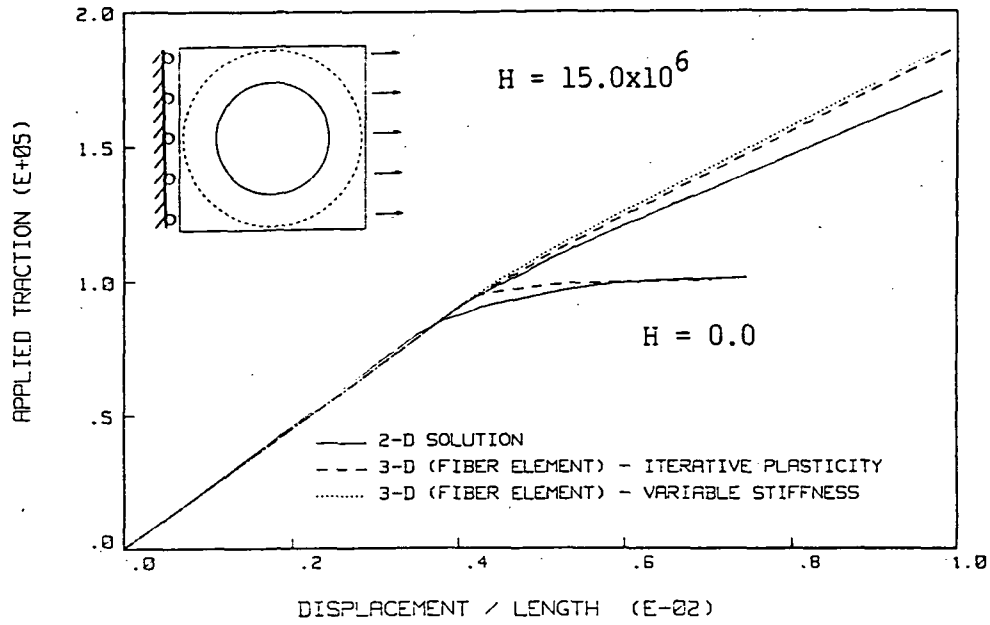

Fig. 8.20.3 Load vs. Displacement Response in a Fiber Composite With and Without Strain Hardening

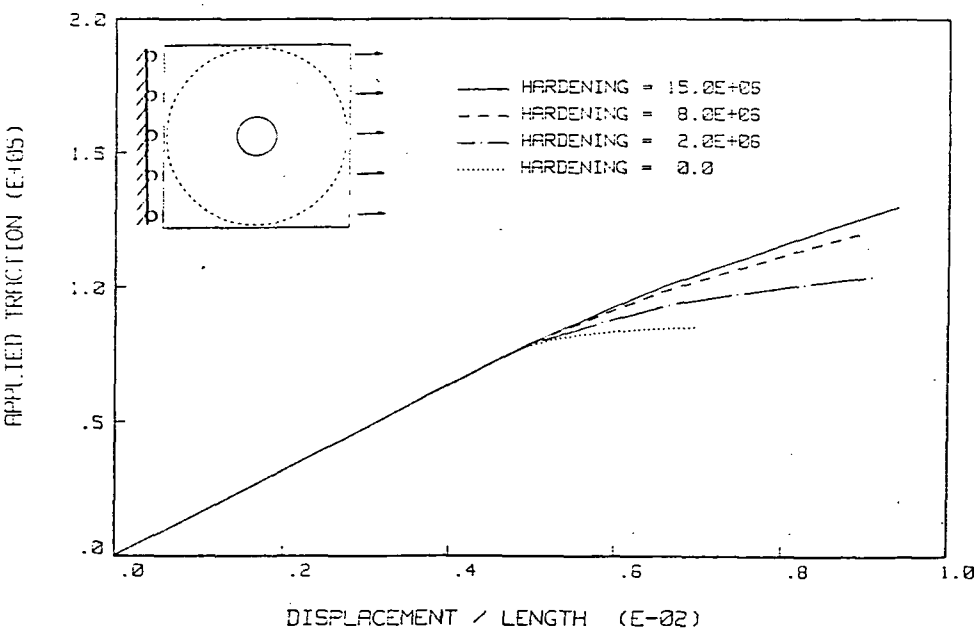

Fig. 8.21.1 Load vs. Displacement Response in a Fiber Composite for Various Strain Hardening Parameters

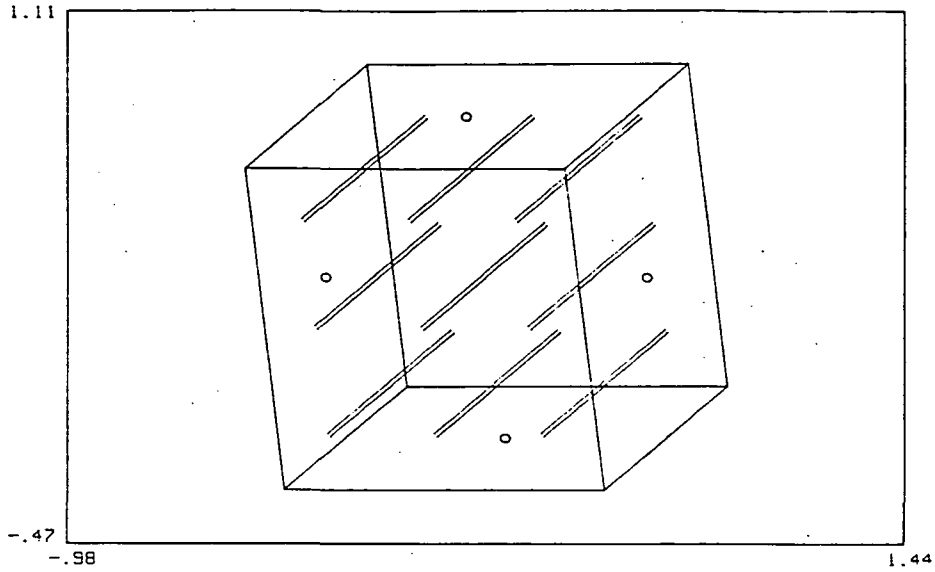

Fig. 8.22.1 Discretization of Nine Fibers in a Unit Cube using Fiber Elements (includes cylindrical volume cells not shown)

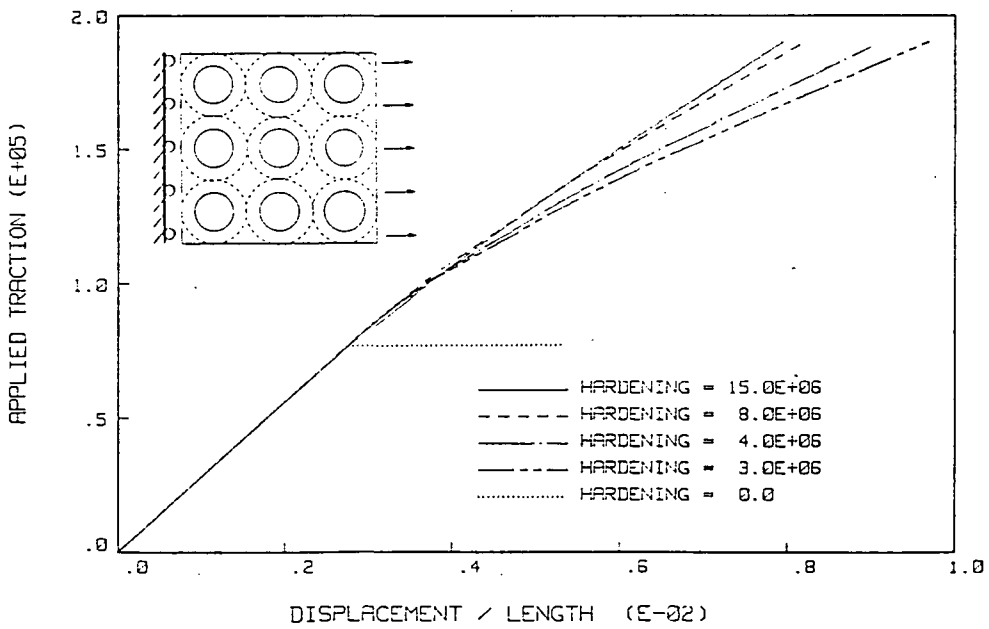

Fig. 8.22.2 Load vs. Displacement Response in a Fiber Composite for Various Strain Hardening Parameters

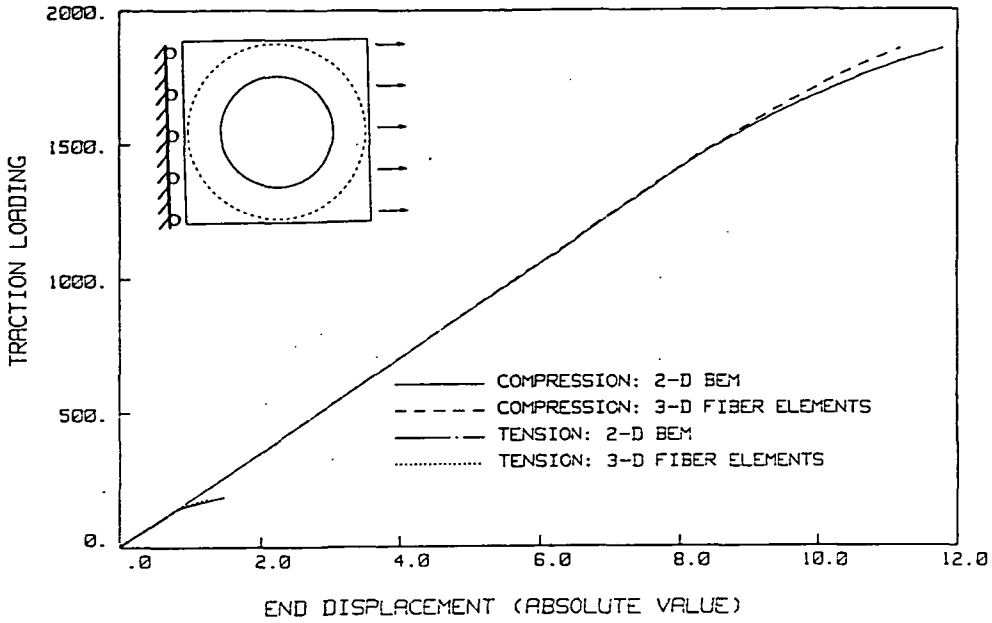

Fig. 8.23.1 Elastoplastic-Fracture Load vs. Displacement Behavior in a Fiber Composite. Response under a Tensile Load and a Compression Load are both shown.

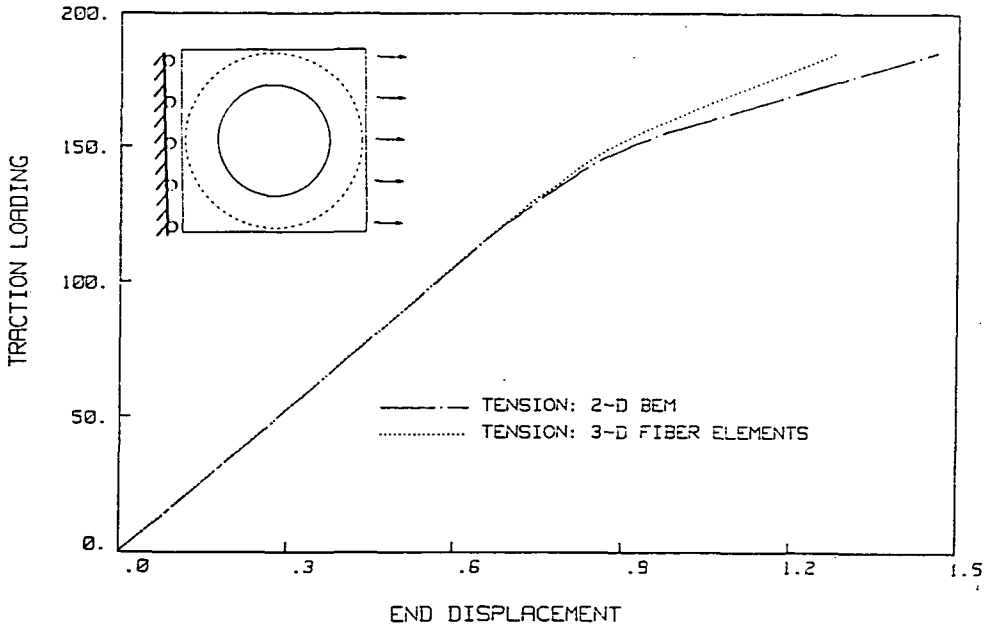

Fig. 8.23.2 Close-up of the Elastoplastic-Fracture Load vs. Displacement Response of the Tensile Load of Fig. 8.23.1

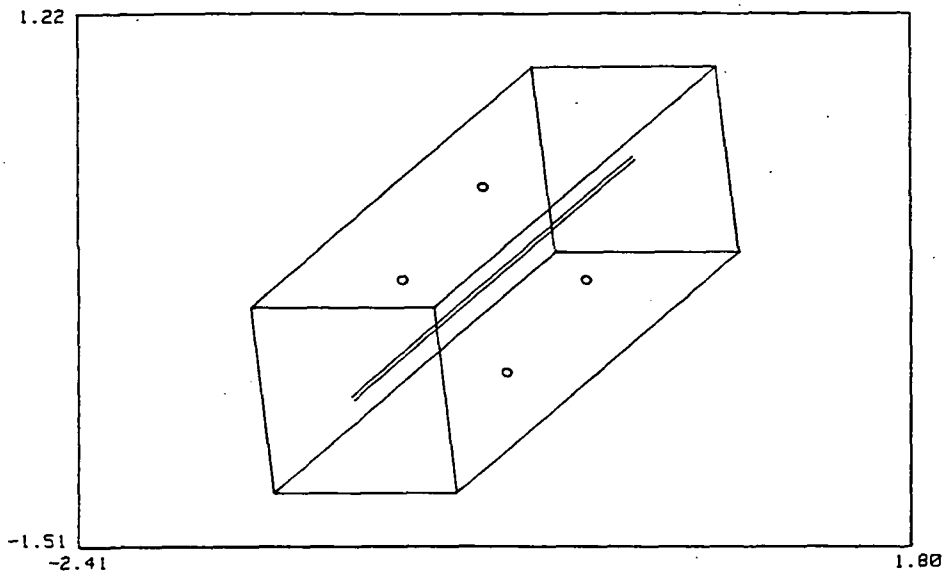

Fig. 8.24.1 Discretization of a Fiber in a Rectangular Block using Fiber Elements (includes a cylindrical volume cell not shown)

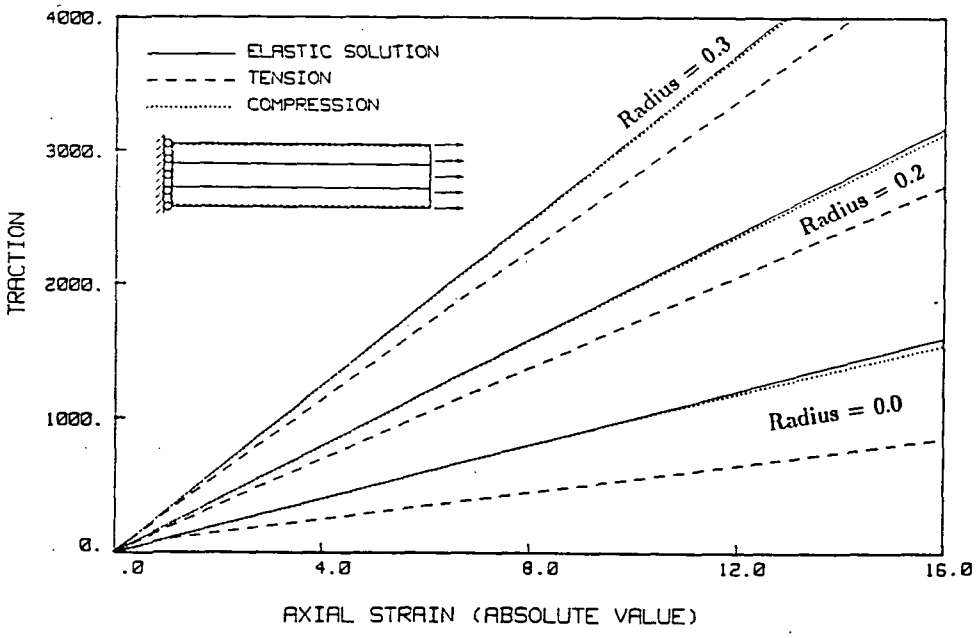

Fig. 8.24.2 Traction vs. Axial Strain (in the Fiber). Elastoplastic-Fracture with Strain Hardening Behavior in Fiber Composites for Various Fiber Radii

9. CURRENT ACHIEVEMENT

9.1 Fourth Year Development

The main focus of the work of this past year has been the development and implementation of a nonlinear formulation that allows yielding of the composite matrix about the fibers. This and other important developments of the past year are outlined below.

9.1.1 General Development

New Quartic Boundary Elements for the Outer Boundary of the Composite Matrix: The fiber composite imposes a strain discontinuity on the fiber-matrix interface. This in turn results in a displacement variation which, although continuous, is quite irregular. To help capture the irregular variation in displacement and in the resulting tractions, quartic boundary elements were introduced to model the functional variation on the outer boundary (geometry remains quadratic). A quartic element has more degrees of freedom than a quadratic element. However, the computational time of an analysis using quartic elements is less than an analysis using quadratic elements when the total number of degrees of freedom are the same since fewer elements are required in the quartic element model and therefore less time is required for their integration. Furthermore, for the same number of degrees of freedom, an analysis using the quartic boundary elements is, in general, more accurate than an analysis using the quadratic elements.

A problem employing quartic boundary elements was demonstrated in example 8.4 of Chapter 8.

9.1.2 Nonlinear Material Behavior of Ceramic Composites

Development of the Integral Equation for Displacement Rates: A formulation of an integral equation for displacement rates in a fiber composite structure undergoing plastic deformation was developed. The nonlinear effects present in the composite matrix are brought into the integral equation via a volume integral.

Development of a Cylindrical Volume Cell: A cylindrical volume cell was developed based on a 30 node shape function. The variation of initial stress rates are quadratic in the axial direction of the volume cell, linear in the radial direction, and trigometric in the circumferential direction. The development of a 5-node circular shape function was required for the circumferential variation. The 30 node shape function can accurately approximate the distribution of initial stress rates about a fiber which were observed in numerical tests.

Semi-analytical Integration of the Volume Cell: A great deal of attention was devoted to the analytical integration of the volume kernel multiplied by the 30 node shape function. To lower the cost of the numerical integration, the volume cell is analytically integrated in the circumferential direction. This reduces the three-dimensional volume integration to a two-dimensional integration which is evaluated numerically.

Development of Integral Equations for Stress Rates: An integral equation for stress rates was developed in which nonlinear effects were incorporated in the equation through a volume integral. this volume integral is strongly singular and had to be given special consideration. The 30 node cylindrical volume cell was once again employed to model the initial stress rates in the system. To reduce computational costs, semi-analytical integration was once again carried out in the circumferential direction.

Development of a Stress Rate Calculation on the Fiber-Matrix Interface: All integrals (including surface integrals) of the stress rate equation are strongly singular and are difficult to integrate numerically, for points on the fiber-matrix interface. For this reason, a special stress rate calculation was developed for the volume cell nodes which lie on the fiber-matrix interface.

Implementation of an Elastoplastic-Fracture Model for Ceramic Composites: An elasto-plastic-fracture model was implemented for the nonlinear constitutive modeling of ceramic

composites. An important feature of this model is its ability to sustain stress in compression many times greater than in tension. The model also includes strain hardening.

Implementation of a Nonlinear Algorithm: In order to solve the nonlinear system, a nonlinear algorithm was implemented based on an iterative algorithm employed in the computer code BEST3D. For fast convergence, the iterative algorithm has an acceleration scheme in which values of initial stress rates are estimated for future time steps based on the past history.

9.1.3 Maintenance and Testing

Considerable effort has been devoted to maintaining the computer program and improving the quality and reliability of the code. Verification problems from previous years are regularly executed to assure their continued operation. Furthermore, the present work was thoroughly tested and verified.

9.2 Summary

Significant progress has been achieved towards the goal of developing the general purpose boundary element program 'BEST-CMS' for the micro- and macro-mechanical studies of advanced ceramic composites (Table 9.1). In the first year of the contract the framework of 'BEST-CMS' was composed based on the advanced boundary element program BEST3D. At that time the formulation for elastostatic analysis of fully-bonded fibers was implemented in the code. All the general purpose features in BEST3D, such as the definition of local boundary conditions and multi-region substructuring, were retained in order to facilitate the analysis of real problems encountered in industry.

In the second year, the ceramic composite formulations for steady-state heat conduction and steady-state uncoupled thermoelasticity were developed and implemented in the elastostatic code developed in the first year. Analytic integration of the kernel functions was performed about the circumference of the fiber, and therefore, the numerical integration of the fiber (and hole) was reduced to an efficient, one-dimensional line integration

along its length. An efficient assembly and solution algorithm was developed for these formulations similar to the algorithm used in the elastostatic analysis. This fiber assembly scheme significantly reduced the number of unknowns in the system, and therefore, it reduced the number of equations and the work required to solve them. Also, the displacement and the heat conduction equations of the thermoelastic analysis are integrated simultaneously, but solved separately for efficiency.

Considerable effort has been focused on the development of nonlinear interface connections between the fibers and the composite matrix. Up to this point only perfectly-bonded connections were considered. The ceramic composite formulations were reformulated to allow the implementation of a variety of sophisticated interface relations such as spring connections, sliding connections with smooth or frictional resistance, progressive debonding, yielding on interfaces, and temperature dependent connections. In addition to the fully-bonded fiber-matrix interface, constitutive relations were derived for spring connections and slide connections with spring-coulomb frictional resistance. These models were implemented in a general manner to facilitate the addition of other interface models to be derived in the future. Since the interface relations are nonlinear and path dependent, an efficient nonlinear algorithm had to be derived. The nonlinear algorithm was implemented in both the elastostatic and the uncoupled thermoelastic analyses.

Overall the cost of the steady-state ceramic composite analysis is just slightly more expensive (for a moderate number of fibers) than the cost of analyzing the matrix without the fibers present. The additional cost is primarily attributed to the integration of the outer surface of the matrix for the additional nodes on the surface of the hole containing the fiber, and towards the expense of solving a slightly larger system. More importantly, the present analysis is far more efficient than the conventional three-dimensional, multi-region approach which requires significantly more nodes in the discretization of the fiber and hole. The additional nodes require additional equations which add to the expense of integration and solution. Furthermore, the conventional approach requires a two-dimensional numer-

ical integration over the surface of the fiber and hole as opposed to a one-dimensional integration used in the present method. The data preparation for the present method is less involved than the conventional multi-region approach and the location of the fibers can be readily changed in a re-analysis. Moreover, the code developed in the present work allows up to 500 (100 per GMR) fiber elements in an analysis. An ordinary multi-region code would require a 500 region capability in order to compete. In terms of computer expense and the cost of data preparation for a 500 region problem, such analyses would be impractical.

In the third year, the implementation of the transient heat conduction and the transient thermoelastic composite analyses was carried out. These analyses are more complicated than their steady-state counterparts due to the presence of the convolution integrals. Since the transient kernels cannot be integrated analytically, a numerical integration scheme was developed for the integration of the fibers. Furthermore a completely new assembly scheme had to be developed for the analysis. This assembly scheme, will also be adopted for the elastodynamic formulations. Although, the transient algorithm costs more than its steady-state counterpart, the present implementation is very efficient relative to the complex nature of the problem.

In the fourth year of development, attention was turned towards the analysis of ceramic composites undergoing plastic deformation. A formulation was developed and implemented for the yielding of the composite matrix about fibers. An elastoplastic-fracture constitutive law was implemented to model the nonlinear behavior of the ceramic composite. Efficient procedures were developed to account for the material nonlinearities and to obtain a solution. The solution time of the iterative nonlinear analysis, varies greatly from problem to problem and is considerably more expensive than the elastostatic analysis. However, without the new procedures developed in this work, an elastoplastic fiber composite analysis would be impractical.

Quartic boundary elements were also implemented throughout all analyses to model

the displacement and traction variation on the outer boundary of the composite matrix. The use of quartic boundary elements improves accuracy in the fiber composite analysis and often leads to computational savings through the reduction of boundary elements required in an analysis.

The ceramic composite formulation for elastostatics, steady-state and transient heat conduction, and steady-state and transient uncoupled thermoelasticity has been successfully implemented and has been proven to be accurate and efficient. Furthermore, the development and implementation of the nonlinear interface and material nonlinearities was successfully carried out in a general manner. Since the boundary element method has already been proven successful in elastodynamic and free vibration analyses, coupled with the success of the present work, the plan to extend the ceramic composite formulations to these other areas holds great potential. In fact, the boundary element method may not only be the best tool, but may also be the only practical tool for the analysis of large ceramic composite problems encountered in industry.

TABLE 9.1

Current State of BEST-CMS

Elastostatic Analysis

Steady-state Heat Conduction Anslysis

Steady-state Uncoupled Thermoelasticity

Transient Heat Conduction Analysis

Transient Uncoupled Thermoelasticity

Nonlinear Interface between the Fibers and the Matrix

Yielding of the Matrix about the Fibers (Elastoplastic-Fracture Model)

The Computer Program BEST-CMS (Version 2.0) and the Associated User's Manual were Last Delivered to NASA-LEWIS Research Center in the Spring of 1990

10. FUTURE DEVELOPMENT

Significant progress has been achieved towards the development of the general purpose, ceramic composite, boundary element code 'BEST-CMS'. Presently, the elastostatic, the steady-state heat conduction, and the steady-state uncoupled thermoelastic formulations for the analysis of fiber composite bodies with linear and frictional fiber-matrix interface connections have been implemented along with the transient heat conduction and the transient thermoelastic analysis of composites with fully-bonded interfaces. During the past year a formulation for the analysis of ceramic composites undergoing plastic deformation was implemented and tested.

In the fifth year of this contract steady-state and transient elastodynamic analyses and a free vibration analysis will be developed. Due to the complexity of these analyses, considerable effort will be required for their development. The framework for the transient elastodynamic analysis, however, is already in place since it closely follows the transient thermoelastic implementation.

The current algorithm for nonlinear interface connections and nonlinear material analysis have been successfully implemented and verified, however, these analyses can not be used simultaneously. Additional work is planned for a combined analysis in which these two failure modes can be studied concurrently. Also, a nonlinear thermoplastic creep model will be developed for an uncoupled thermoelastic nonlinear analysis.

Due to the complex nature of the nonlinear analysis there are a number of parameters that must be set appropriately. Load divisions, convergence tolerances, scale factors, aspect ratios, etc., must be manipulated and this requires patience and an in- depth knowledge of the program in order to obtain a correct solution to a nonlinear problem. With additional development, the algorithms can be refined to remove this burden from the user. The development of an enhanced, user friendly, algorithm is planned in which all parameters would be controlled internally. The user would only need to specify the level of accuracy

(i.e., low, medium or high) that is, desired. The end result will allow analyses of very sophisticated modes of failure with relative ease.

Table 10.1 summarizes the proposed future development of BEST-CMS. The next version of BEST-CMS and associated manuals will be delivered at the end of this year.

'BEST-CMS' will provide a very precise, yet very efficient, user-friendly, design and analysis tool for ceramic composites exposed to severe operating conditions. BEST-CMS will enable an engineer to undertake rapid numerical experiments to gain insight into the micro- and macro-mechanical behavior of ceramic composite materials. Armed with this information, the disposition of fibers can be selected to optimize performance under inelastic, thermal and dynamic loading.

TABLE 10.1

Planned Development of BEST-CMS

Steady-state Elastodynamic Analysis

Transient Elastodynamic Analysis

Free Fibration Analysis

Inclusion of a Temperature Dependent Creep Model in the Nonlinear Analysis (Thermoplastic-Creep Model)

Combine Nonlinear Material Behavior with Nonlinear Interface Conditions

Enhancements to Make Nonlinear Analysis User Friendly

Delivery of the Code BEST-CMS and the Associated User's Manual

APPENDIX A - STEADY-STATE KERNEL FUNCTIONS

This appendix contains the three-dimensional, steady-state kernel functions utilized in Chapters 2-4.

A.1 Heat Conduction

For the temperature kernel,

$$G_{\theta\theta} = \frac{1}{4\pi r}\left(\frac{1}{k}\right)$$

whereas, for the flux kernel,

$$F_{\theta\theta} = \frac{1}{4\pi r^2}\left[\frac{y_k n_k}{r}\right].$$

A.2 Elastostatics

For the displacement kernel,

$$G_{ij} = \frac{1}{16\pi r}\frac{1}{\mu(1-\nu)}\left[\left(\frac{y_i y_j}{r^2}\right) + (\delta_{ij}(3-4\nu)\right]$$

whereas, for the traction kernel,

$$F_{ij} = \frac{1}{8\pi r^2}\frac{1}{1-\nu}\left[-\left(\frac{3y_i y_j y_k n_k}{r^3}\right) - \left(\frac{\delta_{ij} y_k n_k + y_i n_j}{r}\right)(1-2\nu) + \left(\frac{y_j n_i}{r}\right)(1-2\nu)\right]$$

A.3 Steady-State Thermoelasticity

For the displacement kernel,

$$G_{ij} = \frac{1}{16\pi r}\frac{1}{\mu(1-\nu)}\left[\left(\frac{y_i y_j}{r^2}\right) + (\delta_{ij})(3-4\nu)\right]$$

$$G_{i\theta} = 0$$

$$G_{\theta j} = \frac{1}{8\pi}\left(\frac{\beta}{k(\lambda+2\mu)}\right)\left[\left(\frac{y_j}{r}\right)\right]$$

$$G_{\theta\theta} = \frac{1}{4\pi r}\left(\frac{1}{k}\right)$$

whereas, for the traction kernel,

$$F_{ij} = \frac{1}{8\pi r^2}\frac{1}{1-\nu}\left[-\left(\frac{3y_i y_j y_k n_k}{r^3}\right) - \left(\frac{\delta_{ij}y_k n_k + y_i n_j}{r}\right)(1-2\nu) + \left(\frac{y_j n_i}{r}\right)(1-2\nu)\right]$$

$$F_{i\theta} = 0$$

$$F_{\theta j} = \frac{1}{8\pi r}\left(\frac{\beta}{\lambda+2\mu}\right)\left[\left(\frac{y_j y_k n_k}{r^2}\right) - (n_j)\right]$$

$$F_{\theta\theta} = \frac{1}{4\pi r^2}\left[\left(\frac{y_k n_k}{r}\right)\right].$$

APPENDIX B - TRANSIENT KERNEL FUNCTIONS

This appendix contains the detailed presentations of the three-dimensional, transient kernel functions utilized in Chapter 5. For the time-dependent problems, the following relationships must be used to determine the proper form of the functions required in the boundary element discretization. That is,

$$G^n_{\alpha\beta}(X-\xi) = G_{\alpha\beta}(X-\xi, n\Delta t) \qquad \text{for } n = 1$$

$$G^n_{\alpha\beta}(X-\xi) = G_{\alpha\beta}(X-\xi, n\Delta t) - G_{\alpha\beta}(X-\xi, (n-1)\Delta t) \qquad \text{for } n > 1,$$

with similar expressions holding for all the remaining kernels. In the specification of these kernels below, the arguments $(X-\xi, t)$ are assumed.

Note that the indices

i, j, k, l	vary from 1 to 3
α, β	vary from 1 to 4
θ	equals 4

Additionally,

x_i	coordinates of integration point
ξ_i	coordinates of field point

$y_i = x_i - \xi_i \qquad r^2 = y_i y_i.$

For the displacement kernel,

$$G_{ij} = \frac{1}{16\pi r}\frac{1}{\mu(1-\nu)}\left[\left(\frac{y_i y_j}{r^2}\right) + (\delta_{ij})(3-4\nu)\right]$$

$$G_{i\theta} = 0$$

$$G_{\theta j} = \frac{1}{8\pi}\left(\frac{\beta}{k(\lambda+2\mu)}\right)\left[\left(\frac{y_j}{r}\right) g_4(\eta)\right]$$

$$G_{\theta\theta} = \frac{1}{4\pi r}\left(\frac{1}{k}\right)[g_5(\eta)]$$

whereas, for the traction kernel

$$F_{ij} = \frac{1}{8\pi r^2}\frac{1}{1-\nu}\Big[-\left(\frac{3y_iy_jy_kn_k}{r^3}\right) - \left(\frac{\delta_{ij}y_kn_k + y_in_j}{r}\right)(1-2\nu) + \left(\frac{y_jn_i}{r}\right)(1-2\nu)\Big]$$

$$F_{i\theta} = 0$$

$$F_{\theta j} = \frac{1}{8\pi r}\left(\frac{\beta}{\lambda+2\mu}\right)\left[\left(\frac{y_jy_kn_k}{r^2}\right)f_6(\eta) - (n_j)f_7(\eta)\right]$$

$$F_{\theta\theta} = \frac{1}{4\pi r^2}\left[\left(\frac{y_kn_k}{r}\right)f_8(\eta)\right].$$

In the above,

$\eta = r/(ct)^{1/2}$

$c = k/\rho c_\varepsilon$

$erf(z) = \frac{2}{\sqrt{\pi}}\int_0^z e^{-x^2}dx = 1 - erfc(z)$

$h_1(\eta) = erf\left(\frac{\eta}{2}\right) - \frac{\eta}{\sqrt{\pi}}e^{-\eta^2/4}$

$g_4(\eta) = erfc\left(\frac{\eta}{2}\right) + \frac{2h_1(\eta)}{\eta^2}$

$g_5(\eta) = erfc\left(\frac{\eta}{2}\right)$

$f_6(\eta) = erfc\left(\frac{\eta}{2}\right) + \frac{6h_1(\eta)}{\eta^2}$

$f_7(\eta) = erfc\left(\frac{\eta}{2}\right) + \frac{2h_1(\eta)}{\eta^2}$

$f_8(\eta) = 1 - h_1(\eta).$

For the interior stress boundary kernels,

$$E_{\beta ij} = \frac{2\mu\nu}{1-2\nu}\delta_{ij}\frac{\partial G_{\beta l}}{\partial \xi_l} + \mu\left(\frac{\partial G_{\beta i}}{\partial \xi_j} + \frac{\partial G_{\beta j}}{\partial \xi_i}\right) - \beta\delta_{ij}G_{\beta\theta}$$

$$D_{\beta ij} = \frac{2\mu\nu}{1-2\nu}\delta_{ij}\frac{\partial F_{\beta l}}{\partial \xi_l} + \mu\left(\frac{\partial F_{\beta i}}{\partial \xi_j} + \frac{\partial F_{\beta j}}{\partial \xi_i}\right) - \beta\delta_{ij}F_{\beta\theta}$$

where

$$\frac{\partial G_{ij}}{\partial \xi_k} = \frac{1}{16\pi r^2}\frac{1}{\mu(1-\nu)}\Big[\left(\frac{3y_iy_ky_k}{r^3} - \frac{\delta_{jk}y_i}{r} - \frac{\delta_{ik}y_j}{r}\right) + \left(\frac{\delta_{ij}y_k}{r}\right)(3-4\nu)\Big]$$

$$\frac{\partial G_{\theta j}}{\partial \xi_k} = \frac{1}{8\pi r}\left(\frac{\beta}{k(\lambda+2\mu)}\right)\left[\left(\frac{y_jy_k}{r^2} - \delta_{jk}\right)g_4(\eta) - \left(\frac{y_jy_k}{r^2}\right)\eta g_4'\right]$$

$$\frac{\partial F_{ij}}{\partial \xi_k} = \frac{1}{8\pi r^3}\frac{1}{(1-\nu)}\Bigg[-\left(\frac{15y_iy_jy_ky_ln_l}{r^4} - \frac{3y_iy_jn_k}{r^2} - \frac{3\delta_{jk}y_iy_ln_l}{r^2} - \frac{3\delta_{ij}y_jy_ln_l}{r^2}\right) - \left(\frac{3\delta_{ij}y_ky_ln_l}{r^2} - \delta_{ij}n_k + \frac{3y_iy_kn_j}{r^2} - \delta_{ik}n_j + \frac{3y_jy_kn_i}{r^2} - \delta_{jk}n_i\right)(1-2\nu)\Bigg]$$

$$\frac{\partial F_{\theta j}}{\partial \xi_k} = \frac{1}{8\pi r^2}\left(\frac{\beta}{\lambda+2\mu}\right)\Bigg[\left(\frac{3y_jy_ky_ln_l}{r^3} - \frac{y_jn_k}{r} - \frac{\delta_{jk}y_ln_l}{r}\right)f_6(\eta) - \left(\frac{y_kn_j}{r}\right)f_7(\eta) - \left(\frac{y_jy_ky_ln_l}{r^3}\right)\eta f_6' + \left(\frac{y_kn_j}{r}\right)\eta f_7'\Bigg]$$

and the prime, $'$, represents a derivative with respect to η. Thus,

$$f_6' = \frac{\partial f_6(\eta)}{\partial \eta}.$$

APPENDIX C - LIST OF SYMBOLS

A short list of notation used in this report is given below. Bold print is used to identify vectors and matrices.

$\mathbf{A^b}, \mathbf{B^b}, \mathbf{C^b}$ Boundary system matrices in assembled form

$\mathbf{A^\sigma}, \mathbf{B^\sigma}, \mathbf{C^\sigma}$ Matrices of the stress rate equations

$C_{ij}(\xi)$ A tensor dependent on location of the field point ξ

d_i Difference in displacement (and/or temperature) across the matrix-insert interface

$D^e_{ijkl}, D^{ep}_{ijkl}$ The elastic and the elastoplastic constitutive matrix relations, respectively

G_{ij}, F_{ij} Kernel functions

k^{ep}_{ij} Nonlinear interface constitutive relationship

$L^\beta(\eta_1, \eta_2)$ Two-dimensional shape function

$N^\gamma(\eta)$ One-dimensional shape function

$M^\alpha(\theta)$ Circular shape function

t Time

t_i Traction

u_i Displacement

x, X Refers to global coordinates of an integration point

$\mathbf{x}$ System vector of unknown boundary quantities

$\mathbf{y}$ System vector of known boundary quantities

ϵ_{ij} Strain

η Refers to local coordinates of an integration point

ξ refers to coordinates of a field point

σ_{ij} Stress

$\dot{\sigma}^c_{ij}$ Initial stress rates (corrective stress rates)

Subscript

i, j, k Indicial notation

$i, j, k = 1$ for heat conduction analysis (Chapter 2)

$i, j, k = 1, 2, 3$ for elastostatic analysis (Chapter 2) and for elastoplastic analysis (Chapter 6)

$i, j, k = 1, 2, 3, 4$ for thermoelastic analysis (Chapters 3 and 4)

$\alpha, \beta = 4$ for heat conduction (Chapter 5)

$\alpha, \beta = 1, 2, 3, 4$ for thermoelasticity (Chapter 5)

Superscript

H refers to quantities on the surface of the hole (left for fiber) in the ceramic matrix

$F, F2$ refers to quantities on the surface of the fiber

O refers to quantities on the outer surface of the ceramic matrix

$\dot{}$ (Incremental) time rate of change

REFERENCES

Abramowitz, M. and Stegun, I.A., Handbook of Mathematical Functions, Dover, New York (1974).

Ballarini, R. and Shamin, A., 'Finite Element Modeling of Frictionally Restrained Composite Interfaces', NASA Contractor Report 182281 (April 1989).

Banerjee, P.K., 'Integral Equation Methods for Analysis of Piece-wise Non-homogeneous Three-dimensional Elastic Solids of Arbitrary Shape', Int. J. Mech. Sci., 18, pp. 293-303 (1976).

Banerjee, P.K., Ahmad, S. and Manolis, G.D., 'Transient Elastodynamic Analysis of Three-dimensional Problems by Boundary Element Method', Earthquake Engineering and Structural Dynamics, Vol. 14, pp. 933-949 (1986).

Banerjee, P.K. and Butterfield, R., Boundary Element Methods in Engineering Science, McGraw-Hill, London (1981).

Banerjee, P.K. and Butterfield, R., Developments in Boundary Element Methods - I, Applied Sci. Publishers, Barking, Essex, UK (1979).

Banerjee, P.K. and Driscoll, R.M., 'Three-dimensional Analysis of Raked Pile Groups', Proc. of Inst. Civil Engineers, Research and Theory, Vol. 61, pp. 653-671 (1976).

Banerjee, P.K., Henry, D.P. and Dargush, G.F., 'Micromechanical Studies of Composites by BEM', Proceedings from the ASME Annual Winter Meetings, Atlanta, Georgia (1991).

Banerjee, P.K. and Mukherjee, S., Developments in Boundary Element Methods - III, Applied Sci. Publishers, Barking, Essex, UK (1984).

Banerjee, P.K. and Shaw, R.P., Developments in Boundary Element Methods - II, Applied Sci. Publishers, Barking, Essex, UK (1982).

Banerjee, P.K. and Watson, J.O., Editors, Developments in Boundary Element Methods IV, Elsevier Applied Science Publishers, Barking, Essex, U.K. (1986).

Banerjee, P.K., Wilson, R.B. and Miller, N., 'Development of Large BEM System for Three-dimensional Inelastic Analysis', in Advanced Topics in Boundary Element Analysis, ed. T.A. Cruse, A.B. Pifko and H. Armen, AMD-V72, ASME, New York (1985).

Banerjee, P.K., Wilson, R.B. and Miller, N., 'Advanced Elastic and Inelastic Stress Analysis of Gas Turbine Engine Structures by BEM, Int. Jour. Numer. Methods in Engrg., Vol. 26, pp. 393-411 (1988).

Behrens, E., 'Thermal Conductivities of Composite Materials,' J. Composite Materials, Vol. 2, p. 2 (1968).

Butterfield, R. and Banerjee, P.K., 'Analysis of Axially Loaded Compressible Piles and Pile Groups', Geotechnique, Vol. 21, No. 1, pp. 43-60 (1971).

Byrd, P.F. and Friedman, M.D., Handbook of Elliptic Integrals for Engineers and Physicists, Springer-Verlag, Berlin (1954).

Caruso, J.J. and Chamis, C.C., 'Assessment of Simplified Composite Micromechanics Using Three-dimensional Finite-element Analysis', J. Comp. Tech. Res., Vol. 8, No. 8, pp. 77-83 (1986).

Chamis, C.C. and Sinclair, J.H., 'The Effects of Eccentricities on Fracture of Off-axis Fiber Composites', Polym. Eng. and Sci., Vol. 19, No,. 5 (April 1979).

Chen, W.F., Limit Analysis and Soil Plasticity, Elsevier, New York (1975).

Cruse, T.A.,'An Improved Boundary Integral Equation Method for Three-dimensional Elastic Stress Analysis', Comp. and Struct., V4, pp. 741-754 (1974).

Dargush, G.F., 'Boundary Element Methods for the Analogous Problem of Thermomechanics and Soil Consolidation', Ph.D. Thesis, State University of New York at Buffalo (1987).

Dargush, G. and Banerjee, P.K. Development of an Integrated BEM for Hot Fluid Structure Interaction, Earth to Orbit Propulsion System, NASA Conf. Publication No. 3012 (1988).

Dargush. G.F. and Banerjee, P.K., 'Advanced Development of the Boundary Element for Steady-state Heat Conduction', Int. J. Num. Methods in Eng., Vol. 28, pp. 2123-2142 (1989).

Dargush, G.F. and Banerjee, P.K., 'BEM Analysis for Three-dimensional Problems of Transient Thermoelasticity', Int. Jour. Solids and Structures, Vol. 26, pp. 199-216 (1990).

Dargush, G. and Banerjee, P.K., 'Application of the Boundary Element Method to Transient Heat Conduction', Int. Jour. Numer. Methods in Engrg., Vol. 31, pp. 1231-1247 (1991).

Davidge, R.W., 'Fibre-reinforced Ceramics', Composites, Vol. 18, No. 2, pp. 92-97 (1987).

Dongarra, J.J. et al, Linpack Users' Guide, SIAM, Philadelphia, Pa (1979).

Garg, K.S., Svalbonas, V. and Gutman, G., Analysis of Structural Composite Materials, M. Decker, New York (1973).

Hashin, Z. and Rosen, B.W., 'The Elastic Moduli of Fiber Reinforced Materials,', J. Appl. Mech., Vol. 31, p. 223 (1964).

Hastings, C., Jr., Approximations for Digital Computers, Princeton University Press, Princeton (1955).

Henry, D.P., 'Advanced Development of the Boundary Element Method for Elastic and Inelastic Thermal Stress Analysis,' Ph.D. dissertation, State University of New York at Buffalo (1987).

Henry, D. and Banerjee, P.K., 'A Thermoplastic BEM Analysis for Substructured Axisymmetric Bodies', Journal of Engineering Mechanics, ASCE, Vol. 113, No. 12, pp. 1880-1900 (1987).

Henry, D. and Banerjee, P.K., 'A New Boundary Element Formulation for Two and Three-dimensional Problems of Thermoelasticity Using Particular Integrals', Int. Jour. Numer. Methods in Engrg., Vol. 26, pp. 2061-2077 (1988a).

Henry, D.P. and Banerjee, P.K., 'A Variable Stiffness Type Boundary Element Formulation for Axisymmetric Elastoplastic Media', International Journal for Numerical Methods in Engineering, Vol. 26, No. 5, pp. 1005-1027 (1988b)

Henry, D.P. and Banerjee, P.K., 'Elastic Stress Analysis of Three-dimensional Solids with Small Holes by BEM', International Journal for Numerical Methods in Engineering, Vol. 31, pp. 369-384 (1991).

Hill, R., 'Theory of Mechanical Properties of Fibre-strenghtened Materials: III. Self-consistent Model', J. Mech. Phys. Solids, Vol. 13, p. 189 (1965).

Hopkins, D.A. and Chamis, C.C., 'A Unique Set of Micromechanics Equation for High Temperature Metal Matrix Composites', First Symposium on Testing Technology of Metal Matrix Composites, Nashville, Tenessee, NASA Technical Memorandum 87154 (November 1985).

Jones, R.M., Mechanics of Composite Materials, McGraw-Hill (1975).

Lachat, J.C. and Watson, J.O. 'Effective Numerical Treatment of Boundary Integral Equations: A Formulation for Three-dimensional Elastostatics', Int. J. Num. Meth. in Eng., 10, pp., 991-1005 (1976).

McCullough, R.L., Concepts of Fiber-resin Composites, M. Decker, New York (1971).

Rizzo, F.J. and Shippy, D.J., 'A Formulation and Solution Procedure for the General Non-homogeneous Elastic Inclusion Problems', Int. J. Solids and Struct., 4, pp. 1161-1179 (1968).

Rizzo, R.R., 'More On the Influence of End Constraints on Off-axis Tensile Tests', J. Composite Materials, Vol. 3, p. 202 (1969).

Selvadurai, A.P.S., 'Some Aspects of Non-linear Interfaces in Geomechanics: Boundary Element Modelling', Third International Conference in Geomechanics, Niagara Falls, Canada, p. 463 (May 1988).

Sen, R., Kausel, E. and Banerjee, P.K., 'Dynamic Behavior of Axially and Laterally Loaded Piles and Pile Groups Embedded in Inhomogeneous Soil', Int. Jour. Numerical Analytical Methods in Geomechanics, Vol. 9, No. 6, pp. 507-524 (1985).

Stroud, A.H. and Secrest, D., Gaussian Quadratic Formulas, Prentice-Hall, New York (1966).

Tripp, D.E., Hermann, J.H., and Gyekenyesi, J.P., 'A Review of Failure Models for Unidirectional Ceramic Composites Under Monotonic Loads', NASA Technical Memorandum 101421 (June 1989).

Vinson, J.R. and Chou, T.W., Composite Materials and Their Use in Structures, John Wiley and Sons (1975).

Walker, K.P., Research and Development Program for Nonlinear Structural Modeling with Advanced Time-temperature Dependent Constitutive Relationships, NASA CR-165533 (1981).

Walker, K.P., Jordon, E.H., and Freed, A.D., 'Nonlinear Mesomechanics of Composites with Periodic Microstructure: First Report', NASA Technical Memorandum 102051 (June 1989).

Wang, H.C., 'A General Purpose Development of BEM for Axisymmetric Solids', Ph.D. Dissertation, State University of New York at Buffalo (1989).

Watson, J.O., 'Advanced Implementation of the Boundary Element Method for Two- and Three-dimensional Elastostatics', in Banerjee, P.K. and Butterfield, R., Developments in Boundary Element Methods - I, Applied Science Publishers, London, pp. 31-64 (1979).

Whitney, J.M. and Riley,, M.B., 'Elastic Properties of Fiber Reinforced Composite Materials', J. AIAA, Vol. 4, p. 1537 (1966).

Wilson, R.B., Bak, M.J., Nakazawa, S., and Banerjee, P.K., '3-D Inelastic Analysis Method for Hot Section Components (Base Program)', NASA Contract Report 174700 (February 1984).

Wilson, R.B., Snow, D.W. and Banerjee, P.K. 'Stress Analysis of Gas Turbine Engine Structure Using Boundary Element Methods, AMD-Vol. 72, pp. 45-64 (1985).